DISCLAIMER

This report was prepared as an account of work sponsored by an agency of the United States Government. Neither the United States Government nor any agency thereof, nor any of their employees, makes any warranty, express or implied, or assumes any legal liability or responsibility for the accuracy, completeness, or usefulness of any information, apparatus, product, or process disclosed, or represents that its use would not infringe privately owned rights. Reference herein to any specific commercial product, process, or service by trade name, trademark, manufacturer, or otherwise does not necessarily constitute or imply its endorsement, recommendation, or favoring by the United States Government or any agency thereof. The views and opinions of authors expressed herein do not necessarily state or reflect those of the United States Government or any agency thereof. Reference herein to any social initiative (including but not limited to Diversity, Equity, and Inclusion (DEI); Community Benefits Plans (CBP); Justice 40; etc.) is made by the Author independent of any current requirement by the United States Government and does not constitute or imply endorsement, recommendation, or support by the United States Government or any agency thereof.

Final Technical Report (FTR)

Award Number: DE-EE0009305

Project Title:

Designing Recyclable Biomass-Based Polyesters

Federal Agency: Department of Energy
Sponsoring Program Office: Office of Energy Efficiency and Renewable Energy, Bioenergy Technologies Office

Recipient Organization: University of Wisconsin – Madison
Principal Investigator: George Huber, gwhuber@wisc.edu
Business contact: Alina Cuamani, Grant Administrator, alina.cuamani@wisc.edu

Teaming Partners: The University of Oklahoma, Colorado State University, National Renewable Energy Laboratory, Pyran, Amcor, Stora Enso.

Reporting Period: October 1, 2021 to February 28, 2025
Report Date: July 2025

ACKNOWLEDGEMENT: This material is based upon work supported by the U.S. Department of Energy's Office of Energy Efficiency and Renewable Energy (EERE) under the **Bioenergy Technology Office (BETO)** Award Number **DE-EE0009305**.

Executive Summary

This project successfully demonstrated the production of sustainable polyesters from biomass-derived monomers, offering properties on par with or superior to fossil-based plastics such as LLDPE and PBAT. Using renewable chemical platforms like furfural and HMF, we synthesized over eight novel monomers and nearly 100 aliphatic-aromatic polyesters. Among these, PPeAT and PDDF emerged as highly promising candidates for flexible packaging applications, exhibiting excellent mechanical performance, tunable thermal properties, and enhanced barrier characteristics.

Key advances included the development of ring-opening polymerization strategies using cyclic monomer intermediates to produce high molecular weight materials with excellent control. The resulting polymers achieved biobased content of at least 44 wt.%. We also implemented chemical recycling via catalytic methanolysis, recovering over 90% of monomers from PPeAT at semi-pilot scale. This supports a circular economy approach by enabling material reuse without performance loss.

Techno-economic and life cycle assessments confirmed that these polyesters can reduce greenhouse gas emissions by up to 50% compared to petroleum-derived alternatives. Favorable mechanical properties may further reduce material demand, and cost competitiveness was demonstrated under specific market conditions. Feedstock cost and environmental footprint were identified as primary levers for future optimization.

In summary, the project met or closely approached all technical targets, including biodegradability, strength, and processing compatibility. While minor issues such as color and melting point variation remain, the results strongly support continued development and scale-up of these sustainable materials.

1. Background and Project Goals

Since the 1950s, most of plastics produced have ended up in landfills or the natural environment, contributing significantly to environmental degradation.[1] Packaging industry is one of the largest contributors to this problem due to widespread use of plastics in single-use applications.[2] The environmental burden caused by plastics is continuously exacerbated, as the high costs associated with transportation, processing, and recycling of plastic packaging often make the production of new plastic materials more economically viable.[3] Packaging films are typically made from petroleum-derived polymers such as polyethylene (PE), polypropylene (PP), and polyethylene terephthalate (PET), among others, which exhibit attractive features including low production cost, excellent processability, favorable mechanical properties, and strong resistance to physical, chemical, and biological degradation.[4] However, despite these functional advantages, oil-derived polymers lack biodegradability and tend to persist in the environment for centuries.

To address the environmental issues associated with the non-biodegradability of oil-derived polymers, biomass-derived aliphatic polyesters have emerged as viable alternatives. Notable examples include polylactic acid (PLA),[5-7] polyhydroxyalkanoates (PHA),[8, 9] polybutylene succinate (PBS),[10, 11] and polyhydroxybutyrate (PHB)[12] which are bio-based polymers that offer advantages such as biodegradability, high thermal stability, good barrier properties, and acceptable mechanical performance.[13] However, many aliphatic polyesters suffer from brittleness, which limits their mechanical performance compared to conventional polyolefins. To overcome these limitations, aliphatic-aromatic copolyesters such as poly(butylene adipate-co-terephthalate)(PBAT),[14, 15] poly(butylene glycolate-co-furan dicarboxylate),[16] poly-(butylene succinate-co-furandicarboxylate),[17] poly(ethylene succinate-co-furan dicarboxylate),[18] and poly(ethylenesebacate-co-furandicarboxylate)[19] have been developed as new classes of materials that combine biodegradability with improved mechanical properties. These materials aim to bridge the performance gap between aliphatic bio-based polyesters and petroleum-derived polymers.

One of the most widely produced biodegradable aliphatic-aromatic polyesters in 2022 was PBAT, which has been commercialized by companies such as BASF, Eastman, and Novamont as a biodegradable alternative to low-density polyethylene (LDPE) for packaging and other film applications. For instance, BASF's PBAT-based polymer, Ecoflex®, biodegrades into water, CO_2, and biomass losing 90% of its mass in 180 days.[20] Although aliphatic-aromatic offer improved biodegradability compared to LDPE and exhibit a similar melting point to that of polyolefins, their Young's modulus is typically one third that of LDPE. As a result, aliphatic-aromatic polyester films must be approximately 44% thicker than LDPE films to achieve comparable stiffness. This increased thickness raises raw material costs and runs counter to the industry's push toward downgauging.

Consequently, currently available aliphatic-aromatic polyesters such as PBAT have insufficient mechanical properties to fully replace LDPE films in packaging applications.

Based on the above, the primary objective of this project was to design new biomass-derived polyesters with thermal and mechanical properties comparable to those of current polyolefin packaging films, while also being chemically recyclable and biodegradable. These polyesters were intended for use in three different commercial applications. The specific objectives that were targeted were the design of a new class of polyesters with the following properties:

- 50 to 70% lower energy input than conventional petroleum polymers.
- Biomass based content from 50 to 100 wt.%.
- Costs 30-50% lower than PBAT.
- 60% biodegradable in 180 days by ASTMD6400.
- Modulus at least 200 MPa and elongation at break at least 350% (similar to LDPE and linear-low density poly-ethylene (LLDPE)).
- Melting temperature 105-115 °C (similar to LDPE and LLDPE)
- Haze index for a 25 μm film ~10 according to ASTM D1003 (similar to LDPE and LLDPE)
- O_2 transmission rate equal to or lower than ~8000 $cm^3/(m^2$ day) (LDPE and LLDPE)

2. Approach and Report Outline

To achieve the stated goals and targeted performance of the engineered polyester films from bioderived sources, five main topic areas, as show in **Figure 1**, were integrated. The whole project team was assembled to include professionals with experience in the production of bioderived monomers, synthesis and characterization of polyesters, application of polymers, chemical recycling of polyesters, and techno-economic analysis and life cycle assessment. The following sections discuss the approaches followed in this project to interconnect the findings of each area.

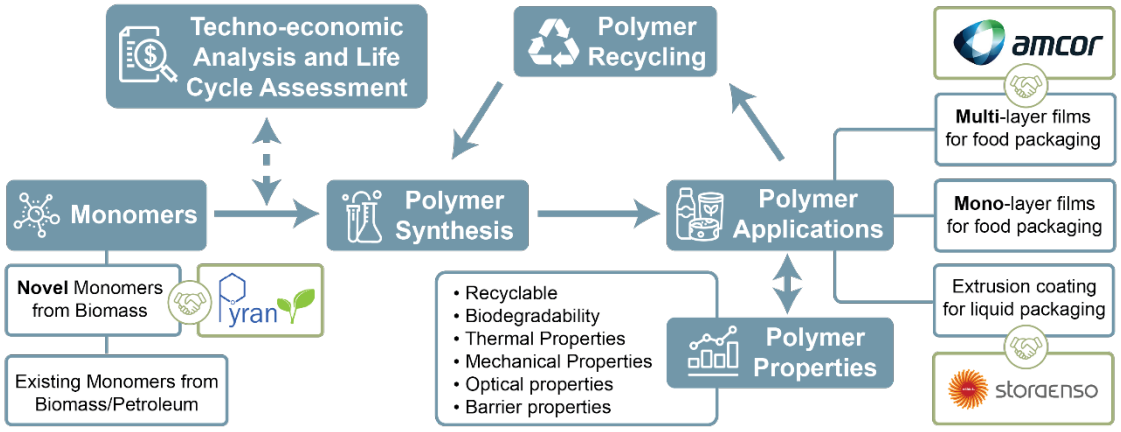

Figure 1. Summary of proposed project.

Area 1 – Monomers from biomass: This section describes the synthesis of monomers from 5-hydroxymethylfurfural (HMF), a biomass-derived platform molecule. Additionally, we outline the purification strategies employed, when necessary, to deliver high-quality monomers suitable for subsequent polymerization. Beyond the successful synthesis of these monomers, the project also included the results obtained for scaling up 1,5-pentanediol as promising monomer for polyesters synthesis.

Area 2 – Polymer synthesis and characterization: We report the synthesis and characterization of two new classes of polyesters, namely, Poly(pentenyl-co-adipate terephthalate) (PPeAT) and Poly(dodecanyl furanoate) (PDDF). Key polymer properties such as biodegradability, thermal stability, mechanical performance, and barrier behavior were systematically evaluated, highlighting the promising potential of these materials. Structure–property relationships were investigated through both computational and experimental approaches, enabled by a synergistic collaboration between experimentalists and the PolyML development team.

Area 3 – Polymer applications: Produced polyesters in this project were meant to be tested in three different commercial applications (mono- and multi-layer films for food packaging, and extrusion coating for liquid packaging) with our industrial partners.

Properties of these polymers were tested and compared with the incumbent PE and PBAT materials. Suggestions for application of the developed materials in the packaging industry based on their properties were made.

Area 4 – Chemical recycling of polyesters: A chemical recycling strategy was developed to depolymerize biobased polyesters back into their monomeric building blocks. This section focuses on the optimization of the methanolysis reaction conditions to enable efficient polymer deconstruction. Key metrics such as monomer recovery yield were quantified to assess depolymerization efficiency. Furthermore, the recovered monomers were subjected to re-polymerization reactions, followed by full re-characterization of the resulting materials. These experiments collectively demonstrate the feasibility of a circular lifecycle for the synthesized polyesters, supporting sustainable production and end-of-life management of these biobased materials.

Area 5 – Techno-economic analysis and Life cycle assessment: A comprehensive techno-economic analysis (TEA) and life cycle assessment (LCA) were conducted to evaluate the economic viability and environmental impact of the proposed biobased monomer and polyester production and recycling pathways. The TEA quantified capital and operating costs associated with monomer synthesis and polymerization, while the LCA assessed energy consumption, greenhouse gas emissions, and overall environmental burden across the full production lifecycle. Comparative analyses were performed against commercially available biodegradable polyesters, such as poly(butylene adipate-co-terephthalate) (PBAT), to contextualize the performance and sustainability of the proposed materials. These assessments provide critical insights into the feasibility and circularity of implementing these new biopolyesters at scale.

The following key outcomes were anticipated in the original project plan and served as the primary drivers for the successful completion of the work:

- ✓ A new class of chemically recyclable and biodegradable biomass-derived polyesters that have mechanical and thermal properties similar to PE.
- ✓ Demonstration of new polyesters in three commercial applications.
- ✓ The relationship between the structure of the polyesters and their properties.
- ✓ Material and energy balances for chemical recycling of the biomass polyesters.
- ✓ Continuous production of biomass-derived monomers in laboratory-scale reactors.
- ✓ TEA and LCA models for polymers synthesis based on experimental data.
- ✓ LCA of production and recycling of biomass-derived polyesters.

Area 1 – Monomers from biomass

This project leveraged a broad portfolio of biomass-derived monomers developed at the University of Wisconsin–Madison over the past two decades. As illustrated in **Figure 2**, the monomers synthesized for this study predominantly consist of diols with diverse chemical functionalities, including saturated aliphatic chains (e.g., 1,5-pentanediol), saturated and unsaturated furan rings (e.g. THFDM and FDM, respectively), and other furan-based structures with varying degrees of hydrogenation (e.g. HAH, PHAH, and FHAH). To enable tunable cross-linking within the resulting polymer networks, 1,2,5,6-Hexanetetrol (tetrol) was incorporated in the pool of synthesized monomers. In addition, 2,5-furandicarboxylic acid (FDCA) was included as a bio-based alternative to terephthalic acid.

The central hypothesis of this work was that the incorporation of these structurally diverse, renewable monomers into polyester backbones enable the production of bio-based polyesters with improved recyclability, biodegradability, and enhanced thermal, mechanical, and barrier properties compared to conventional or recently developed sustainable polyesters. Monomers syntheses were carried out under **Task 2.0 – *Synthesis and Characterization of Biomass-Derived Polyesters***, specifically within **Milestones 2.1.3** and **2.2.3**, while scale-up efforts of a promising bio-based diol was addressed under **Task 5.0** – ***Scaling Up of Polyester Synthesis and Application***, as outlined in **Milestone 5.3**.

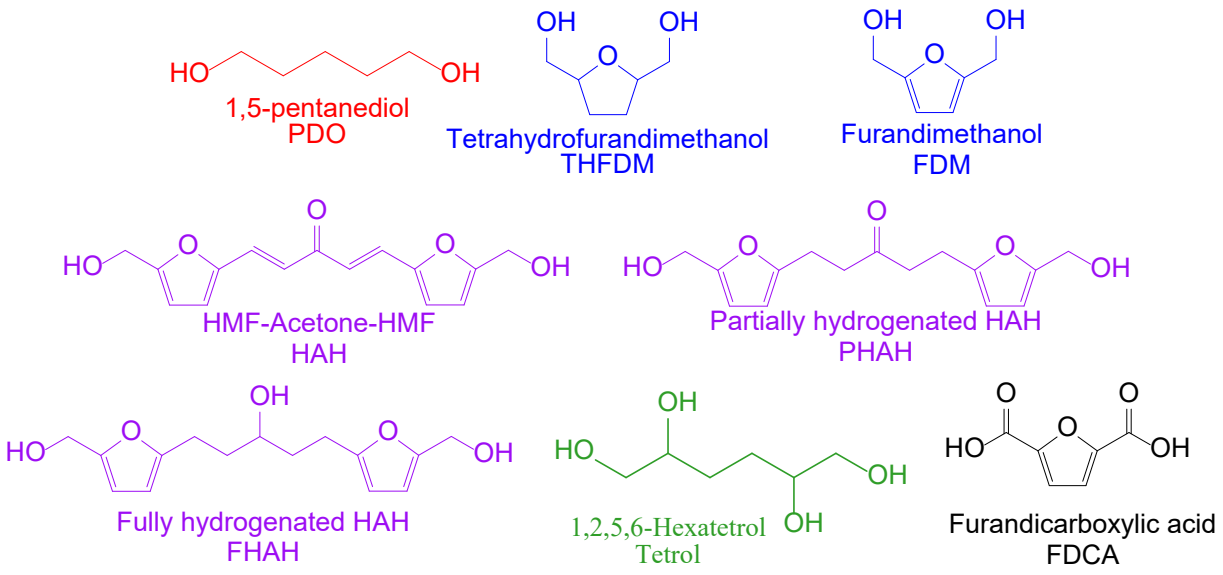

Figure 2. Biomass-derived monomers employed in this project.

M. 2.1.3 - Synthesis of 100g FDCA from glucose/fructose in laboratory: The synthesis of FDCA was not pursued at the laboratory scale within this project, as our industrial partner, Stora Enso, has been actively developing a continuous-flow pilot plant in Belgium to produce FDCA under the commercial name FuraCore®.[21] **Figure 3** illustrates the chemical pathway employed by Stora Enso, where the chemical route involves hydrolysis of cellulose to yield glucose, enzymatic isomerization of glucose to fructose, and subsequent acid-catalyzed dehydration to form HMF. HMF is then subjected to a pretreatment step for humins removal and catalytic oxidation to obtain FDCA. At the pilot plant scale, more than 100g of FDCA were synthesized by our industrial collaborator, therefore this milestone was satisfactorily demonstrated.

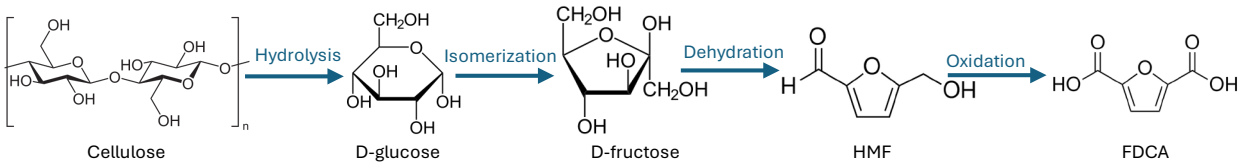

Figure 3. Chemical route followed by Stora Enso for synthesis of FDCA departing from cellulose.

M. 2.1.3 – Catalytic production of THFDM and FDM from HMF in laboratory reactors: As with the production of FDCA from 5-hydroxymethyl furfural (HMF), the use of HMF as a platform chemical requires previous conditioning of the commercially available material. Crude HMF is typically supplied as a dark brown solid with a nominal purity of 95-98%, but it contains a range of impurities including degradation products (e.g. levulinic acid, formic acid), residual acidic catalysts used during its synthesis, and polymeric byproducts commonly referred to as humins. Although refined grades of HMF (visibly lighter in color – typically yellow) are available commercially and exhibit reduced humins content, they still contain acidic impurities that can promote undesired side reactions during catalytic conversion. Therefore, rigorous purification of the starting HMF is essential to ensure reproducibility and selectivity in the synthesis of target monomers such as tetrahydrofuran dimethanol (THFDM) and furan dimethanol (FDM). The following section describes the protocols developed and implemented to effectively remove humins and neutralize residual acidic species present in commercial HMF, thereby enhancing consistency and efficiency of catalytic processes.

HMF purification through packed bed filtration:

Hydroxymethylfurfural (HMF) is a low-melting-point solid (melting point ~31.5 °C) that exhibits thermal instability and readily degrades into polymeric byproducts known as humins upon heating. To mitigate degradation and facilitate handling, HMF is commonly dissolved in a protic solvent such as water, alcohols, or tetrahydrofuran. After HMF dissolution in a solvent, the molecule becomes more stable and can be heated up to the reaction temperature. In the example presented below, ethanol was chosen as the reaction solvent. Therefore, HMF purification is presented for an HMF-ethanol solution.

A typical purification procedure involved the preparation of a 5–10 wt.% solution of commercial HMF in ethanol, which was subsequently pumped through a packed bed of γ-alumina. The γ-alumina served a dual function: it physically retained high-molecular-weight polymeric humins and adsorbed lower molecular weight oligomeric humins as well as acidic impurities commonly present in commercial HMF. **Figure 4** illustrates the filtration system employed to condition the HMF feed for monomer synthesis. As shown, the humins-rich HMF solution (orange solution, right bottle) was delivered through the γ-alumina column using an HPLC pump. The γ-alumina effectively removed both polymeric and acidic contaminants. The purified solution (yellow filtrate) was collected at the column outlet and further clarified using a 0.22 µm syringe filter to remove any residual particulates. This filtered HMF solution was then used directly in the catalytic synthesis of the targeted monomers.

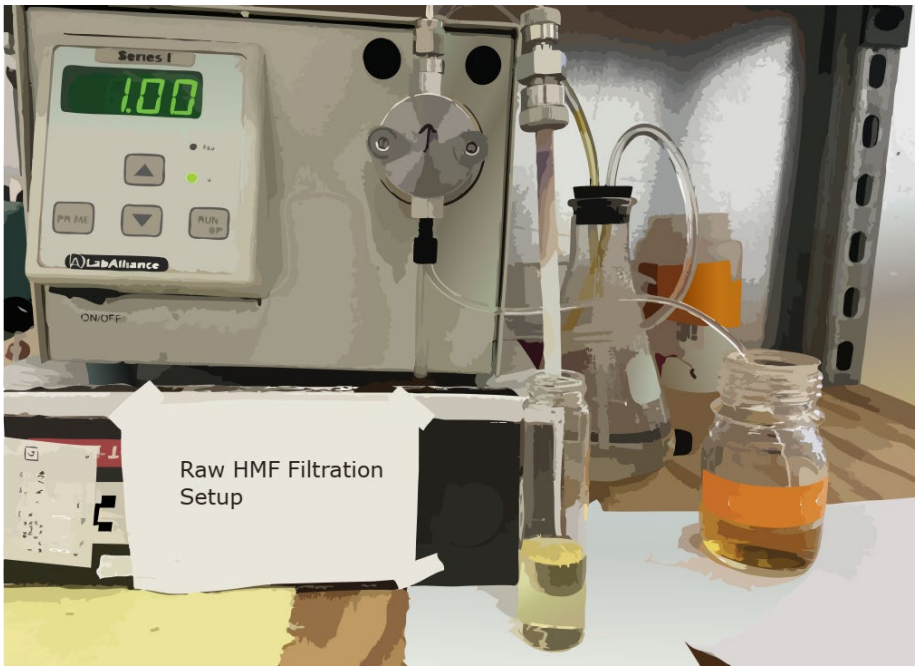

Figure 4. Filtration setup for crude HMF purification.

To determine the optimal column length required for effective humins removal from crude HMF solutions, a study was conducted varying the length of the γ-alumina filtration bed, as presented in **Figure 5**. Because humins are structurally undefined and lack a standardized analytical reference, their quantification was conducted using a colorimetric method. Specifically, the concentration of humins in the filtrate was measured via UV-Vis spectroscopy (Evolution 300, Thermo Scientific), and normalized against the feed solution used in the filtration experiments.

In a typical experiment, collected samples were filtered using a 0.22 µm PES syringe filter, placed into UV-grade fused quartz cuvettes, and analyzed at a wavelength of 380 nm,

where humins exhibit characteristic absorption. This approach enabled a semi-quantitative estimation of humins concentration based on absorbance intensity. As illustrated in **Figure 5**, the relative concentration of humins (represented by purple data points) decreased significantly with increasing bed length, reaching a minimum at approximately 1.5 cm. Beyond this length, no further improvement in humins removal was observed, indicating that 1.5 cm of bed length is sufficient for effective purification under the conditions tested. Additionally, a slight decline in HMF concentration was detected along the column, suggesting partial adsorption of HMF onto the γ-alumina surface. This tradeoff underscores the importance of balancing impurity removal and monomer recovery when optimizing filtration parameters for scale-up.

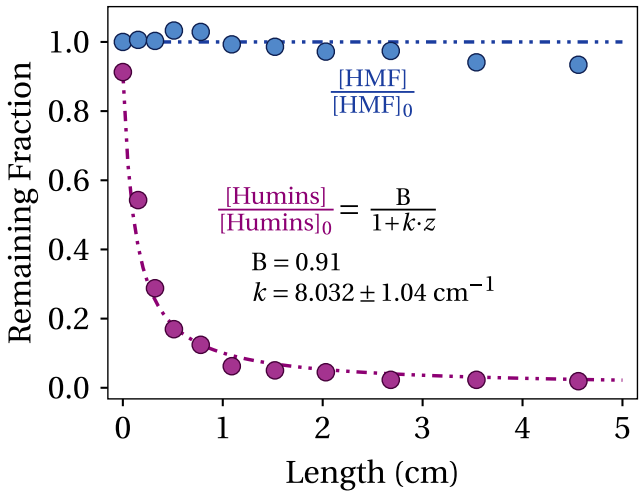

Figure 5. Remaining fraction of humins (purple) and HMF (blue) in the filtrate as a function of column length (z). Scattered data is representative for a time on stream (TOS) of 3.12 min. The dot-dashed lines represent: the adsorption kinetic model (purple) and a reference line at 1 (blue) to highlight the decrease in HMF concentration.

Figure 6 provides visual confirmation of this purification process. It shows a series of vials containing HMF solutions after filtration through increasing bed lengths. A clear color transition from orange to yellow is observed, consistent with the progressive removal of humins (which are primarily responsible for the orange coloration in crude HMF solutions). This result further supports the effectiveness of the γ-alumina filtration approach in conditioning HMF for subsequent catalytic transformations.

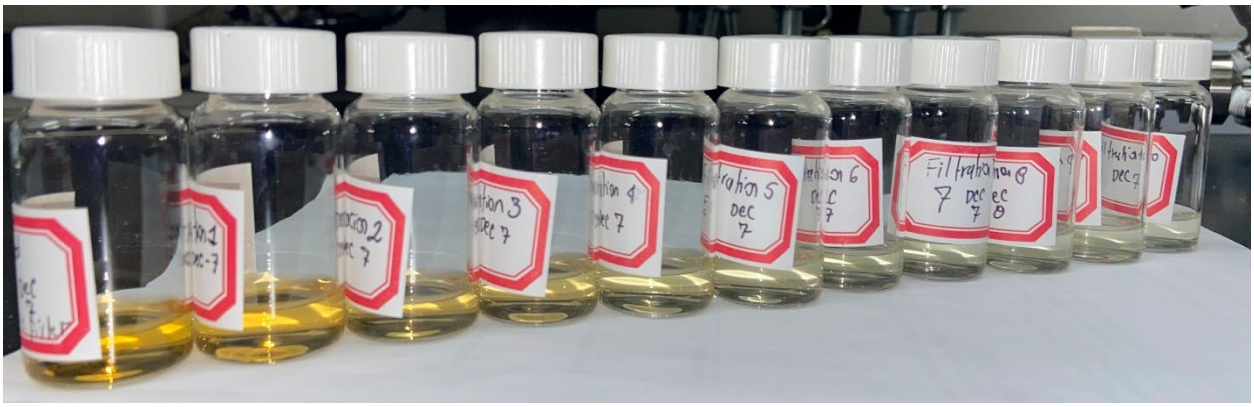

Figure 6. Evolution of the coloration of the permeate for an HMF solution at multiple points along the filtration column. Vials at the right were filtered with longer column bed with respect to vials at the left.

The following paragraphs detail the synthesis the proposed bio-derived monomers, departing from the purified HMF feed.

2,5 - Furandimethanol (FDM): The synthesis of FDM was performed in a continuous flow reactor. In a typical experiment a mass of an in-house synthesized $CuZrO_2$ catalyst ranging between 10-130 mg was packed in a tubular reactor and reduced at 300 °C under hydrogen flow. After reduction the reactor was cooled down to 100 °C and pressurized up to 500 psig of hydrogen atmosphere. Subsequently, a previously purified 5 wt.% HMF solution in ethanol was pumped through the packed bed at 60 μL min^{-1}, cofed with hydrogen at 60 mL min^{-1}. After reaction, reaction products were collected in a chilled vessel and prepared for analysis through gas chromatography. At these reaction conditions HMF hydrogenation occurs selectively displaying exclusively the reaction presented in **Figure 7**.

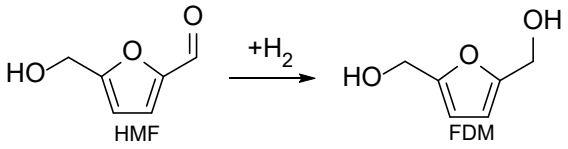

Figure 7. Hydrogenation of HMF to FDM over Copper catalysts.

Figure 8 presents the concentration profiles of HMF and its hydrogenation product, FDM (also commonly referred to as BHMF (2,5-bis(hydroxymethyl)furan)). The hydrogenation kinetics were systematically studied under continuous flow conditions, and a kinetic model was developed to describe the transformation. Model parameters were regressed based on experimental data to predict optimal reaction conditions, specifically the contact time (τ) required to achieve complete HMF conversion. The model revealed that virtually complete hydrogenation could be achieved at a residence time of approximately $\tau \approx 660\ g_{cat} h\ mol_{HMF}^{-1}$, under which >99% yield of BHMF was obtained. This was confirmed

by the chromatographic analysis shown in **Figure 9**, which illustrates full HMF conversion and exclusive formation of BHMF.

Following reaction, the solvent was removed via rotary evaporation, and the purified BHMF was forwarded to the polymer development team for evaluation in polyester formulations. These results demonstrate the feasibility of producing FDM (a.k.a. BHMF) in a continuous flow system with high efficiency and scalability for downstream polymer applications.

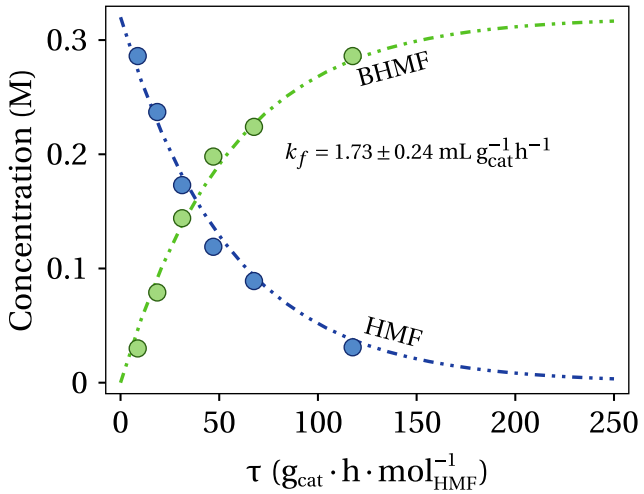

Figure 8. Concentration profile of HMF and BHMF over contact time (τ). Circles represent the collected data, while dot dashed lines represent the regressed model. Conditions: 5 wt.% humins-free HMF in ethanol (0.31 M, feed at 60 µL min^{-1}), 100 °C, 35 bar H_2, 60 mL min^{-1} H_2, 10-135 mg 10 wt.% $CuZrO_2$.

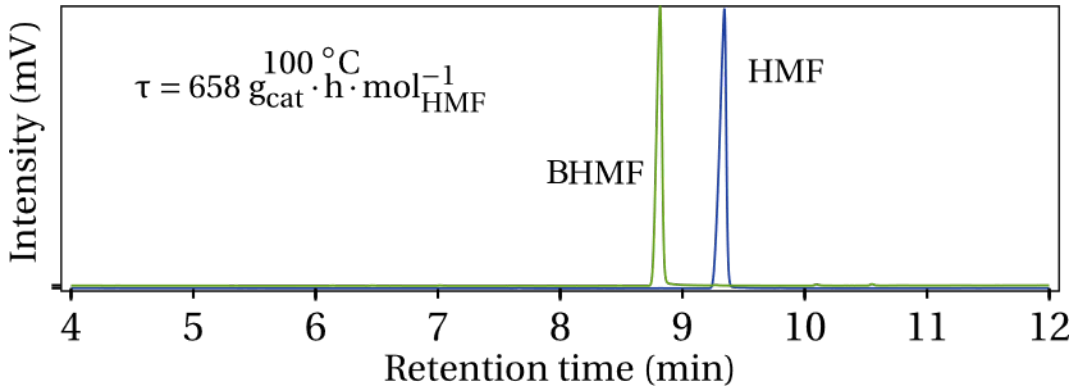

Figure 9. Chromatogram of Purified HMF for reaction (blue curve) and reaction product at 100 °C and τ = 658 $g_{cat} h\ mol_{HMF}^{-1}$ (green curve).

<u>2,5 - Tetrahydrofurandimethanol (THFDM)</u>: The synthesis of THFDM was conducted in a 2 L stainless steel batch reactor equipped with a mechanical stirrer. In a representative experiment, 60 g of HMF were dissolved in 340 g of ethanol to prepare a 15 wt.% HMF solution, which served as the reaction feed. Subsequently, 10 g of a commercial 64 wt.% Ni/SiO_2 catalyst were added directly to the reactor without any pretreatment (i.e., no

reduction or passivation). The hydrogenation reaction was carried out at 100–120 °C under 950 psi of H_2 for approximately 60 hours to ensure complete conversion. After reaction completion, ethanol was removed via rotary evaporation, yielding 55 g of THFDM per batch at 92% isolated yield. Over the course of the project, a consistent production of 85.5 g of THFDM per week was achieved, corresponding to an average yield of 95.1%. To further enhance the purity of the synthesized monomer, THFDM was subjected to flash chromatography. This step successfully reduced the monoalcohol content to 0.3–0.4 wt.%, meeting the purity threshold required for polymerization applications (<0.5 wt.% monoalcohol). **Figure 10** illustrates the reaction network for THFDM formation from HMF. As shown, the hydrogenation proceeds through the intermediate 2,5-furandimethanol (FDM). Incomplete conversion of this intermediate can reduce the overall selectivity to THFDM, emphasizing the importance of achieving full hydrogenation for process efficiency.

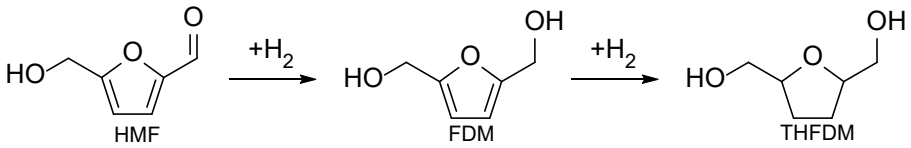

Figure 10. Hydrogenation network of HMF to THFDM over Nickel catalyst.

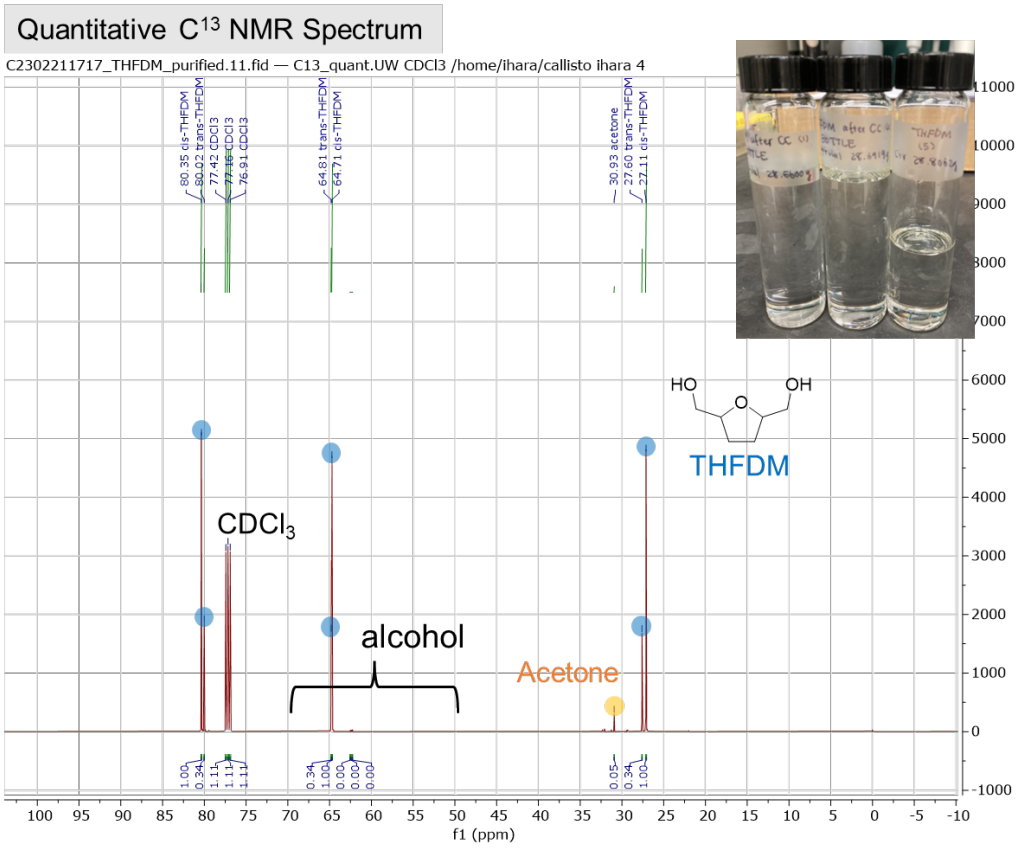

Figure 11. ^{13}C NRM of synthesized *cis*- and *trans*-THFDM.

Figure 11 displays the ^{13}C NMR spectrum of the purified THFDM monomer, along with a photograph illustrating its physical appearance. The spectrum confirms the successful synthesis of THFDM, showing characteristic chemical shift signals corresponding to both *cis*- and *trans*-isomers of the molecule. Additionally, a minor peak attributed to residual acetone is observed. This signal originates from the acetone used as an eluent during the flash chromatography step, which was applied to eliminate traces of monoalcohols and improve monomer purity. The accompanying image shows that the final THFDM product is a colorless, viscous liquid, consistent with expectations for this fully hydrogenated diol monomer.

HMF-Acetone HMF (HAH): The synthesis of HAH was conducted in batch mode in an aqueous NaOH solution using a round-bottom glass flask. Stoichiometric amounts of HMF and acetone were reacted at atmospheric pressure at 35 °C for 60 minutes. **Figure 12** presents the chemical reaction ruling the synthesis.

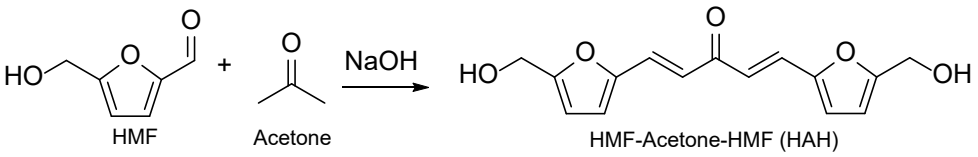

Figure 12. Hydrogenation of HMF to FDM

Upon completion, the reaction mixture was neutralized, leading to the precipitation of HAH, which was recovered by vacuum filtration and washed thoroughly with deionized water. The resulting solid was dried in a vacuum oven at 40 °C for 2 hours. The synthesis afforded approximately 20 g of HAH per liter of solution, corresponding to a 99% isolated yield.

Figure 13. Left: Reaction setup employed for the synthesis of HAH, showing the glassware configuration used during the reaction. Right: Image of the isolated HAH product collected in a Büchner funnel, illustrating its solid, yellow appearance upon filtration.

Figure 14 presents the quantitative ^{13}C NMR spectrum of the synthesized HAH. As shown, complete conversion of HMF was achieved, resulting in a 99% isolated yield of HAH. Quantitative analysis of ^{13}C NMR and HPLC confirmed the presence of less than 0.1 wt.% of monoalcohol side products. A total of 90 g of HAH were successfully synthesized and subsequently delivered to our collaborators at the University of Oklahoma for evaluation in polyester synthesis experiments.

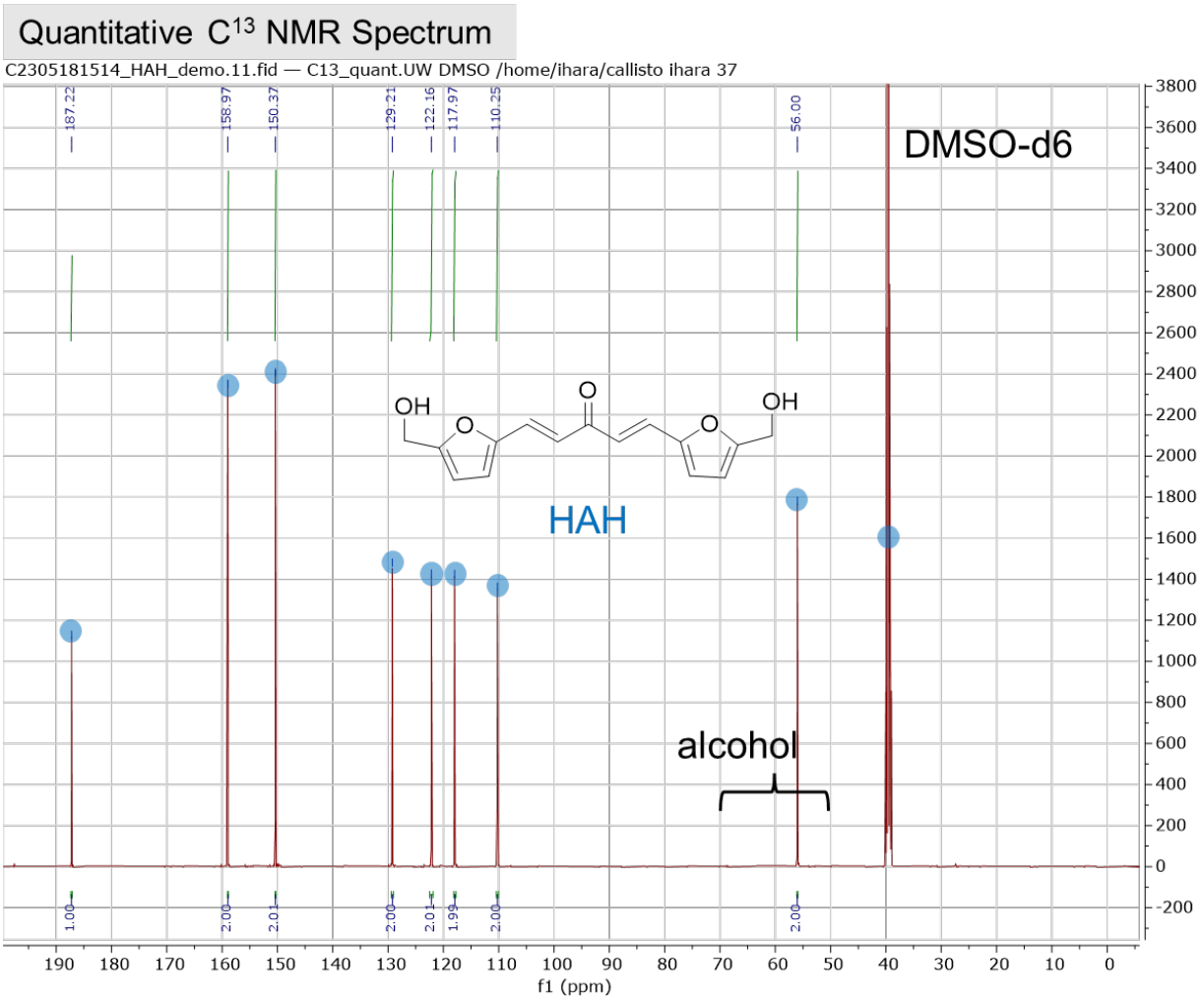

Figure 14. Left: reaction glassware for HAH synthesis. Right: HAH in Büchner filter displaying its solid yellow color.

Partially and Fully Hydrogenated HAH (PHAH and FHAH): The synthesis of partially hydrogenated HAH (PHAH) was carried out following a previously reported procedure by the Huber group.[22] The reaction proceeds via sequential hydrogenation steps: first, the two carbon–carbon double bonds present in HAH are fully saturated, yielding a ketone-containing intermediate (PHAH=O); subsequently, the carbonyl group is hydrogenated to form the corresponding alcohol (PHAH-OH). For demonstration purposes, 1.1 g of HAH were dissolved in 30 mL of an equimolar isopropanol/water mixture, and 0.25 g of Cu/γ-

Al_2O_3 catalyst was added to the reaction vessel. The reaction was conducted at 120 °C and 35 bar of H_2 for 450 minutes. Upon completion, the solvent was removed via rotary evaporation. Under these conditions, a production rate of 5.4 g/week was achieved. However, due to solubility limitations of the starting material in the IPA/water mixture, it was found that the use of tetrahydrofuran (THF) as the reaction solvent substantially improves solubility and, consequently, reaction efficiency.

The hydrogenated products, PHAH=O and PHAH-OH, present distinct chemical functionalities that influence the properties of the resulting polyesters. Specifically, the alcohol functionality in PHAH-OH enables cross-linking during polymerization, while the ketone form (PHAH=O) lacks this reactivity. Kinetic studies demonstrated that PHAH=O can be selectively obtained in up to 80% yield, as it serves as a transient intermediate for PHAH-OH synthesis. In contrast, prolonged contact time under optimized hydrogenation conditions might enable near-quantitative conversion to PHAH-OH (>99% yield). However, side reactions, primarily dehydration pathways, are typically observed under these conditions, which can reduce the overall yield of the desired products. These byproducts are indicated in **Figure 15**. **Table 1** summarizes the product distribution obtained from catalytic hydrogenation of HAH in both isopropanol (IPA) and tetrahydrofuran (THF) at 120 °C and 30 bar of H_2. As shown, PHAH-OH was the predominant product under these conditions, followed by PHAH=O. Nonetheless, dehydration-derived byproducts such as DH-PHAH-(OH or =O) were also detected, indicating the need for further optimization to suppress side reactions and maximize monomer purity.

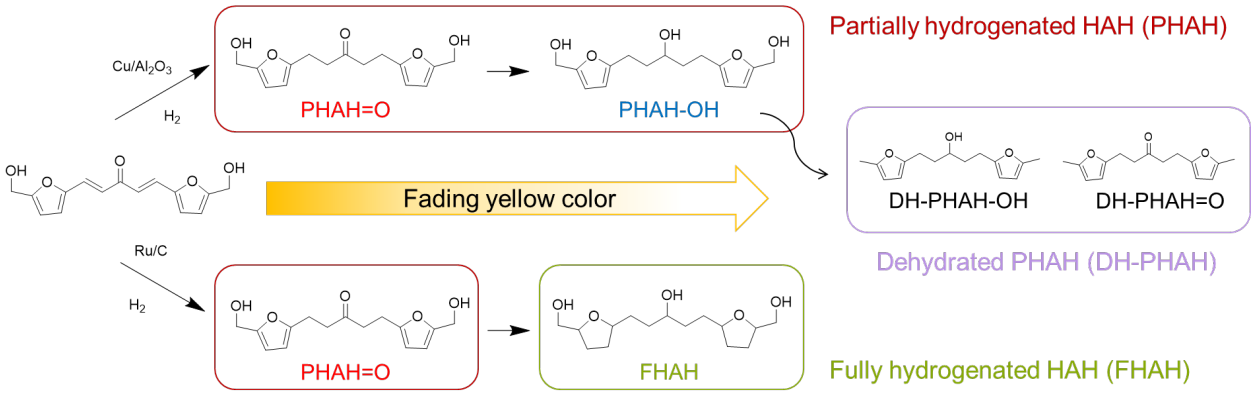

Figure 15. Hydrogenation of HMF to FDM

Table 1. Product composition of HAH hydrogenation over Cu/γ-Al_2O_3. Reaction conditions: 56 mM HAH with 100 mg cat. reacted at 120℃ under 30 bar H2 for 1800 min

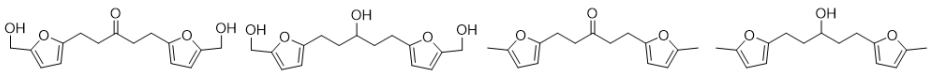

		PHAH=O	PHAH-OH	DH-PHAH=O	DH-PHAH-OH
Composition from NMR	IPA	43.7%	43.7%	7.0%	5.7%
	THF	8.6%	71.4%	10.0%	10.0%
Composition from GC-FID	IPA	44.2%	44.8%	5.6%	5.5%
	THF	7.2%	75.9%	6.1%	10.8%
Yield (mol)	IPA	44.4%	45.0%	5.6%	5.5%
	THF	5.7%	60.2%	4.8%	8.5%

FHAH can be synthesized under reaction conditions similar to those employed for PHAH production, with the key distinction that a Ru/C catalyst is required. The use of Ru/C enables activation and hydrogenation of the furan ring, which is otherwise resistant to saturation over copper based catalsyts.

1,2,5,6-Hexanetetrol (Tetrol): The synthesis of tetrol was carried out following a protocol adapted from a previous report by the Huber group,[23] as presented in **Figure 16**. Initially, 350 g of pure Cyrene® (dihydrolevoglucosenone) was subjected to hydrogenation in a 2 L batch reactor at 100 °C and 1000 psig of H_2 for 60 hours using a commercial Ru/C catalyst. This reaction yielded levoglucosanol (Lgol) with >99% selectivity. Subsequently, a 50 wt% aqueous solution of Lgol was reacted with a Pt/SiAlOx catalyst (15 mg catalyst per g of Lgol) at 150 °C and 1000 psig of hydrogen for 50 hours. Upon completion, the catalyst was removed via filtration, and water was eliminated using rotary evaporation followed by SpeedVac concentration. The resulting crystallized tetrol contained minor impurities such as tetrahydrofuran dimethanol (THFDM) and unreacted Lgol. To enhance the purity of the synthesized monomer, THF was added to the crystallized product. Owing to its limited solubility in THF, tetrol remained largely undissolved, while the more soluble impurities were extracted. The purified, undissolved tetrol was then filtered and dried. A total of 300 g of 1,2,5,6-hexanetetrol was obtained and subsequently sent to the polymerization group at the University of Oklahoma for further studies.

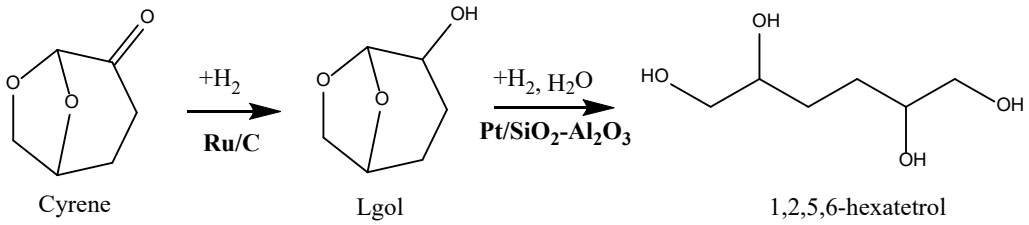

Figure 16. Dihydrolevoglucosenone (cyrene) and into tetrol.

Figure 17. Left: Crude tetrol dissolved in tetrahydrofuran (THF) for impurity removal and purification. Right: Purified and dried tetrol in solid form, ready for subsequent use in polyester synthesis.

M. 5.3 – Scaling up synthesis of one biomass-based monomer to produce 1 kg of monomer: Along with producing biodegradable polymers, it is important to utilize biobased monomers to reduce GHG emissions throughout the life cycle of the polymer. Pyran, Inc. is scaling the production of their biobased monomer, 1,5-pentanediol (1,5-PDO), which is a C5 diol with the potential to replace petroleum-based C4-C6 diols like 1,4-butanediol and 1,6-hexanediol. Pyran's 1,5-PDO is produced through a four-step process (as shown in **Figure 15**) from commercially available, biobased furfural or furfuryl alcohol. As a replacement for current petroleum-based diols, 1,5-PDO can be used in a large variety of polymers such as polyesters, polycarbonates, polyurethanes, and acrylates. At the start of the BOTTLE project, Pyran began scaling 1,5-PDO production in lab reactors reaching 10-100 g/day.

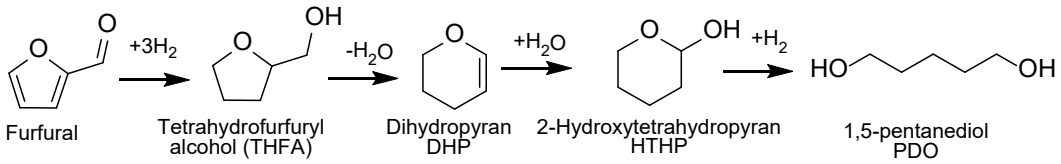

Figure 18. Pyran's proprietary pathway for 1,5-PDO synthesis from furfural

During the BOTTLE project, Pyran has been scaling our reactors in the lab as well as in a 2022-2023 toll manufacturing (contract manufacturing, funded separately through investors and an NSF grant). Demonstrating scale up is important for commercialization of our process and for further production of samples to validate applications of our 1,5-PDO. Pyran's lab scale reactors for each of the four reactor steps (**Figure 15**) have been scaled over 30x in lab, with most being scaled a further 100-1000x during toll manufacturing. Pyran's first step, furfural or furfuryl alcohol hydrogenation to tetrahydrofurfuryl alcohol, has been scaled from 10 g/day to over 350 g/day in our lab-scale continuous flow reactors. The second step, tetrahydrofurfuryl alcohol dehydration to 3,4-dihydropyran, has also been scaled up from 10 g/day up to 3 kg/day. This step was further demonstrated at over 600 kg/day during our 2022-2023 toll manufacturing. The

third step, hydration of 3,4-dihydropyran to 2-hydroxytetrahydropyran, has reached up to 3 kg/day in the lab and 750 kg/day during toll manufacturing. Our final step, 2-hydroxytetrahydropyran hydrogenation to 1,5-PDO, was scaled from 10 g/day up to 1 kg/day in the lab and up to 750 kg/day at toll manufacturing. Integration of our steps has also been key to scaling to a commercial plant. Our toll manufacturing campaign integrated from tetrahydrofurfuryl to distilled 1,5-PDO, while our lab has further integrated back to furfural/furfuryl alcohol. All our sourced furfural or other intermediates are biobased, demonstrating the handling of impurities throughout the process.

With the scaling of our lab reactors in addition to our 2022-2023 toll manufacturing, we have greatly exceeded our synthesis goals of 1 kg of biobased monomer. In our lab, we are able to produce >350 g/day in all reactors with most being >1 kg/day. Our toll manufacturing campaign demonstrated >600 kg/day production of distilled 1,5 PDO, producing more than 4 tons of on-spec 1,5 PDO while providing valuable reaction data for further scale up and derisking of our process. The toll production also provided enough material for larger scale testing of our 1,5-PDO in various polymer applications. Pyran's 1,5-PDO has been certified as 100% biobased by the United States Department of Agriculture (USDA) BioPreferred® Program. Pyran has also recently demonstrated that our biobased 1,5-PDO has up to 99% reduction in GHG emissions compared to petroleum-derived 1,6-hexanediol through an independent cradle-to-gate life cycle analysis (LCA).

Pyran is continuing to pilot larger reactors in our lab while working towards demonstration scale production. Currently, Pyran is working towards larger toll manufacturing campaigns in 2026 and 2027 targeting >100 tons and >1000 tons, respectively, with the commercial production goal of 20,000 tons by 2028.

Final Remark

Overall, this project successfully demonstrated the feasibility of synthesizing all proposed biomass-derived monomers, either at laboratory scale (using both batch and continuous flow reactors) or at pilot scale through collaboration with industrial partners. High-purity monomers were consistently obtained by conditioning the reaction feed and, when necessary, further purified using flash chromatography. All milestones outlined at the beginning of this chapter were achieved, and in several instances, the production targets were exceeded by achieving synthesis at scales beyond the originally proposed metrics.

Area 2 – Polymer synthesis and characterization

The synthesis of polyesters using biomass-derived monomers was addressed in Task 2.0 - *Synthesis and characterization of biomass-derived polyesters.* The report of this area is going to be presented as three different parts summarizing the work performed by (1) NREL on the use of PolyML for computational guidance on design of biobased polymers, (2) Colorado State University showing their progress on aliphatic-aromatic polyesters containing furan rings, and (3) Oklahoma University showing their findings on PPAT synthesis as a viable replacement for LLDPE and PBAT.

1. Work from NREL

Task 2.0: Synthesis and characterization of biomass-based polyesters

The goal of PolyML modeling was to develop a relationship between newly designed bio-based polymer's structure and physical properties by leveraging both computational predictions and experimentation. A secondary goal was to improve the accuracy of the model by adding experimental data to the training database.

M 2.1.1 - Prediction of 1,5-PDO-derived polyesters properties using PolyML: The PolyID™ machine learning tool was used to predict properties of 1,5-PDO containing polymers that were combined with 4 different diacids of interest and to set the initial benchmark of the performance of the prediction model for thermal properties. This work successfully completed the predicting properties of polyesters containing 1,5-PDO with various diacid comonomers in different molar ratios. A total of 66 different formulations were predicted. Predicted properties were compared with experimental properties and it was found the prediction accuracy was generally in line with performance of the model based on validation and test set loss for glass transition and melt temperature. The structural overlap between the predicted polymers and polymers in the training set was found to be acceptable.

M 2.2.1 - Prediction of THFDM, HAH, FDM- derived polyesters properties using PolyML: The PolyID machine learning tool was used by the NREL team to predict properties for 3144 formulations of hypothetical polymers using various combinations of 6 diols and 4 diacids at different molar percentages. Of these hypothetical polymers, 69 polyester formulations were predicted to meet the screening criteria of a $T_m \geq 100$ °C and $T_g \leq 0$ °C, shown in red in **Figure 19**. Results from PolyID were used to guide the formulations that were synthesized by the OU polymer team.

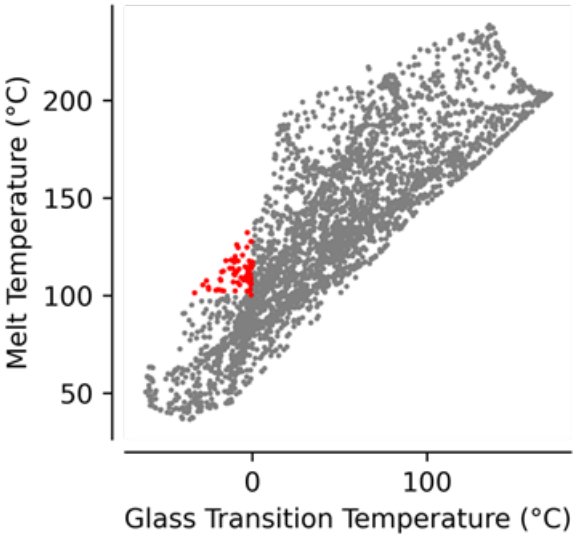

Figure 19. Scatter plot showing predicted melt temperature as function of predicted glass transition temperature.

M 2.3 - Improve the prediction accuracy of PolyML by incorporating experimental data into 1 new training set and retraining the network: Two rounds of experimental data from the synthesized polymers were incorporated into the base PolyID database to further improve this tool. Model predictions were improved for mechanical data (**Figure 20**) and in the accuracy of predictions (**Figure 21** and **Figure 22**).

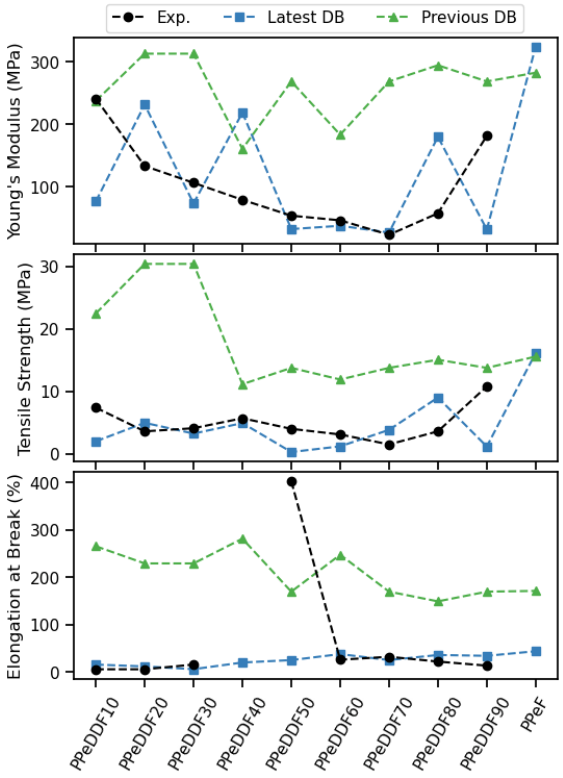

Figure 20. Young's Modulus, Tensile Strength, and Elongation at Break for the previous database (DB) model predictions, new database model predictions, and experimental data for select polymers.

A 10-fold cross-validation comparison mean absolute error (MAE) shows improvement of the accuracy of the predictions (**Figure 21**), but the greatest decrease in MAE is for polyesters (**Figure 22**).

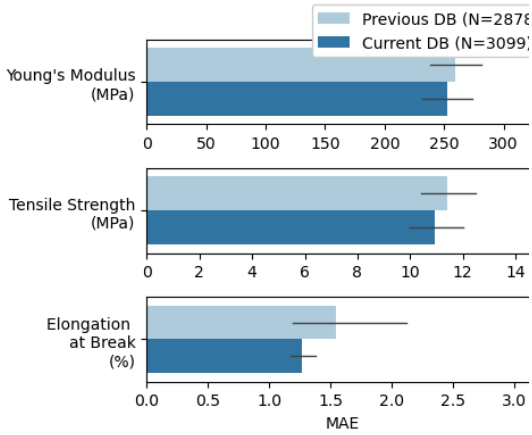

Figure 21. 10-fold Cross-Validation comparison Error (MAE)

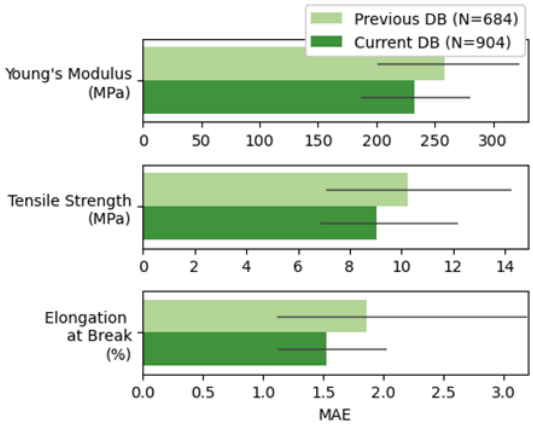

Figure 22. Polyesters show the greatest Mean Absolute decrease in MAE

The improved accuracy of the model would have been beneficial at the beginning of the project to avoid investigating certain unsuitable chemicals. Additionally, PolyID still struggles to capture the effects of crystallinity when varying copolymer monomer ratios. More experimental data will continue to improve the accuracy of the model predictions.

2. Work from Colorado State University

M. 2.1.4 – Tensile property measurements to meet target polyethylene films: In this milestone we aimed to elucidate structure-property relationships in bio-based aliphatic-aromatic polyesters by correlating chemical structure and molecular weight with thermal, mechanical, and barrier performance. Copolymers were synthesized from renewable monomers including 1,5-pentanediol (1,5-PDO), dimethyl tetrahydrofuran-2,5-dicarboxylate (dmTHFDCA), and 2,5-furandicarboxylic acid (FDCA). Additional monomers such as 1,12-dodecanediol (1,12-DD) were used to tailor flexibility, crystallinity, and extensional viscosity, critical for applications such as film formation.

The polyester synthesis was performed *via* a two-stage melt polycondensation as follows:

1. Stage I - Esterification: Conducted under inert atmosphere with excess diol and acid catalysis, targeting >90% conversion.
2. Stage II - Polycondensation: Titanium (IV) tert-butoxide catalyzed polymerization under reduced pressure and elevated temperature to achieve high molecular weight. Process variables (e.g., time, temperature, catalyst) were optimized for each monomer set. Molecular weight could be further enhanced via solid-state polymerization and modified by filler incorporation.

In parallel, a ring-opening polymerization (ROP) approach using chemically recycled cyclic oligomers was developed. Low-M_n prepolymers were depolymerized (Bu_2SnO-catalyzed) to cyclic macromers, which underwent entropically driven chain-growth ROP to regenerate high-M_n polymers. This closed-loop recycling strategy improves resource and energy efficiency by avoiding full-monomer depolymerization.

Together, these methods aim to deliver high-performance, recyclable bio-based polyesters with tunable processability-supporting circular polymer design for sustainable material applications.

Synthesis and Properties of Biobased Polyesters: PPeF, PDDF, and PDDTHF

- **Poly(pentamethylenefuranoate)(PPeF):**

PPeF cyclic oligomers were synthesized via two routes: (1) a two-step process involving chlorination of 2,5-furandicarboxylic acid (FDCA) to 2,5-furandicarbonyldichloride, followed by esterification with 1,5-pentanediol in the presence of triethylamine (Et_3N), affording pure cyclic dimer (PeFL) in 13% yield; and (2) a more efficient ring-closing depolymerization (RCDP) of the corresponding linear polyester (PPeFL), yielding 35.6%. Structural characterization was confirmed by $^1H/^{13}C$-NMR and single-crystal X-ray diffraction (SCXRD), which revealed stabilizing two different intramolecular C–H···O interactions.

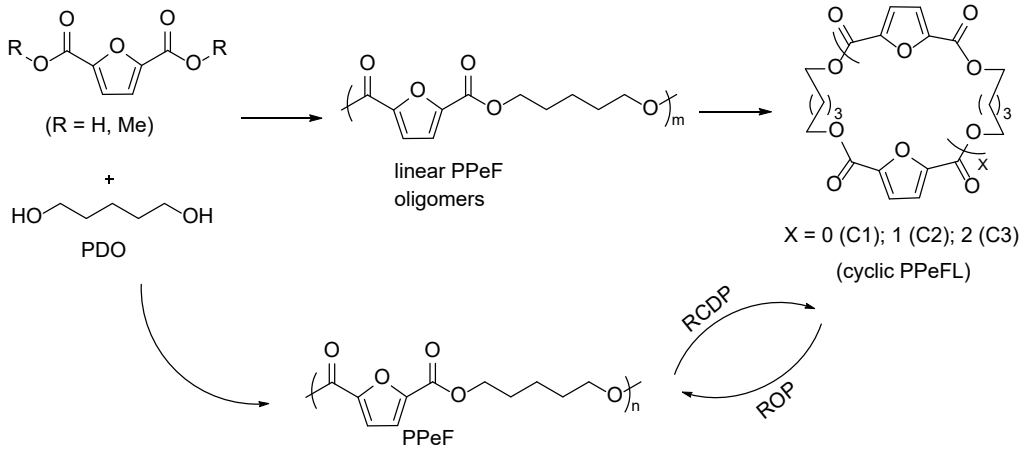

Figure 23. Synthesis and chemical circularity of PPeF through dual circular paths via ring-opening polymerization (ROP)/ring-closing depolymerization (RCDP) and step-growth polymerization (SGP) routes.

Thermal analysis of the cyclic oligomers (DSC) showed a melting point of 187 °C (mixture) and 207 °C (C1). Decomposition temperatures ($T_{d,5\%}$) were 272 °C (C1–C3) and 266 °C (C1), with glass transition temperatures (T_g) from 18.2 to 25.8 °C. Ring-opening polymerization (ROP) of the purified oligomers (5 g scale) yielded PPeF with Mn = 47.8

kDa, *Đ* = 1.2. The polymer exhibited semicrystalline behavior (T_g = 16.7 °C, T_m = 71.6 °C, ΔH_m = 11.9 J/g), high thermal stability ($T_{d,5\%}$=350 °C), and excellent mechanical properties: elongation at break (ε_B) of 620 ± 65%, tensile strength (σ_B) of 2.9 ± 1.1 MPa, and Young's modulus (E) of 4.0 ± 0.7 MPa. Oxygen transmission rates (OTR) were up to 8× lower than PET, attributed to dense supramolecular hydrogen bonding networks.

Closed-loop recycling was achieved by depolymerizing PPeF at 180 °C under vacuum with Bu_2SnO (3 mol%), yielding purified PPeFL oligomers (35.6%) that could be repolymerized.

- **Poly(dodecylene2,5-furanoate) (PDDF):**

Initial synthesis of cyclic dimer DDFL was achieved via Yamaguchi esterification or diacid chloride esterification, isolated in 19% yield. An improved RCDP route from PDDF yielded DDFL in 71%. SCXRD confirmed monoclinic packing with significant intermolecular H-bonding and van der Waals interactions.

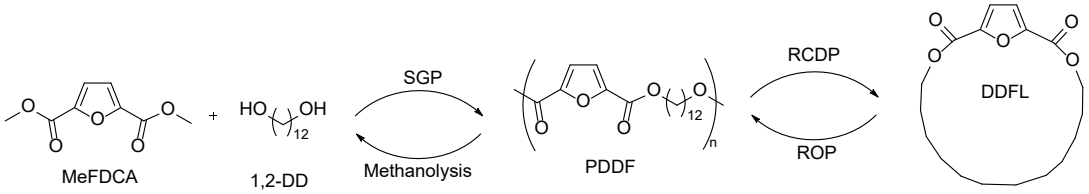

Figure 24. Synthesis and chemical circularity of PDDF through dual circular paths via ring-opening polymerization (ROP)/ring-closing depolymerization (RCDP) and step-growth polymerization (SGP)/ methanolysis routes.

ROP of DDFL using a lanthanum catalyst and benzyl alcohol initiator enabled precise control over M_n (18.3 kDa to 764 kDa; M_w up to 1.08 MDa, Đ = 1.41). PDDF exhibited semicrystalline character with excellent thermal stability ($T_{d,5\%}$ = 349 °C), T_g = –8.53 °C, T_m = 95.0 °C, and ΔH_m = 35.0 J/g. Mechanical testing showed PDDF-ROP had δ_b = 30 ± 3 MPa, ε_b= 280 ± 60%, and E = 165 ± 7 MPa; PDDF-SGP had E = 247 ± 7 MPa, δ_b = 21 ± 2 MPa, and ε_b = 220 ± 32%. Barrier performance studies revealed PDDF had significantly lower WVTR, CO_2, and O_2 permeability than PBAT and LLDPE.

Chemical recycling was achieved via two methods: (1) superbase-catalyzed depolymerization with tBu-P_4 at 120 °C, recovering 71% pure DDFL; and (2) methanolysis to dimethyl FDCA (MeFDCA) and 1,12-DD with 30 wt% Et_3N at 120 °C for 18 h, affording quantitative recovery. Both ROP and SGP-derived PDDF showed full recyclability under mild conditions.

Ring-Opening Polymerization (ROP)

Synthesis of 1,12-dodecane 2,5-furanoate lactone (DDFL)

Two methods were used to prepare DDFL, a Yamaguchi esterification route and an acid chloride route.

Method 1. Yamaguchi esterification

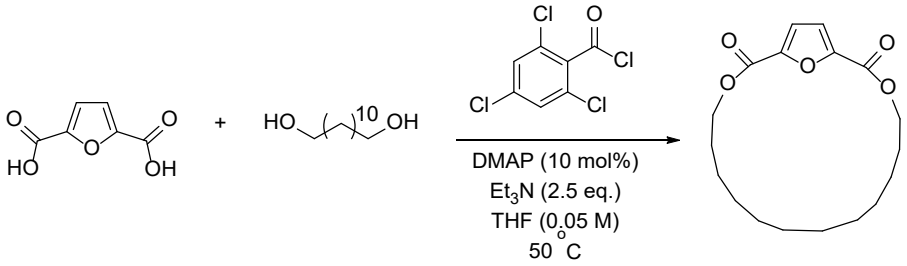

Figure 25. Synthesis of dodecane 2,5-furanoate lactone (DDFL) by Yamaguchi esterification

The Yamaguchi esterification (see **Figure 25**) began by dissolving FDCA (1.0 g, 6.41 mmol) in THF in a dry round-bottom flask under an inert atmosphere. To this solution, 2,4,6-trichlorobenzoyl chloride (the Yamaguchi reagent) (3.11 g, 12.8 mmol) was added, followed by the addition of 2.5 equiv. Et_3N to neutralize the hydrogen chloride generated during the reaction. The mixture was stirred at a slightly elevated temperature (around 40–50 °C) to form the mixed anhydride. Once the formation of the mixed anhydride was confirmed using thin-layer chromatography (TLC), the alcohol DD was added along with a catalytic amount of 4-dimethylaminopyridine (DMAP, 10 mol%). The reaction mixture was then stirred at slightly elevated temperatures (50–60 °C) for 6 h to produce the desired product. After removal of the solvent under reduced pressure, the residue was washed with brine solution and extracted with dichloromethane. The extracted organic layer was dried over anhydrous Na_2SO_4, and the solvent was removed. The resulting mixture was purified by column chromatography (ethyl acetate, 15%), yielding 19% of DDFL

Method 2. Acid Chloride Route

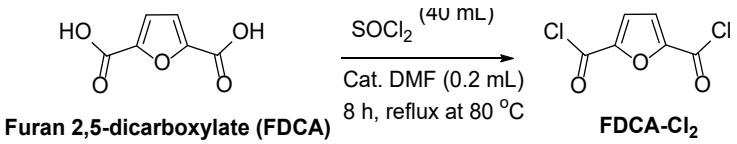

Figure 26. Synthesis of FDCA-Cl_2

FDCA-Cl_2 precursor (see Scheme S2) was prepared by reacting FDCA (20 g, 0.128 mol) with $SOCl_2$ (40 mL, 0.336 mol) and catalytic amount of DMF (0.2 mL, 0.0026 mol) under reflux at 80 °C for 8 h.

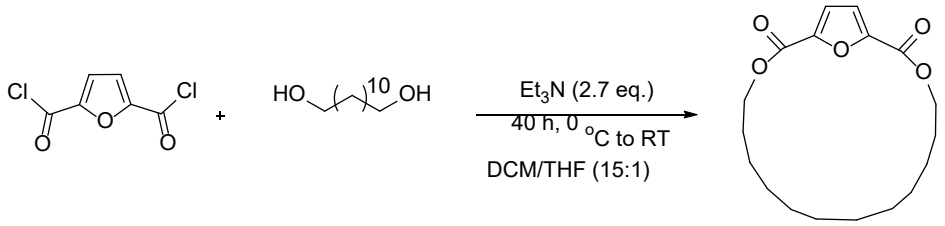

Figure 27. Synthesis of dodecane 2,5-furanoate lactone (DDFL)

To prepare the DDFL from the acid chloride as shown in **Figure 27**, a round-bottom flask was charged with 150 mL of dichloromethane and cooled to 0 °C. Under stirring, 64.8 mmol (6.50 g) of Et_3N were added. Then, 27.0 mmol (5.49 g) of DD in 10 mL of THF were introduced into the reaction solution. Subsequently, 25.9 mmol (5.00 g) of FDCA-Cl_2 in 100 mL of DCM were added dropwise to the reaction mixture using a pressure-equalizing funnel at 0 °C. After stirring for 48 h at room temperature, the solvent was removed under reduced pressure. The mixture was washed with brine solution and extracted with dichloromethane. The organic layer was dried over anhydrous Na_2SO_4 and evaporated. The reaction mixture was purified by column chromatography (ethyl acetate, 15%), yielding 19% of DDFL.

The structure and purity for the DDFLs was confirmed by ^1H and ^{13}C NMR spectra (figure not shown here). The monomeric nature and molecular structure of DDFL was further confirmed by single-crystal X-ray diffraction analysis (**Figure 28**). DDFL crystallizes in a monoclinic system with unit cell parameters a = 9.4333 Å, b = 9.4417 Å, c = 11.1036 Å, and α = 85.420 ° β = 66.219°, γ = 74.516°. Notably, significant intermolecular interactions, including H-bonding and van der Waals forces, were observed, contributing to the stability of the crystal structure. The expanded packing structure reveals close intermolecular interactions between the C–H hydrogen on the furan ring and the carbonyl oxygen of the ester, with a O–H distance of 2.433 Å and H–O–C angle of 143.38° (**Figure 28**). The pK_a of a phenyl hydrogen is 43-45, while the pK_a of a 2/5 (*ortho*)-hydrogen in furan is 35.6 for significantly higher acidity (i.e., a better H-bonding donor), owing to the inductive electron-withdrawing effect of the oxygen on the furan ring, which stabilizes the resultant anion. Although the hydrogen atoms in DDFL are 3/4 (*meta*) rather than 2/5 (*ortho*), the presence of two electron-withdrawing ester groups on both sides of the furan ring is expected to further assist in stabilizing the resultant anion. A pK_a of 27.5 was calculated for a 3-H in a related furan heterocycle.[24] Overall, these observations indicate significantly greater polarization of the C–H bond in furan rings over the equivalent in phenyl rings, suggesting that weak H-bonding could occur,[24] verified experimentally here.

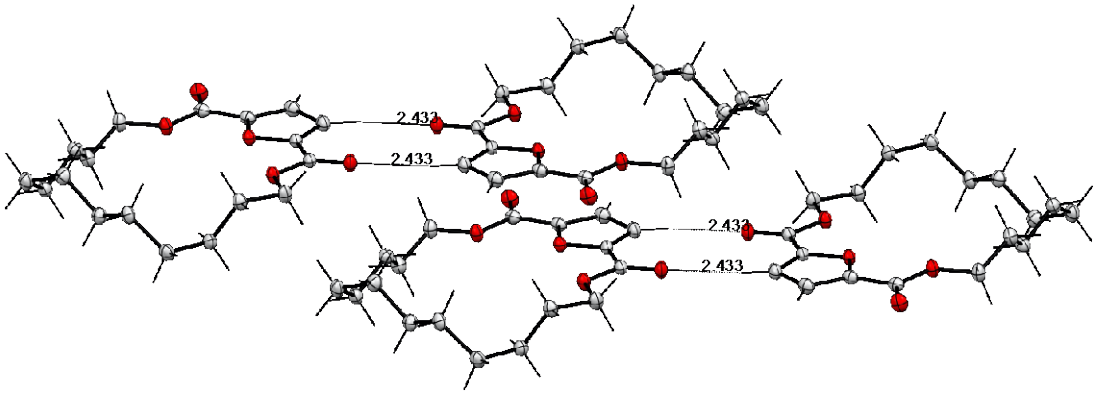

Figure 28. The molecular structure of the cyclic monomer DDFL obtained by single-crystal X-ray diffraction analysis and its expanded packing structure (*a* + 2, *b* + 1.5, *c* + 0). Carbon atoms in gray, oxygen atoms in red, and hydrogen atoms in black. The crystal data was deposited at the Cambridge Crystallographic Database Centre as CCDC-2359161.

Although these H-bonding interactions observed in the cyclic DDFL monomer could vary in the corresponding linear polymer upon the ROP reaction, all structural motifs are identical, except for cyclic vs. linear forms, which should render such interactions intact in the polymer. Hence, it can be expected the H-bonding network would also exist in the polymer structure, which is a commonly practiced extrapolation made from monomer to polymer in the context of hydrogen bonds (as obtaining single-crystal structures of synthetic polymers is not possible). Overall, the detailed analysis of the crystal structure of the monomer DDFL provided insights into the chain packing structure of the corresponding polymer PDDF and thus its suitability for packaging applications in the context of barrier performance, mechanical robustness, and thermal stability, all of which would be enhanced by the presence of a H-bonding network structure present in the polymer material.

ROP of dodecane 2,5-furanoate lactone (DDFL)

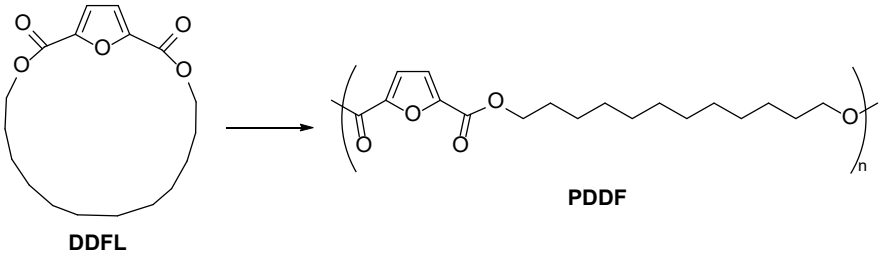

Figure 29. Synthesis of poly(dodecane furanoate) by ROP

Polymerization was conducted in a small, oven-dried Schenk tube. Inside a glovebox, the reactor was charged with specified amounts of monomer, catalyst, and initiator as detailed in the polymerization tables. The mixture was stirred in a solvent at ambient

temperature (~25 °C) as well as under different temperature conditions, both with and without solvent (neat conditions). After the reaction, the mixture was quenched with acidic CH_2Cl_2 and precipitated in methanol. The product was analyzed by ^{1}H-NMR to determine the percent monomer conversion. The ROP of DDFL was performed in solution or in melt, and selected results were summarized in **Table 2**. Several molecular catalysts were screened, including a commercial lanthanum [La]-based catalyst, La[N(SiMe$_3$)$_2$]$_3$,[24] and a commercial superbase catalyst, ^{t}Bu-P$_4$ (1-*tert*-Butyl-4,4,4-tris(dimethylamino)-2,2-bis[tris(dimethylamino)-phosphoranylidenamino]2λ^5,4λ^5-catenadi(phosphazene)).[24] At first, ^{t}Bu-P$_4$ was shown to be an effective catalyst for the ROP of DDFL (**Table 2**, runs 1-3); however, attempts to produce high-molecular-weight PDDF with ^{t}Bu-P$_4$ by employing a [DDFL]/[^{t}Bu-P$_4$] ratio of 300:1 resulted in a low monomer conversion of only 19% (**Table 2**, run 4). On the other hand, the [La] complex, when combined with an initiating alcohol, $PhCH_2OH$ (BnOH), was shown to be highly effective for this ROP, producing PDDF with controlled molecular weight from low number-average molecular weight (M_n) = 18.3 kDa to high M_n = 764 kDa or weight-average molecular weight (M_w) = 1.0 MDa (**Table 2**, runs 5-12). Several organic and metal-based catalysts, including 1,8-diazabicyclo[5.4.0]undec-7-ene and tin(II) 2-ethylhexanoate (Sn(Oct)$_2$), were also screened, but they were much less effective than the [La] catalyst. Using La(NTMS)$_3$ as the catalyst, the monomer conversion reached 100%, and the isolated yield of PDDF was 95.0%.

Table 2. Selected results of the ROP of DDFL

Run	catalyst	[M]/ [Cat.]/[I]	Solvent	Temp. (°C)	Time (h)	Conv. (%) [b]	M_n (kDa) [c]	$Đ$ [c]
1	^{t}Bu-P$_4$	100:1.1	neat	110	4.5	74	61.7	3.05
2	^{t}Bu-P$_4$	100:1.1	THF	25	3	69	15.1	2.09
3	^{t}Bu-P$_4$	100:1.1	THF	60	3	61	10.9	2.40
4	^{t}Bu-P$_4$	300:1.1	THF	60	3	19	/	/
5	[La]	100:1.3	neat	110	4.5	100	31.2	1.36
6	[La]	100:1.3	DCM	25	0.5	100	25.6	1.47
7	[La]	100:1.3	DCM	25	3	100	25.0	2.30
8	[La]	100:1.3	DCM	60	3	100	18.3	2.43
9	[La]	1000:1.3	DCM	25	3	100	134	2.19
10	[La]	3300:1.3	DCM	25	1.5	97	227	1.60
11	[La]	6700:1.3	DCM	25	1.5	39	520	1.60
12	[La]	20000:1.3	neat	125	14	38	764	1.31

(a) Conditions: Monomer (M) (0.5 mmol); catalyst (cat.) = ^{t}Bu-P$_4$, or [La] = La[N(SiMe$_3$)$_2$]$_3$; initiator (I) = BnOH; solvent (0.2 mL), THF = tetrahydrofuran, DCM = dichloromethane, neat = no solvent. (b) Determined by ^{1}H NMR in $CDCl_3$. (c) Number-average molecular weight (M_n) and dispersity index ($Đ$ = M_w/M_n) determined via size exclusion chromatography (SEC) at 40 ℃ in $CHCl_3$ coupled with a Wyatt DAWN HELEOS II multi (18)-angle light scattering detector and a Wyatt Optilab TrEX dRI detector for absolute molecular weight.

- **Poly(dodecylenetetrahydro-2,5-furanoate)(PDDTHF):**

To address FDCA color and enhance flexibility (lower T_g), hydrogenated dimethyl FDCA (dmTHFDCA) was synthesized via $Pd(OH)_2/C$-catalyzed hydrogenation of dmFDCA in MeOH under 4 MPa H_2 at 50 °C, yielding colorless dmTHFDCA (99.9% yield, 99% purity).

Step-growth polymerization of dmTHFDCA with 1,12-dodecanediol produced PDDTHF with Mw = 46.2 kDa, Đ = 1.40. The polymer is semicrystalline with excellent thermal stability (Td,5% = 344 °C) and target-matching thermal transitions: Tg = –19.5 °C, Tm = 91.2 °C (ΔHm = 40.2 J/g), and Tc = 44.5 °C (ΔHc = 47.1 J/g), supporting its potential as a sustainable polyethylene alternative.

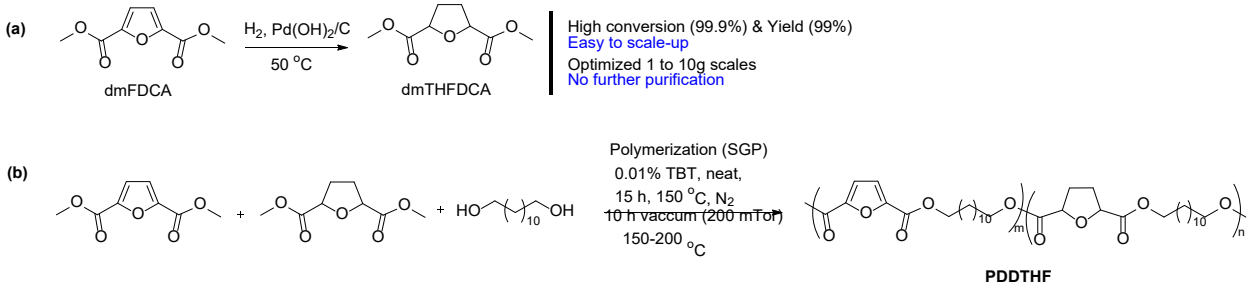

Figure 30. (a) Synthesis of dimethyl-2,5-tetrahydrofurandicarboxylate (dmTHFDCA) by catalytic hydrogenation (b) PDDTHF via the step-growth polymerization (SGP)

3. Work from University of Oklahoma

The University of Oklahoma has actively contributed to the development of PPeAT as a bio-derived surrogate for PBAT. Substantial efforts have been dedicated to the synthesis and characterization of biobased copolyesters derived from pentanediol, including poly(pentylene dodecanoate-co-furandicarboxylate) PPeDF and poly(pentylene adipate-co-terephthalate) PPeAT. Complete experimental details and characterization data for these materials are available in Singh et al, Polym Eng Sci. 2024; 64(10): 4935-4946 and Aboukeila et al. Polym Eng Sci. 2024; 64(10): 4746-4759.

The following sections of this report describe recent advancements in the repolymerization of chemically depolymerized PPeAT and scale-up of its production, which have not been published to date.

Furthermore, the University of Oklahoma has made additional progress in the development of PDDF. As this work also remains unpublished, full experimental procedures and results are detailed in subsequent sections. The University was responsible for delivering milestones 2.1.4 through 2.1.6 and 2.2.2 through 2.2.7. We confirm that milestones 2.1.4 to 2.1.6 and 2.2.4 to 2.2.7 have been fully met for both PPeAT and PDDF.

M. 2.1.4 – Tensile property measurements to meet target of polyethylene films
M. 2.1.5 – Viscosity measurements similar to film blowing grade LLDPE
M. 2.1.6 – Melt temperature equal to film blowing grade LLDPE
M. 2.2.2 – Synthesis of THFDM/FDM + TPA + AA and THFDM/FDM + FDCA
M. 2.2.4 - Tensile property measurements to meet target of polyethylene films
M. 2.2.5 - Viscosity measurements similar to film blowing grade LLDPE
M. 2.2.6 - Melt temperature equal to film blowing grade LLDPE
M. 2.2.7 - Oxygen transmission rate equal to or better than film blowing grade LLDPE

Unpublished details on Repolymerization of PPeAT

Chemical depolymerization/repolymerization of polyesters: Here we present the repolymerization occurred for chemically decomposed PPeAT and PDDF polyesters, and the comparison of virgin and repolymerized products.

PPeAT

Materials and Methods: A 300 mL stainless steel mechanically stirred pressure reactor (Parker Autoclave) was used for the reaction, operated under a nitrogen atmosphere at 300 PSI. The polymer was loaded at 20 wt% in methanol (MeOH), and 5 wt% of dimethylethanolamine (DMEA) was added relative to the polymer repeat unit. The reactor, equipped with a heating jacket and thermocouple, was heated to 190 °C and stirred at 600 rpm for 3 hours. After completion, the product was recovered by vacuum filtration. The reactor used is shown in Figure 1. The products of methanolysis were dimethyl adipate (DMA), dimethyl terephthalate (DMT) and PDO as shown in **Figure 31**.

RP-PPeAT synthesis followed the exact same procedure as the virgin PPeAT, as presented in our previous publications. The only difference was that instead of using AA and TPA as monomers, we used the products of methanolysis, DMA and DMT, as our linear and aromatic diacids. Temperatures, ratios and reaction times were kept the same.

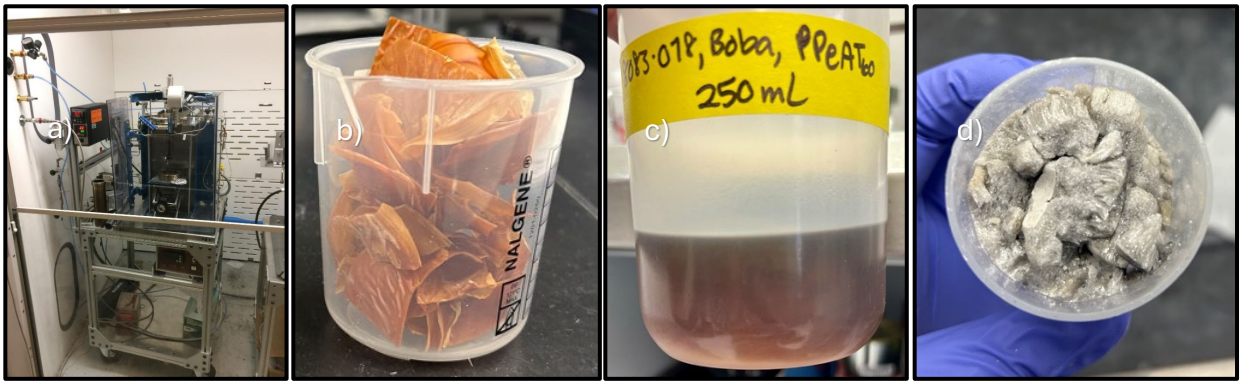

Figure 31. a) Parker-Autoclave 300 mL stirred tank reactor used for the methanolysis process, b) Original PPeAT, c) DMA, PDO and DMT in methanol and d) Solid DMT

Molecular weight and Composition Analysis

Number average molecular weight (M_n), weight average molecular weight (M_w) and dispersity (Đ), are reported in **Table 3**. The variation in molecular weight is due to the difficulty of controlling molecular weight in a SGP at high conversions in a batch system. Also, ^{1}H NMR spectra, shown in **Figure 33** with the chemical structure and triad assignments shown in **Figure 32**. Both PPeAT and RP-PPeAT showed identical peaks, and no difference was found between both polyesters. Of particular note is that no evidence appears of an impurity.

Table 3. Gel permeation chromatography results for PPeAT and RP-PPeAT.

Sample	M_n	M_w	Đ
	g/mol	g/mol	-
PPeAT	90,270	291,110	3.2
RP-PPeAT	78,890	111,500	1.4

Figure 32. Chemical structure of PPeAT and triad assignments.

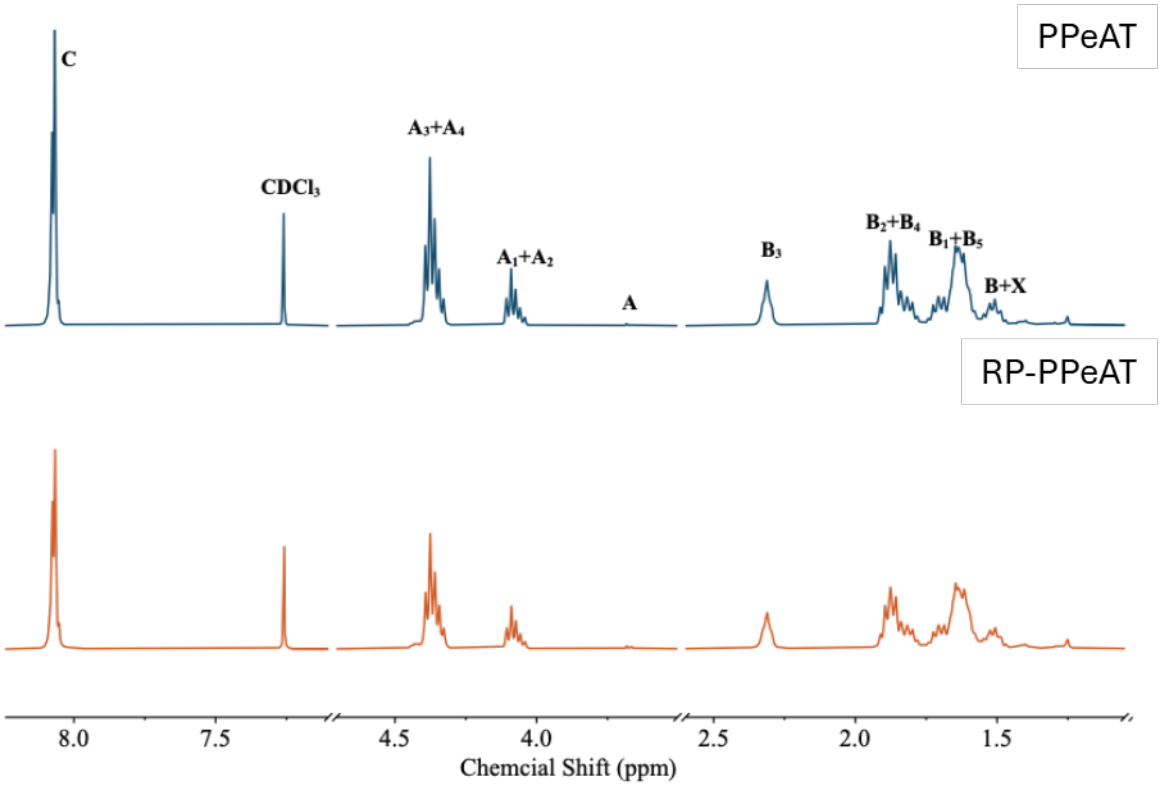

Figure 33. ^{1}H NMR Spectra of PPeAT and RP-PPeAT.

PPeAT and RP-PPeAT were analyzed for carbon, hydrogen, nitrogen and oxygen, with the CHN analysis results presented in **Table 4**. Additionally, the actual monomer compositions of the synthesized polymer were calculated based on the CHN analysis and is also reported in **Table 4**. The oxygen content was calculated as the difference between 100% and the total measured carbon, hydrogen, and nitrogen content with nitrogen composition equal to zero. The actual monomer composition ratios of PPeAT and RP-PPeAT were almost identical, showing no deviations from the measured stoichiometric ratio.

Table 4. CHN analysis for PPeAT and RP-PPeAT.

Sample	*Carbon*	*Hydrogen*	*Nitrogen*	*Oxygen*	*Adipic acid*	*Terephthalic acid*
	%	%	%	%	%	%
PPeAT	66.0 ± 0.4	7.1 ± 0.3	0	26.9 ± 0.6	41 ± 8	59 ± 8
RP-PPeAT	65.4 ± 0.1	7.0 ± 0.2	0	27.7 ± 0.3	40 ± 6	60 ± 6

Thermal Properties

DSC curves for PPeAT and RP-PPeAT are shown in **Figure 34**. The first heating cycle of both PPeAT and RP-PPeAT showed a clear endothermic peak due to the melting temperature of the polymer. However, for the cooling cycle an exothermic peak was not observed due to slow crystallization rate of PDO-based polyesters which was reported

previously [59]. The absence of an endothermic melting peak in the second heating cycle for PPeAT confirmed the assumption of a slow crystallization rate. However, for RP-PPeAT, a small cold crystallization peak followed by a small melting peak can be observed in the second heating cycle. The relevant parameters are summarized in **Table 5**. For RP-PPeAT, T_{cc} and $T_{m,2}$ were found be 62.2°C and 98.3°C, respectively which are consistent with crystallization temperature and melting temperature of nucleated PPeAT measured by our group. Other than these differences that are clearly due to crystallization kinetics, RP-PPeAT has a lower T_g and lower T_{m1}; the source of these small differences is not understood.

$T_{d,5\%}$, $T_{d,max}$ and $R_{600°C}$ from TGA are shown in **Figure 34**. **Figure 34**. shows PPeAT and PPeAT had identical thermal stability with similar $T_{d,5\%}$ and $T_{d,max}$. Both PPeAT and RP-PPeAT left a residue of 6% at 600°C due to the pyrolysis of the aromatic fraction leading to the formation of stable char.

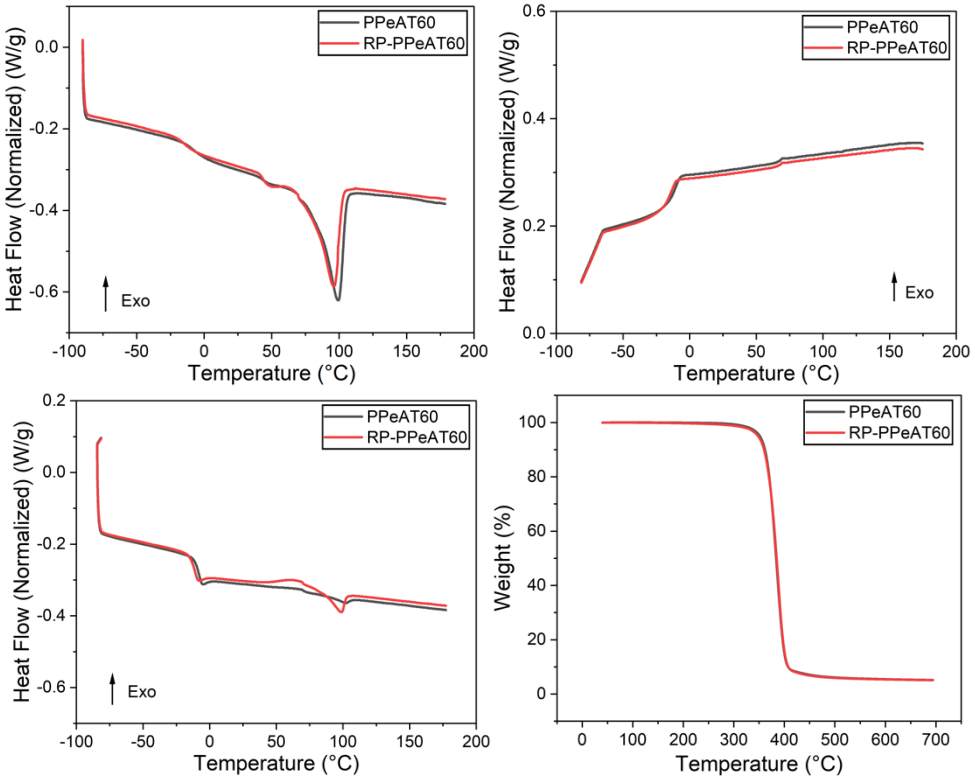

Figure 34. Differential scanning calorimetry curves of PPeAT and RP-PPeAT, (a) the first heating scan, (b) cooling scan and (c) second heating scan. d) Thermogravimetric analysis curves of PPeAT and RP-PPeAT

Table 5. Thermal properties from DSC, TGA and DMA for PPeAT and RP-PPeAT.

Sample	First Heating		Cooling	Second Heating				DMA	TGA		
	$T_{m,1}$ °C	$\Delta H_{m,1}$ J/g	T_c °C	T_g °C	T_{cc} °C	$T_{m,2}$ °C	$\Delta H_{m,2}$ J/g	T_g °C	$T_{d,5\%}$ °C	$T_{d,max}$ °C	$R_{600°C}$ %
PPeAT	99.2	27.4	-	-8.7	-	-	-	-5.9	351	364	5.8
RP-PPeAT	95.8	28.1	-	11.6	62.2	98.3	4.8	-8.9	348	366	5.7

Additionally, isothermal crystallization kinetics of PPeAT and RP-PPeAT were investigated at 40°C using DSC and the results are presented in **Figure 35**. As expected, for RP-PPeAT, the rate of crystallization was faster than the rate of crystallization of PPeAT. That improvement in crystallization rate could be attributed to the presence of an unknown impurity, which was not detected by CHN, NMR or TGA, that acted as a nucleating agent. The Avrami model was utilized to gain deeper insights into the isothermal crystallization process such as nucleation and crystal growth. The crystallization half-time ($t_{1/2}$) and the Avrami model parameters are presented in **Table 6**. The Avrami exponent for PPeAT and RP-PPeAT were 2.65 and 3. Therefore, the growth mechanism for PPeAT is a combination of 1D and 2D growth while for RP-PPeAT, the growth rate is more 2D growth [52]. Furthermore, the $t_{1/2}$ of RP-PPeAT was found to be half that of PPeAT. This reduction was due to the doubling of the crystallization rate constant in RP-PPeAT compared to PPeAT, indicating a significantly enhanced crystallization process. This significant enhancement in the crystallization kinetics was the primary factor responsible for the observed cold crystallization and subsequently the small melting peak from the second heating cycle for RP-PPeAT.

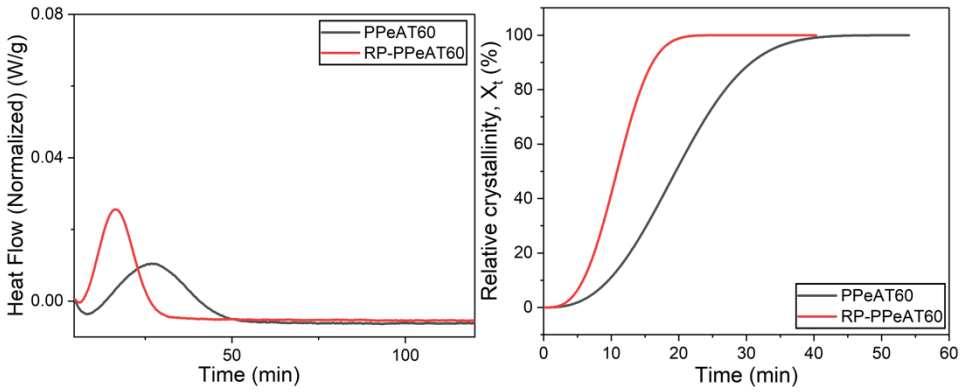

Figure 35 a) Isothermal crystallization for PPeAT and RP-PPeAT b) Avrami model results for PPeAT and RP-PPeAT.

Table 6. Avrami model parameters and half-time crystallization for PPeAT and RP-PPeAT.

Sample	k	n	$t_{1/2}$
	min^{-1}	-	min
PPeAT	$2.64*10^{-4}$	2.65	19.6
RP-PPeAT	$5.04*10^{-4}$	3.03	10.9

Crystallinity

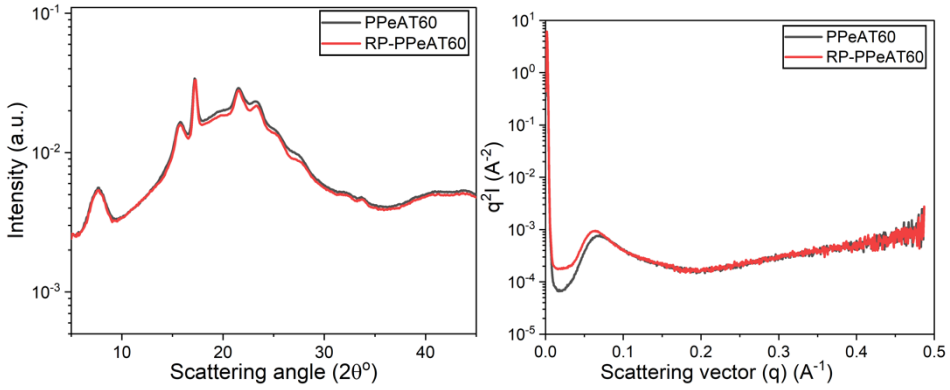

Figure 36. a) WAXS *results for PPeAT and RP-PPeAT. b) SAXS results for PPeAT and RP-PPeAT*

Figure 36 illustrates WAXS spectra of PPeAT and RP-PPeAT, while **Table 7** provides the percent crystallinity values for these polymers. For both PPeAT and RP-PPeAT, scattering angles (2θ°) observed are 7.6°, 15.7°, 17.2°, 21.6°, 23.2° and 25.2° corresponding to the planes (011), (010), (102), (100), and (111) respectively for the latter five consistent with the literature.[59] PPeAT and RP-PPeAT showed identical WAXS spectra and hence an identical percent crystallinity. Therefore, the depolymerization and repolymerization processes didn't affect the percent crystallinity.

Figure 36 and **Table 7** show SAXS results for PPeAT and RP-PPeAT. The values of lamellar thickness are reported in **Table 7** are derived from the multiplication of fractional crystallinity with d-spacing values. The d-spacing of RP-PPeAT was found to be larger than that of PPeAT, also with a slightly greater lamellar thickness for RP-PPeAT. However, the difference in lamellar thickness was minimal.

Table 7. Crystallinity properties for PPeAT and RP-PPeAT.

Sample	**WAXS**	**SAXS**		
	χ_c	q_{max}	d-spacing	Lamellar Thickness
	%	$Å^{-1}$	Å	Å
PPeAT	13.92	0.070	90.1	12.5
RP-PPeAT	13.88	0.064	97.9	13.6

Mechanical Properties

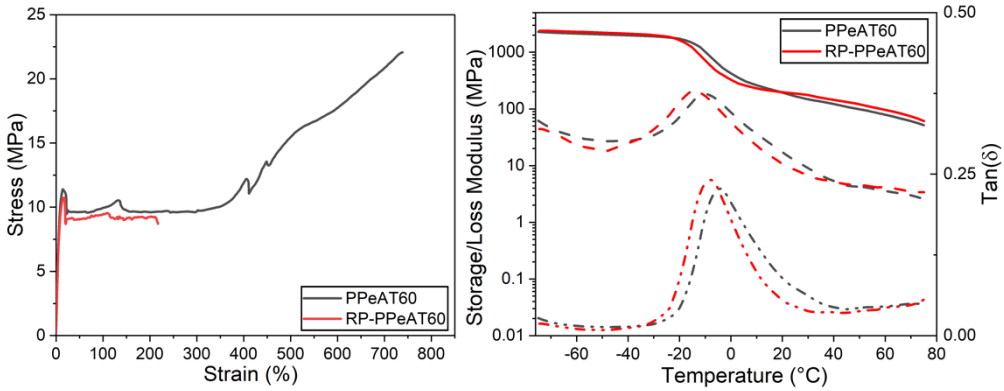

Figure 37. a) Stress-strain curves for PPeAT and RP-PPeAT. b) DMA results for PPeAT and RP-PPeAT. Storage modulus is represented as (- solid lines), loss modulus is represented as (- - dashed lines) and damping factor is represented as (-··- dashed lines).

Stress-strain curves for PPeAT and RP-PPeAT are shown in **Figure 37** with the relevant parameters reported in **Table 8**. Both polymers exhibit ductile behavior with a high elongation at break. The E, δ_y, ε_y, δ_b and ε_b values for PPeAT are in agreement with literature results [59]. Although RP-PPeAT had a similar E, δ_y and ε_y to PPeAT, δ_b and ε_b for RP-PPeAT were significantly lower than PPeAT. Using a polymeric nucleating agent causes no change in the mechanical properties. Hence, we believe that the impurity is a particulate of some sort. Given the inability to find any evidence in CHN, NMR or TGA of such a particle, the concentration must be less than 1% and likely less than 0.1%. With other polyesters, gives a factor of ~2 decrease in $t_{1/2}$. mentioned in the crystallization kinetics section could have acted as a stress concentrators, promoting premature failure at lower strain values due to poor adhesion between the said particle and the polymer [72]. Additionally, Viora et al. observed a reduction in elongation at break for repolymerized polyethylene terephthalate compared to virgin polyethylene terephthalate, while its Young's modulus remained similar [73].

Rheological Properties

DMA results for PPeAT and RP-PPeAT are shown in **Figure 38**. E' for PPeAT and RP-PPeAT was found to be similar. The E'' and tan δ peaks for RP-PPeAT were shifted to a lower temperature compared to PPeAT indicating a lower T_g. T_g was determined by the temperature that corresponded to the peak in tan δ curve for both PPeAT and RP-PPeAT and are reported in Table 5. T_gs for DSC and DMA are not the same, but the difference in T_gs between PPeAT and RP-PPeAT is the same with experimental error for the two measurements.

Table 8. Tensile properties for PPeAT and RP-PPeAT.

Sample	E	δ_y	ε_y	δ_b	ε_b
	MPa	MPa	%	MPa	%
PPeAT	154 ± 6.2	11 ± 0.3	14.9 ± 1.3	20.7 ± 1.8	715 ± 43
RP-PPeAT	150 ± 5.7	11 ± 0.2	17.8 ± 1.6	8.3 ± 1.4	192 ± 93

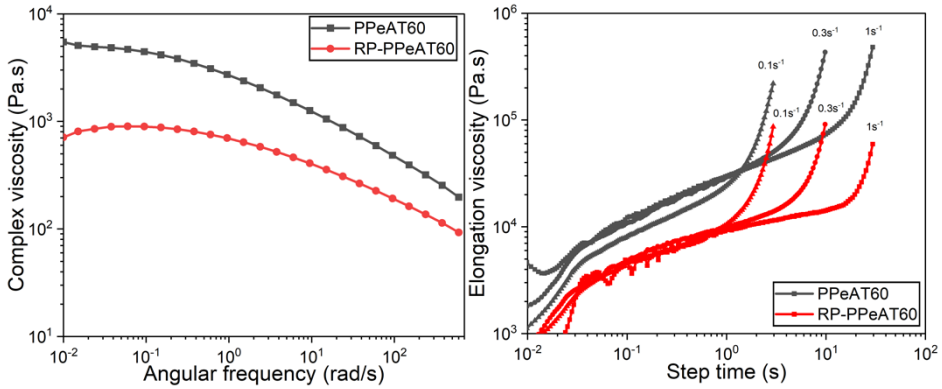

Figure 38. a) Complex viscosity curve of PPeAT and RP-PPeAT. b) Elongation viscosity curves for PPeAT and RP-PPeAT

Complex shear viscosities vs angular frequency at 190°C for PPeAT and RP-PPeAT are shown in **Figure 38**. Shear-thinning behavior at high frequency and a Newtonian plateau at low frequencies can be observed for both polyesters. The higher viscosity of PPeAT vs. RP-PPeAT was expected due to the much higher weight average molecular weight of the former.

The five-parameter Carreau-Yasuda was used to model complex viscosities. Fitted data show good agreement with the experimental results. RP-PPeAT had a higher transition and a lower characteristic relaxation time than PPeAT reflective a narrower transition from shear thinning region to a Newtonian region and a wider Newtonian plateau region, respectively. Additionally, PPeAT had a higher zero-shear viscosity than RP-PPeAT due to the higher molecular weight of the former.

Extensional viscosities vs. time for PPeAT and RP-PPeAT at 130°C at three different elongation rates (0.1 s^{-1}, 0.3 s^{-1} and 1 s^{-1}) were plotted in **Figure 38**. A lower temperature was chosen compared to the temperature used for shear viscosity measurements, as high temperatures lead to sample sagging. A Hencky strain of 2.5 at an elongational rate of 0.3 s^{-1} were found to be representative values for film blowing [14] and these values are found in Table 7. The higher elongation viscosity of PPeAT compared to RP-PPeAT was due to the much higher weight average molecular weight of PPeAT. High elongational viscosity serves as an indicator of elevated melt strength, consequently contributing to a more stable bubble during the film blowing process. Strain hardening of PPeAT was previously reported in the literature [59].

Table 9. Rheological properties for PPeAT and RP-PPeAT.

Sample	Shear viscosity				Elongational viscosity at Hencky strain of 2.5 and 0.3 s^{-1}
	η_o	n	a	λ	η_E
	Pa.s	-	-	s	Pa.s
PPeAT	5437.9	0.6	0.9	6.3	234,366
RP-PPeAT	845.9	0.7	2.0	1.6	48,593

Barrier Properties

P_{O_2}, P_{CO_2} and WVTR results for PPeAT shown in Figure 9 were consistent with results reported in the literature. However, RP-PPeAT had a higher P_{O_2}, P_{CO_2} and WVTR compared to PPeAT. A possible explanation is that poor interfacial adhesion between the particle and the polymer could have introduced a low-resistance path for gas diffusion. An increase in permeability with the addition of particles has been reported previously in the literature [74].

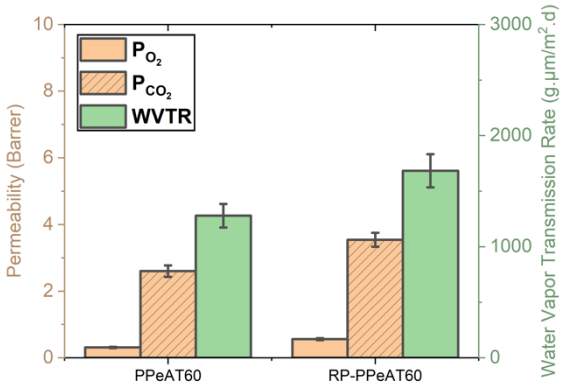

Figure 39. H2O, O2 & CO2 permeation of PPeAT and RP-PPeAT.

PDDF

Materials and Methods

ROP produces condensation-type polyesters through a chain-growth mechanism, consisting of initiation, propagation, and termination steps. Without termination, polymers can reach an equilibrium with monomers, known as reversible polymerization. For propagation, both enthalpy (ΔH_p) and entropy (ΔS_p) of polymerization are typically negative, meaning polymerization occurs at low temperatures, below its ceiling temperature (T_{ce}). Conversely, depolymerization occurs at high temperatures, above T_{ce}. For pure monomers, $T_{ce} = \Delta H_p/\Delta S_p$, but in solution, solvents increase monomer's entropy,

lowering T_c or raising the floor temperature (T_{fl}), as described by the Dainton and Ivin Equation (5)[75]:

$$T_{ce}\,(or)T_{fl} = \frac{\Delta H^{\circ}_{P}}{\Delta S^{\circ}_{P} + R\ln[M]_0} \quad (5)$$

In ROP, small- to medium-sized strained rings result in negative ΔH_p and ΔS_p, where polymerization is driven by enthalpy. Depolymerization can be facilitated by high dilution or reactive distillation; the former shifts the equilibrium position towards the monomer state, favored by their higher translational entropy, whilst the latter ensures equilibrium is never established via constant monomer removal. For macro-lactones (ring size >12 atoms) with non- or negligible ring strain, polymerization is driven by entropy (i.e., the gain in conformational entropy upon ring-opening can effectively offset the loss in translational entropy due to polymerization) and thus regulated by T_{fl}: high temperatures favor polymer formation and low temperatures favor monomer formation (the case for DDFL, a 19-membered lactone).

Results of Depolymerization

Guided by the above thermodynamic principles, depolymerization of a ROP-derived PDDF (M_n = 50.8 kDa, $Đ$ = 1.84) film-grade sample was first performed at room temperature (RT), considering the floor temperature phenomenon of this macro-lactone monomer. Although the polymer indeed depolymerized to the cyclic monomer at RT in the presence of strong bases such as ^{t}BuOK and ^{t}Bu-P$_4$, the conversion was low when the equilibrium between the polymer and monomer was reached. Lewis acid catalysts such as phosphomolybdic acid and $ZnCl_2$ were ineffective, recovering products that are mostly oligomers mixed with the olefinic side products caused by decomposition. To drive the reaction forward, a sublimation apparatus was employed, achieving ~40% yield of the desired cyclic monomer (DDFL) with ^{t}BuOK at the catalyst at 120 °C. Notably, polymer decomposition was observed at both RT and higher temperatures with ^{t}BuOK. Switching to organic superbase ^{t}Bu-P$_4$ as the catalyst, depolymerization at 120 °C afforded 71% of the pure DDFL (Figure 8). Additionally, the recovered monomer DDFL can be fully repolymerized to PDDF, demonstrating the closed-loop circularity of this biobased material (**Figure 40**). Through consecutive polymerization-depolymerization cycles, a circular cyclic monomer – linear polymer – cyclic monomer loop was achieved.

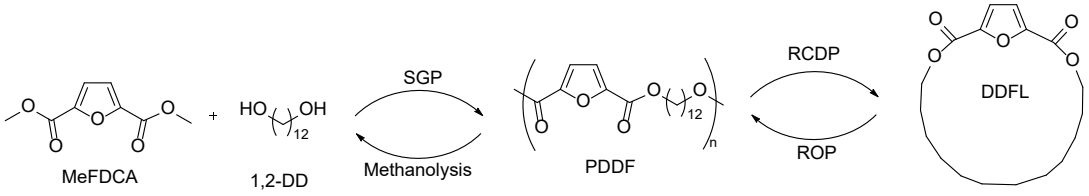

Figure 40. Dual closed circular chemical loops established by catalyzed ring-closing depolymerization (RCDP)/repolymerization (ROP) and methanolysis (MET)/repolymerization (SGP).

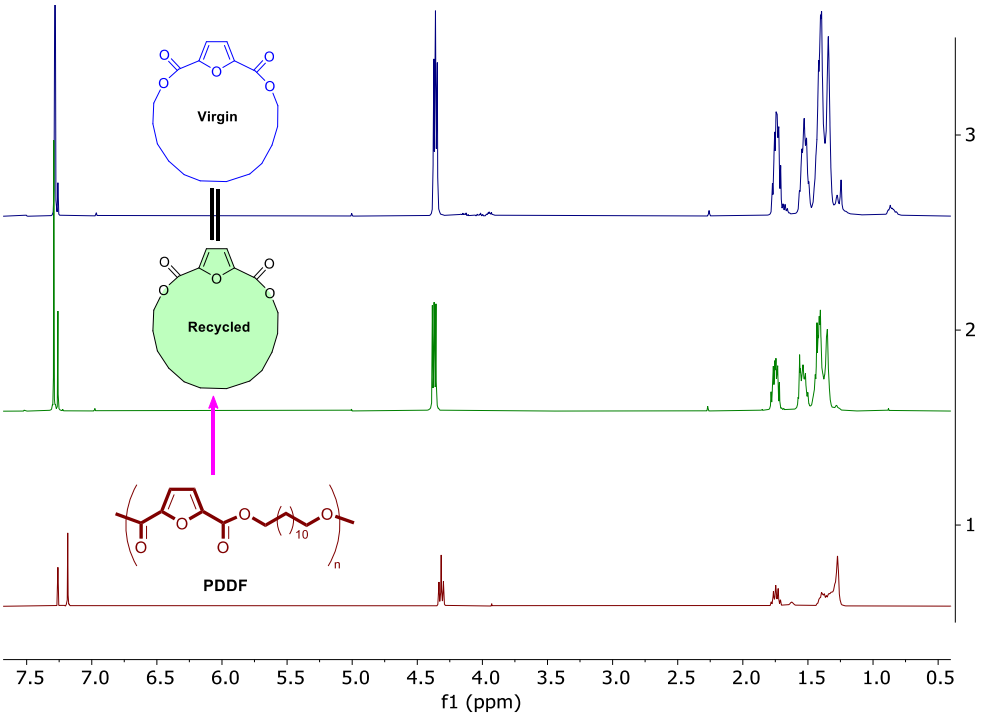

Figure 41. Chemical recyclability demonstration for PDDFL. ^{1}H NMR spectra ($CDCl_3$) of starting virgin monomer DDFL (top), recycled DDFL (second from top) monomer, and PDDF polymer by ROP (bottom).

A second pathway to establish closed-loop chemical recycling is through methanolysis of PDDF to the corresponding diester and diol monomers for repolymerization by SGP. Thus, the diester, dimethyl furan-2,5-dicarboxylate, and the diol, 1,12 dodecanediol, were recovered in quantitative yields using 30 wt% Et_3N at 120 °C for 18 h. The recovered diester and diol were used for repolymerization via the SGP protocol (see section 2.3) without additional purification, although no properties were measured.

Unpublished details on Scaling up of PPeAT

Scale up the process to produce 2.5 kg of resin per week for polyesters that meet criteria 1: To meet the production target of 2.5 kg of resin per week for polyesters that satisfy Criterion 1, an early strategic decision was made to conduct all polymer synthesis in glass reactors. The rationale for this choice was that only the reactor vessel would need to change with scale, while the rest of the synthesis setup would remain consistent, allowing all budgetary resources to be allocated to a single scalable design.

However, approximately halfway through the project, it became evident that this approach was not feasible for scale-up. Achieving high molecular weights requires operating under high vacuum conditions (pressures below 1 mbar) during the second-stage polycondensation. This necessitates a very tight seal at the stirrer shaft. When attempting to stir high-viscosity melts at these scales, the torque required exceeded the mechanical

limits of the glassware, resulting in repeated seal failures and, in some cases, glass breakage. Despite considerable effort over several months to engineer around this limitation, no viable solution was identified.

As a result, the process was constrained to batch sizes of 0.25 kg, with each batch requiring two days to achieve the desired molecular weight. This inherently limited weekly output to a maximum of 0.875 kg/week under ideal conditions.

A viable alternative emerged in the form of diisocyanate coupling, which circumvents the need for the high-vacuum polycondensation step. This method enables an increase in molecular weight from approximately 10,000 to ~100,000, as shown in **Figure 42**, while avoiding the severe mechanical and vacuum constraints associated with melt polycondensation in glass reactors. This coupling strategy offers a practical route to scale production up to the required 2.5 kg/week capacity.

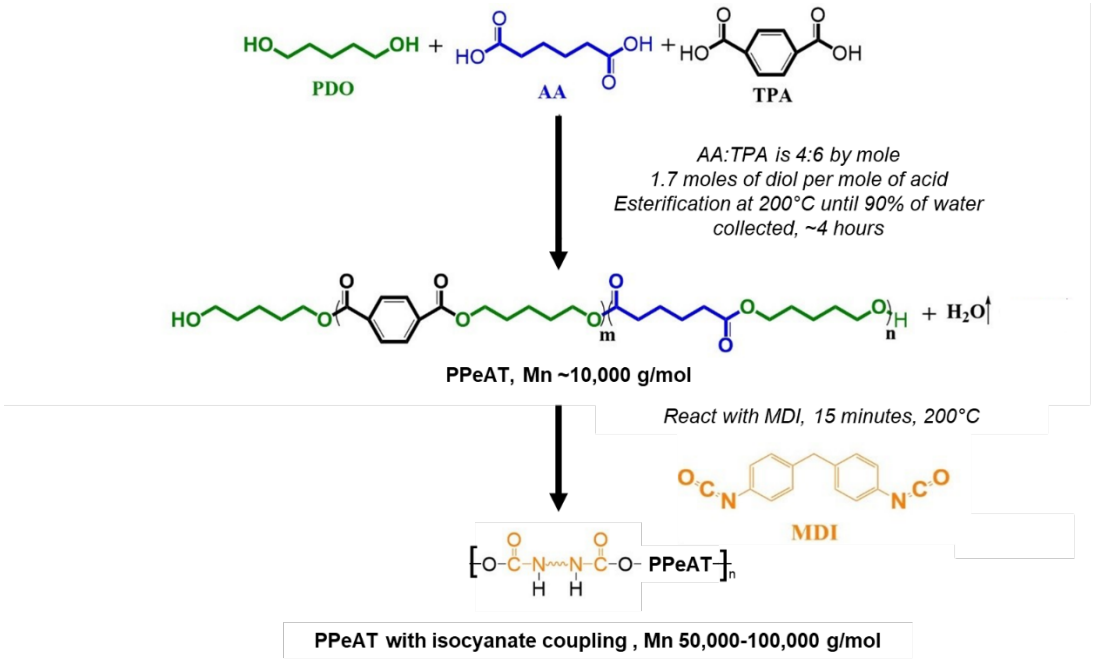

Figure 42. Schematic diagram of synthesis of PPeAT with diisocyanate coupling

The diisocyanate reaction does not require vacuum, and hence achieving this 2.5 kg/week is now possible. The reason for the switch was not because of the 2.5 kg/week problem; a metal reaction system has no problem reaching this volume without diisocyanate coupling. Also of course, diisocyanates would be by far the most dangerous chemical in the polyester synthesis process. Rather, the results described here forced us to adopt this solution. Namely, the cast films were extremely poor in mechanical properties because of larger chain orientation in the machine direction. The diisocyanate coupling reaction is labile at the high temperatures used for cast film production, and we hypothesize that using a diisocyanate-coupled material would reduce or eliminate this

issue as any temporary reduction in molecular weight would allow for relaxation of the chains and hence reduce orientation. However, our ability to diisocyanate couple was not complete until shortly before the project ended, and hence no results are presented in this report on diisocyanate-coupled materials, although we continue to work on this aspect of the project.

Also, in the last year of the project, we developed a collaboration with Korean Research Institute of Chemical Technology who has both 10 and 40 L metal reactors for polyester synthesis. They can make larger batches. Even more importantly, the color of their material is significantly better than our material, which is not surprising because a larger system will be able to better exclude colorants. We are continuing this collaboration as well. No efforts were made to scale up PDDF, although we would not anticipate any problems.

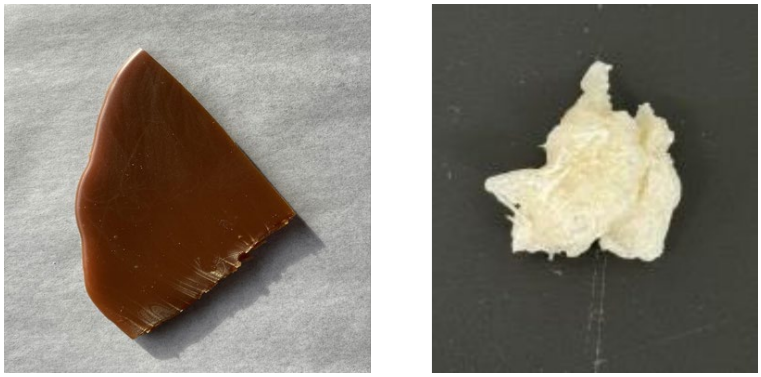

Figure 43. High molecular weight PPeAT made in our lab (left) and medium molecular weight PPeAT made in Korea (right).

Experimental details on production of PDDF

The traditional diacid (A_2) and diol (B_2) SGP route was also employed for the synthesis of PDDF (PDDF-SGP) with a medium molecular weight, which was performed through a two-step procedure, esterification followed by polycondensation. In the first step, DD was melted by slowly increasing the temperature to 100 ℃ under a slow nitrogen flow and continuous agitation. FDCA was then added to the molten DD, and the temperature gradually increased to 170 ℃. At this temperature, titanium isopropoxide (0.1 mol % of acid) was introduced and the temperature was further raised to 200 ℃ at a controlled rate of 5 ℃/30 min. The esterification reaction was allowed to proceed for the next 24 h. Following the esterification reaction, in the second step another portion of titanium isopropoxide (0.1 mol % of acid) was added and the vacuum was reduced to less than 0.1 mbar, initiating the polycondensation phase. The temperature then increased to 230 °C and polycondensation continued until a Weissenberg effect was observed. The

average molecular weight and dispersity (*Đ*) of PDDF-SGP are compared to commercial PBAT in **Table 10**.

Table 10. Molecular weights for PBAT and PDDF prepared by SGP and ROP

Sample	M_n	M_w	
	kDa	kDa	Đ
PBAT [a]	59.9	97.9	1.60
PDDF-SGP [a]	31.6	52.6	1.70
PDDF-ROP [b]	227	363	1.60

(a) Relative to polystyrene standards. (b) From run 10, Table 1, absolute molecular weight.

Thermal stability, crystallization, and melting behaviors

Figure 44 and **Table 10** show the temperatures for different decomposition stages obtained from thermogravimetric analysis (TGA). PBAT exhibits similar thermal stability to PDDF but with slightly higher $T_{d,5\%}$ (by ~6 °C) and $T_{d,max}$ (by ~10 °C) values, likely due to the slightly higher stability of the phenyl ring vs. the furan ring (**Figure 44**d,e). PDDF polyesters have a lower residue at 600 °C compared to PBAT, again attributed to the presence of the furan ring in PDDF versus the phenyl ring in PBAT. Additionally, PDDF-ROP showed a lower residue at 600 °C (0.8%) compared to PDDF-SGP (3.1%). One possible explanation is that the ROP of the cyclic monomer was more controlled and performed under relatively milder conditions (25 to 125 °C), thus eliminating or suppressing possible reaction by-products occurred under the harsh SGP conditions (230 °C, vacuum).

Table 11. Thermal properties measured by DSC, TGA and DMA

Sample	First Heating		First Cooling		Second Heating			DMA	TGA		
	T_m	ΔH_m	T_c	ΔH_c	T_g	T_m	ΔH_m	T_g	$T_{d,5\%}$	$T_{d,max}$	$R_{600℃}$
	℃	J/g	℃	J/g	℃	℃	J/g	℃	℃	℃	%
LLDPE	116	131	106	109	-	116	127	-	441	453	0
PBAT	115	34	38	20	-30	118	20	-27	358	376	4.3
PDDF-SGP	108	80	58	63	-9	102	52	-6	351	366	3.1
PDDF-ROP	102	78	60	52	-10	95	61	2	352	363	0.8

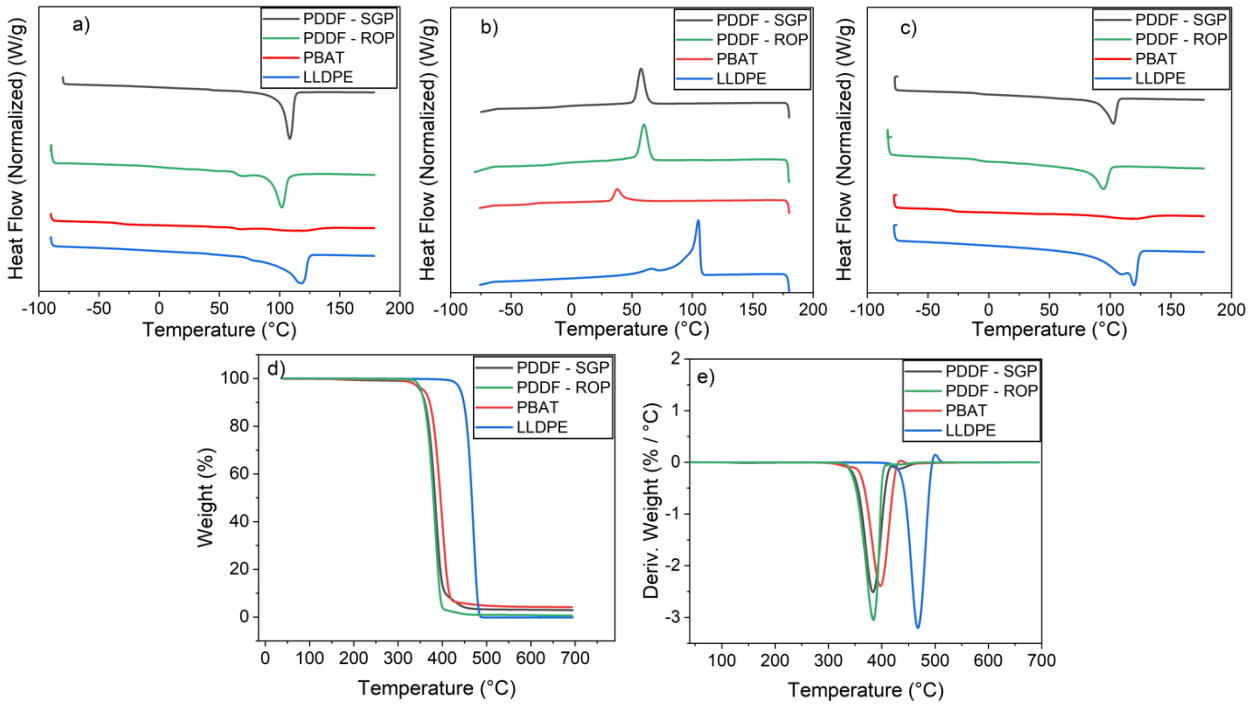

Figure 44. Thermal properties of PDDF, compared to commercial materials PBAT and LLDE. a) DSC first heating cycle. b) DSC first cooling cycle. c) DSC second heating cycle. d) TGA thermogram overlays. e) Derivative TGA (DTGA) thermogram overlays.

Crystallization and melting behaviors of PDDF polyesters were investigated using differential scanning calorimetry (DSC), as shown in **Figure 45**, with the results summarized in **Table 10**. Upon heating, PDDF polyesters presented a well-defined melting peak, indictive of their semi-crystalline nature. A sharp endothermic melting peak was observed for PDDF and LLDPE during both the first and second heating cycles, whereas a broader peak was noted for PBAT (**Figure 45**a,c). PDDF polyesters exhibited a peak at higher temperature during cooling vs. PBAT, indicative of a faster crystallization rate (**Figure 45**b), likely due to the longer methylene sequence in the PDDF chain. High-molecular-weight PDDF-ROP (M_n = 227 kDa) displayed a lower T_m (by ~7 °C) and similar T_g compared to medium-molecular-weight PDDF-SGP (M_n = 31.6 kDa). A lower T_m indicates thinner crystals, an indication that was confirmed by SAXS measurements (*vide infra*). Notably, PDDF polyesters showed a significantly higher ΔH_m (by ~3×) compared to PBAT, presumably due to the presence of the longer alkyl chain in PDDF, suggestive of a higher degree of fractional crystallinity that was confirmed by WAXS measurements (*vide infra*). Owing to differences in molecular weights and DSC conditions, the T_m and T_g values of the current PDDF materials differed somewhat from those reported in literature (T_m ~ 110 °C, T_g ~ –22 °C).[25,26]

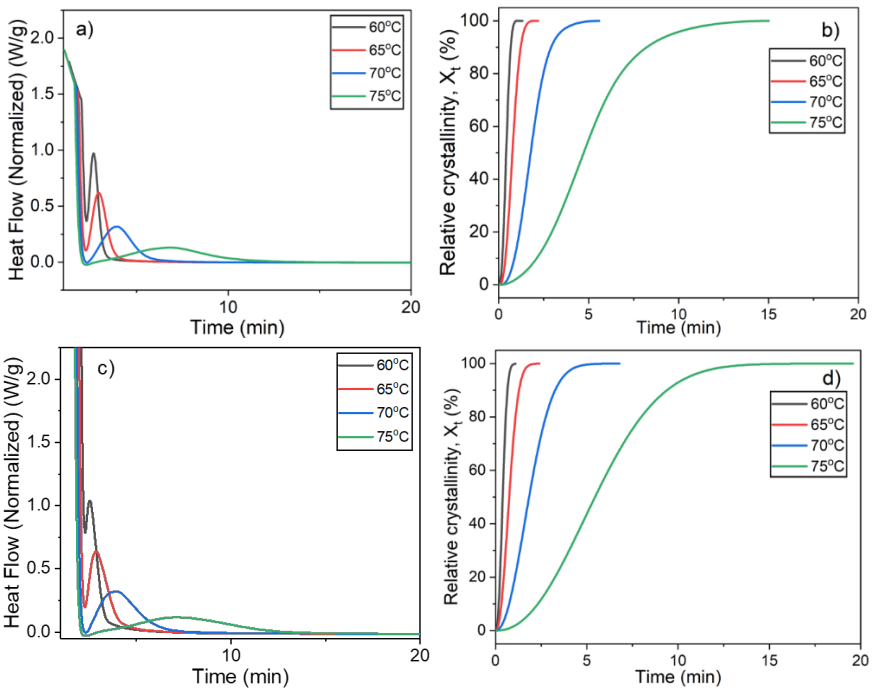

Figure 45. Isothermal crystallization kinetics. a) Isothermal crystallization for PDDF-SGP. b) Avrami model results for PDDF-SGP. c) Isothermal crystallization for PDDF-ROP. d) Avrami model results for PDDF-ROP.

Isothermal crystallization kinetics of PDDF polyesters were studied at different temperatures using DSC with results reported in **Figure 45**. The well-known Avrami model was utilized to gain insights into the isothermal crystallization process. The Avrami model illustrates the time-dependent relative crystallinity (X_t) at a constant temperature, as presented in Equation (1):

$$X_t = 1 - \exp(-kt^n) \quad (1)$$

The half-time for 100% relative crystallization ($t_{1/2}$) was calculated using Equation (2):

$$t_{\frac{1}{2}} = \left(\frac{\ln 2}{k}\right)^{\frac{1}{n}} \quad (2)$$

where k is the rate constant for crystallization that is a function of nucleation and growth rates, and n is the Avrami exponent. The crystallization half-time ($t_{1/2}$) and the Avrami model parameter are reported in **Table 12**. The rate of crystallization decreases with the increase in crystallization temperature, with no substantial difference between the two PDDF materials of different synthetic origins (SGP vs. ROP), although there is a significant difference in molecular weight. The lack of difference here is not reflected in the non-isothermal crystallization results presented in **Table 12**.. The Avrami exponent for all temperatures is between 2 and 3 but decreases as temperature increases. The growth

mechanism changes from one that is equally distributed between two and one-dimensional growth to one that is more one-dimensional growth.[27]

Table 12. Avrami model parameters for PDDF

Sample	T_c (°C)	$t_{1/2}$ (min)	k min^{-n}	n
PDDF-SGP	60	0.42	6.42	2.54
	65	0.77	1.39	2.58
	70	1.78	0.16	2.50
	75	4.72	0.02	2.25
PDDF-ROP	60	0.39	6.27	2.35
	65	0.75	1.32	2.21
	70	1.86	0.19	2.09
	75	5.01	0.02	2.20

Characteristics of PDDF crystallites

Figure *46* illustrates the WAXS patterns of the PDDF polyesters, compared to PBAT and LLDPE, while Table 5 provides percentage crystallinity values for these polymers. For PBAT, scattering angles (2θ°) observed are 16.2°, 17.3°, 20.4°, 23.2° and 24.8° corresponding to the planes (011), (010), (102), (100), and (111) respectively, consistent with the literature. For LLDPE, two sharp crystalline peaks can be observed at the 2θ° values of 21.4° and 23.6° which are assigned to (110) and (200) planes. For PDDF, 2θ° are 9.8°, 17.9°, 21.6° and 23.8° with the latter two scattering angles at approximately at the same angles as the planes (110), and (200) of LLDPE. The percentage crystallinity of PDDF (30.2%) is a bit more than half the percent crystallinity of LLDPE (50.4%); the ratio of these two values is roughly consistent with the ΔH_m values (**Table 11**). Moreover, PDDF has a higher percent crystallinity than PBAT (19.4%), which is due to the presence of a higher number of methylene units in PDDF leading to a more crystalline polyester. The increase in the molecular weight of PDDF-ROP compared to PDDF-SGP resulted in a decrease in percent crystallinity. The ratio of the peak heights for PDDF-ROP and PDDF-SGP observed in DSC analysis for the first heating, which also had room temperature annealing and hence should approximately correspond to the sample measured in WAXS, aligns (0.7) closely with the ratio of percent crystallinity for PDDF-ROP and PDDF-SGP derived from WAXS measurements (0.76).

Figure *46* and **Table 11** also summarized SAXS results for PDDF, PBAT, and LLDPE. As the crystallites are anticipated to have a lamellar shape, the peak observed in $q^2I(q)$ vs q represents the characteristic long spacing drived from Bragg's law. The long period (*d*-spacing) is calculated using Equation (3) where q_{max} is the value where $q^2I(q)$ vs q.

$$d = \frac{2\pi}{q_{max}} \tag{3}$$

The values of lamellar thickness reported in **Table *13*** are derived from the multiplication of fractional crystallinity from WAXS by the d-spacing, i.e., the difference in density between the two phases is ignored. The *d*-spacing between PBAT and PDDF is the same so the lamellar thickness of PBAT is smaller. As mentioned earlier, the lamellar thickness for the PDDF-SGP is larger than that for the PDDF-ROP, consistent with DSC T_m data. In addition, the broadness of the SAXS peak for the PBAT is larger, consistent with the much broader peak in DSC heating scans. Consistent with the higher percentage crystallinity, the lamellar thickness for LLDPE is much larger.

To observe the change in orientation between the PDDF-SGP and PDDF-ROP in the thickness direction, 0° and 180°, samples were cut so that the beam was perpendicular to the thickness direction. SAXS patterns were examined for change in the transmissional intensities as a function of the azimuthal angle and the results are shown in **Figure *46***c. The scattering vector range used was the width of the scattering peak, *i.e.*, 0.03 and 0.1 A^{-1} for PDDF-SGP and 0.02 and 0.1 A^{-1} for PDDF-ROP. The lamellar thickness direction is aligned in the same direction as the thickness direction for both, with much higher alignment for the PDDF-SGP. Presumably, the much higher molecular weight of PDDF-ROP led to a higher number of entanglements which restricts the chain mobility needed for lamellar alignment.

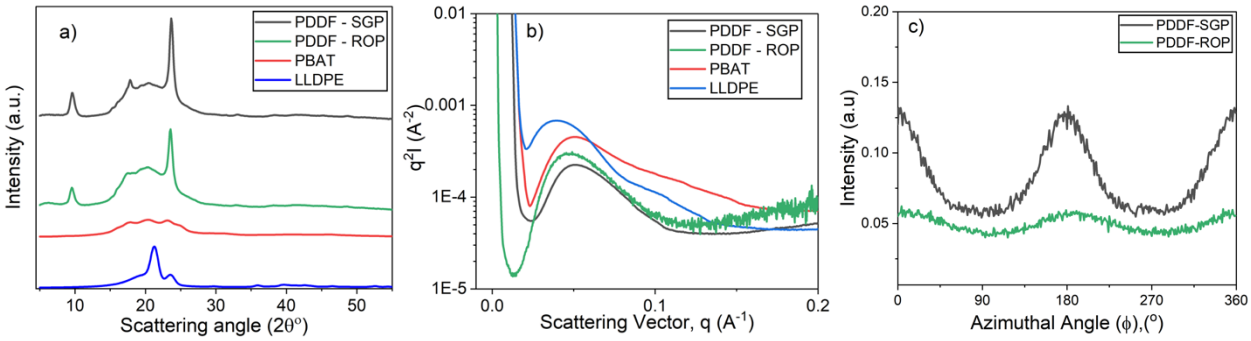

Figure 46. Properties of PDDF crystallites, compared to PBAT and LLDPE. a) WAXS profiles for PDDF, PBAT, and LLDPE. b) SAXS profiles for PDDF, PBAT, and LLDPE. c) Orientation from SAXS for PDDF-SGP and PDDF-ROP in the thickness (0° and 180°) direction.

Table 13. Crystallinity properties for PDDF polyesters, compared to PBAT and LLDPE

Sample	WAXS	SAXS		
	χ_c	q_{max}	*d*-Spacing	Lamellar Thickness
	%	$Å^{-1}$	Å	Å
LLDPE	50.4	0.039	160	80.8
PBAT	19.4	0.051	124	24.2
PDDF-SGP	30.2	0.051	124	37.5
PDDF-ROP	23.1	0.049	128	29.6

Mechanical and rheological properties

Stress-strain curves for PDDF-SGP and PDDF-ROP, compared to PBAT and LLDPE, are overlaid in **Figure 47**a. The relevant parameters are reported in **Table 14**. All four polymers exhibit ductile behavior with a high elongation at break. The measured E, δ_y, ε_y, δ_b and ε_b values for LLDPE and PBAT agree with those reported in literature.[28, 29]

PDDF demonstrates outstanding mechanical performance, with Young's modulus E = 247 ± 7 MPa for the PDDF-SGP and E = 165 ± 7 MPa for the PDDF-ROP; both are significantly higher than PBAT's 78 ± 10 MPa, while the former is comparable to that of LLDPE (E = 255 ± 33 MPa). The higher modulus is a result of the higher crystallinity of the PDDF-SGP. PDDF-ROP exhibited a higher stress at break (δ_b= 37 ± 3 MPa) and elongation at break (ε_b= 280 ± 60%) compared to PDDF-SGP (δ_b= 21 ± 2 MPa, ε_b= 220 ± 32%). As expected, PDDF is stiffer and has a lower elongation at break than PBAT due to PDDF's higher fractional crystallinity. Moreover, the mechanical properties of PDDF in this study significantly differ from those reported by Papageorgiou et al.,[25] denoted as PDDF[1] in **Table 14** where showed much lower $\delta_b$and $\varepsilon_b$values, likely due to variations in molecular weights, synthesis processes, such as the completeness of transesterification, or differences in cooling methods after compression molding.

Table 14. Mechanical properties of PDDF, compared to PBAT and LLDPE

Sample	E	δ_y	ε_y	δ_b	ε_b
	MPa	MPa	%	MPa	%
LLDPE	255 ± 33	11 ± 0.3	19 ± 21	37 ± 4	645 ± 71
PBAT	78 ± 10	-	-	26 ± 3	815 ± 67
PDDF-SGP	247 ± 7	-	-	21 ± 2	220 ± 32
PDDF-ROP	165 ± 7	-	-	30 ± 3	280 ± 60
PDDF[25]	181 ± 16	9.5 ± 1.1	-	11 ± 0.9	130 ± 10

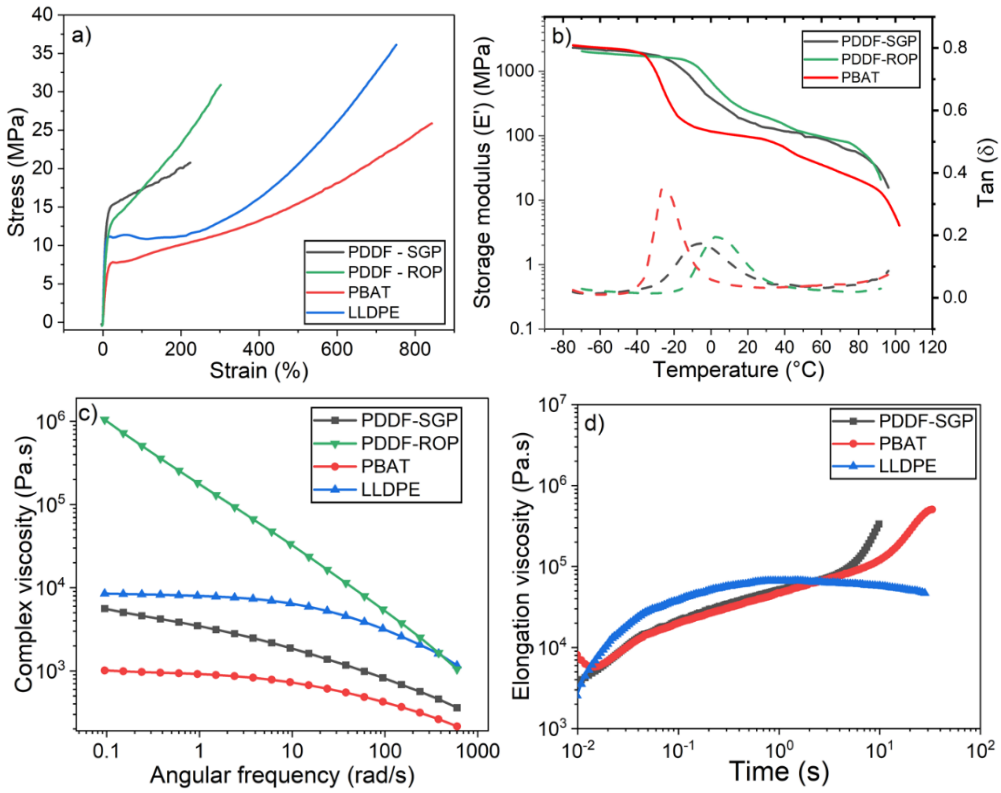

Figure 47. Mechanical, dynamic mechanical, and rheological properties of PDDF, compared to PBAT and LLDPE. a) Stress-strain curves for PDDF, PBAT, and LLDPE. b) DMA results for PDDF and PBAT. Storage modulus is represented as (- solid lines), and damping factor is represented as (- - dashed lines). c) Complex viscosity curve of PDDF, PBAT, and LLDPE. d) Elongation viscosity curves for PDDF, PBAT, and LLDPE.

Figure 47b presents the *E'* and tan *δ* as a function of temperature, measured by DMA. The DMA T_g was determined by the temperature that corresponded to the peak in tan *δ* curve. This T_g value was consistent with that obtained from DSC for PDDF-SGP and PBAT; however, for PDDF-ROP, the T_g obtained from DMA was higher (by 12 C°) than the T_g obtained from DSC as shown in Table 3. This difference is likely related to the much higher number of entanglements in the glass which shifts a mechanical T_g to a higher temperature.

Complex shear viscosities vs angular frequency at 190 °C for PDDF polyesters, compared to LLDPE and PBAT, are plotted in ***Figure 47***c. Shear-thinning behavior at high frequencies and a Newtonian plateau at low frequencies can be observed for PDDF-SGP, LLDPE, and PBAT. The higher melt viscosity of PDDF-SGP vs. PBAT is somewhat surprising, given that the molecular weight of the former is ~1/2 the molecular weight of the latter. A possible explanation is the long chain of the aliphatic diol causes the critical entanglement molecular weight of PDDF to be less than PBAT, while the other is that the friction coefficient is higher for the former. The very long chain of PDDF-ROP showed very high melt viscosity due to its very high molecular weight, as well as a much lower

frequency for the transition to the zero-shear viscosity region. PDDF-ROP showed a crossover viscosity at high frequencies with LLDPE and likely would have shown a crossover with PDDF-SGP at a few thousand radians/sec. The shear rate within the extruder during film blowing is expected to be 45 s^{-1} [30] which corresponds to a frequency of 283 radians/sec on ***Figure 47***c. Hence, if the Cox-Merz rule is applicable to these polymers, then the extrusion energy required for PDDF-ROP is about the same as that needed for LLDPE while for PDDF-SGP the extrusion energy required is significantly lower. The low frequency tested limit was quite high because of thermal degradation of FDCA.[31, 32]

The five-parameter Carreau-Yasuda was used to model the complex viscosities. Fitted data showed good agreement with the experimental results; although the lack of a turnover frequency for PDDF-ROP means that η_o, ***a***, and λ are not very accurate for this polymer. PDDF-SGP had a lower flow index and a higher characteristic relaxation time than PBAT, reflective of a decrease in shear thinning behavior and a narrower Newtonian plateau region, respectively.

Table 15. Rheological properties of PDDF, compared to LLDPE and PBAT

Sample	Shear viscosity				Extensional viscosity at Hencky strain of 2.5 and 0.3 s^{-1}
	η_o	n	a	λ	η_E
	Pa.s	-	-	s	Pa.s
LLDPE	8711	0.12	0.62	0.01	47,000
PBAT	1006	0.67	0.76	0.12	350,000
PDDF - SGP	9168	0.45	0.29	0.28	225,000
PDDF - ROP	61741097	0.17	0.82	1354	-

Elongation viscosities vs. time for PDDF polyesters, LLDPE, and PBAT at 130 °C and 0.3 s^{-1} are plotted in ***Figure 47***d. A lower temperature was chosen compared to the temperature used for shear viscosity measurements, as high temperatures lead to sample sagging. In addition, a Hencky strain of 2.5 at an extensional rate of 0.3 s^{-1} was found to be representative values for film blowing[30] and these values are listed in **Table *15***. High elongation viscosity serves as an indicator of elevated melt strength, consequently contributing to a more stable bubble during the film blowing process. Strain hardening is characterized by an increase in elongation viscosity above the linear viscoelastic plateau.[33] In this context, PDDF-SGP and PBAT exhibit strain hardening, while the absence of strain hardening in LLDPE is attributed to the presence of short branches that allow the polymer chains to stretch without any entanglements. Strain hardening has been attributed to certain long chains remaining stretched until the sample's failure.[34] Micic ***et al.*** reported that strain hardening is linked to improved stability of the bubble during the film blowing process.[35] The very high elongation viscosity of PDDF-ROP prevented the accurate measurement of elongation viscosity at 130 °C. The sample continued to slip

because adequate adhesion to the grip requires a slight melting of the material. In other words, 130 °C was insufficient to lower the viscosity of the PDDF-ROP sample to a level compatible with the equipment limits.

Biodegradation

Biodegradation of PDDF-SGP was conducted in freshwater, soil, and compost environments, and the results are summarized in **Figure 48**. The test is considered valid if the degree of the biodegradation of the reference material (glucose or microcrystalline cellulose (MCC)) is more than 60% at the end of the test for the freshwater environment, more than 70% in 6 months for the soil environment, and 70% after a specific timeframe (usually around 45 days) for compost environment. The results for PBAT were reported previously by Zheng *et al*.[36] In the freshwater environment, PDDF-SGP achieved approximately 17% biodegradation in 72 days, while PBAT reached around 35% within the same period. Therefore, the estimated EoL time, based on first-order kinetics, is 395 days for PBAT, whereas for PDDF-SGP, it is projected to be 990 days under the same conditions. In the soil environment, PBAT reached around 20% biodegradation in 96 days but for PDDF no measurable biodegradation was observed after 96 days. However, in the compost environment, PDDF-SGP reached about 28% biodegradation in 62 days, with an estimated EoL time of 475 days based on first order kinetics. The slower biodegradation rate of PDDF-SGP compared to PBAT may be attributed to two key factors. First, PDDF-SGP has a higher degree of crystallinity, which makes the polymer structure more rigid and less accessible to microbial attack.[37] Second, the incorporation of a long-chain alkyl in PDDF-SGP results in fewer ester groups per unit length of the polymer chain. Since ester groups are the primary sites for hydrolytic degradation, their lower density in PDDF likely reduces its susceptibility to biodegradation.[38]

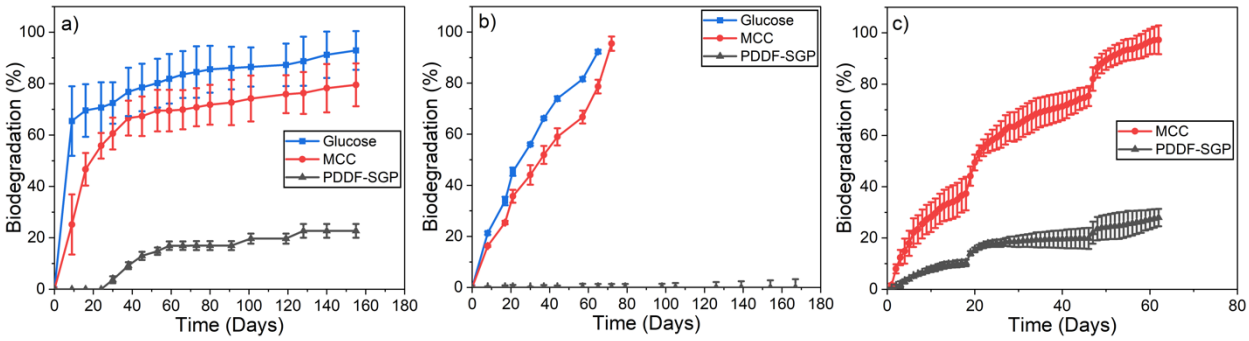

Figure 48. PDDF biodegradability tests against reference materials (glucose and/or micro-crystalline cellulose (MCC)). a) Freshwater biodegradation profile. b) Soil biodegradation profile. c) Compost biodegradation profile.

Area 3 – Polyester applications

Demonstration of the performance of the polyesters synthetized in this project in packaging applications was addressed in Task 5.0 – Scaling up of Polyester Synthesis and Application under milestones 5.6 – 5.8.

M. 5.6 - Testing of biomass-derived polyester in mono-layer film for food packaging: This milestone has been achieved in terms of successfully producing biomass-derived polyesters (e.g., PPeAT and PDDF) with mechanical and barrier properties comparable to linear low-density polyethylene (LLDPE). However, a potential limitation for their application in food packaging is the inherent coloration of these materials, which may affect their aesthetic appeal and market acceptance.

Table 16. Mechanical properties for blown film (MD is the machine direction, TD is the transverse direction).

Samples		E / MPa	δ_b / MPa	ε_b / %
LLDPE	MD	165.5 ± 35.5	16.7 ± 0.8	673 ± 27
	TD	165.8 ± 31.1	13.5 ± 2.1	580 ± 79
PPeAT	MD	131.7 ± 14.4	12.2 ± 1.5	334 ± 17
	TD	124.3 ± 29.3	9.5 ± 1.1	266 ± 38
PDDF	MD	163.4 ± 33.0	15.1 ± 2.5	147 ± 17
	TD	154.4 ± 24.0	18.7 ± 2.1	270 ± 47

Table 17. Oxygen, CO_2 and water vapor transmission rates for three blown films.

Samples	P_{O_2} / Barrer	P_{CO_2} / Barrer	WVTR g.mm/m².d
LLDPE	3.56 ± 0.32	14.5 ± 1.28	0.17 ± 0.1
PPeAT	0.60 ± 0.11	4.31 ± 0.79	2.14 ± 0.34
PDDF	0.58 ± 0.19	3.80 ± 1.3	1.08 ± 0.20

M. 5.7 - Testing of biomass-derived polyester in multi-layer film for food packaging: This milestone could not be achieved due to the unavailability of sufficient starting material for film production. The polymer synthesis team encountered technical difficulties with the glass reactors used in the polymerization process, leading to significant delays in the project timeline. As a result, it was not possible to produce the required quantities of polyester needed for testing in multi-layer film applications within the project's execution window.

M 5.8 - Testing of biomass-derived polyester in extrusion coating for liquid packaging: The following sections summarize the key findings related to the production and evaluation of cast films prepared from these biomass-derived polyesters. This includes an assessment of their processability, mechanical behavior, and barrier properties in extrusion coating formats.

Materials and Methods

Linear low-density polyethylene (LDPE), polylactic acid (PLA), Poly(butylene adipate-co-terephthalate) (PBAT) were graciously provided by Amcor, plc. PPeAT was synthesized in our lab via direct esterification and polycondensation, following a method previously developed and published by our group. Two different weight percentages were tested, as summarized in **Table 18**. Two types of PBAT/PLA blends were considered: a commercially available formulation and a physically blended formulation prepared by compounding individual PBAT and PLA components during the extrusion process.

Table 18. Cast film compositions

	Sample	Commercial Name	PBAT	PLA	PPeAT	LDPE	Notes
-	**LDPE**	Petrothene NA214000	-	-	-	100	
1	**PBAT**	Ecoflex C1200	100	-	-	-	
2	**PBAT/PLA**	Ecovio F2224	55	45	-	-	Commercial
3	**PBAT/PLA**	-	55	45	-	-	Component
4	**PPeAT/PLA**	-	-	45	55	-	
5	**PBAT/PLA**	Ecovio F2341	90	10	-	-	Commercial
6	**PBAT/PLA**	-	90	10	-	-	Component
7	**PPeAT/PLA**	-	-	10	90	-	

Note: Percentages are weight percent

Cast film extrusion using a multilayer co-extrusion cast film line manufactured by Labtech Engineering. The extrusion parameters are summarized in **Table 19**. All barrel temperature zones were maintained at a constant temperature of 350 °C, while the die temperature was set to 380 °C. The screw speed was held constant across all formulations, except for the LDPE film. The casting rates was kept constant for all films to ensure consistent processing conditions.

Table 19. Cast film extrusion conditions. Numbers in top row refer to **Table 2**

Description	Units	LDPE	1	2	3	4	5	6	7
Barrel Zone 1	**°F**	350	350	350	350	350	350	350	350
Barrel Zone 2	**°F**	350	350	350	350	350	350	350	350
Barrel Zone 3	**°F**	350	350	350	350	350	350	350	350
Barrel Zone 4	**°F**	350	350	350	350	350	350	350	350
Filter/Clamp	**°F**	350	350	350	350	350	350	350	350
Adapter Pipe	**°F**	350	350	350	350	350	350	350	350
Feed Block	**°F**	350	350	350	350	350	350	350	350
Die Left	**°F**	380	380	380	380	380	380	380	380
Die Middle	**°F**	380	380	380	380	380	380	380	380
Die Right	**°F**	380	380	380	380	380	380	380	380
Screw Speed	**rev/min**	50	18	18	18	18	18	18	18
Motor Load	**%**	53	50	49	50	48	49	50	49
Back Pressure	**Bar**	30	50	48	50	52	44	50	64
Melt Temperature	**°F**	395	396	393	394	393	395	394	393
Casting Rate	**m/min**	1.0	1.0	1.0	1.0	1.0	1.0	1.0	1.0
Die Width	**mm**	250	250	250	250	250	250	250	250
Die Gap	**µm**	635	635	635	635	635	635	635	635
Chill Roll Temperature	**°F**	100	100	100	100	100	100	100	100

WAXS and SAXS

The percentage of crystallinity for MD and TD were calculated from the WAXS spectra is reported in **Table 20**. The addition of PLA didn't significantly affect the percent crystallinity of PBAT and PPeAT blends except for film 4 where a drop in percent crystallinity can be observed. The percent crystallinity in TD for all the cast films was found to be slightly higher than percent crystallinity in the MD. **Table 20** show SAXS results for the cast films in MD and TD. TD films had a higher percentage crystallinity than MD films and these results show that the lamellar thickness were also higher. Additionally, PPeAT Films 4 and 7 showed a smaller d-spacing and thinner lamellar thickness in MD and TD compared to PBAT Films 3 and 6, respectively. To observe the degree in orientation of the cast films, SAXS patterns were examined for change in the transmissional intensities as a function of the azimuthal angle, with results are shown in **Table 20**. More orientation can be observed for PPeAT film 7 compared with the roughly equivalent PBAT cast films 5 and 6. Similar degree of orientation can be observed for PPeAT film 4, PBAT film 2 and LDPE film.

Table 20. WAXS and SAXS results for the cast films

Sample		Orientation		WAXS	SAXS		
		Orientation	f	Percent Crystallinity (%)	q_{max} (Å^{-1})	d-spacing (Å)	Lamellar Thickness (Å)
LDPE	MD	0.23	-0.16	20.7	0.056	112.5	23.3
	TD	0.45	0.17	34.8	0.060	105.2	36.6
1	MD	0.32	-0.02	21.1	0.061	103.3	21.7
	TD	0.35	0.02	20.8	0.059	107.2	22.3
2	MD	0.25	-0.12	17.8	0.060	104.2	18.5
	TD	0.43	0.15	19.9	0.066	95.4	18.9
3	MD	0.32	-0.03	20.1	0.063	100.5	20.2
	TD	0.35	0.02	22.6	0.071	88.0	19.9
4	MD	0.22	-0.16	3.5	0.078	80.5	2.8
	TD	0.45	0.18	8.3	0.094	67.1	5.6
5	MD	0.32	-0.02	24.3	0.048	130.3	31.7
	TD	0.34	0.01	36.7	0.048	131.9	48.4
6	MD	0.28	-0.08	22.0	0.059	106.2	23.4
	TD	0.39	0.08	22.5	0.056	112.5	25.3
7	MD	0.17	-0.25	5.5	0.070	89.4	4.9
	TD	0.53	0.29	15.5	0.078	81.1	12.5

Mechanical Properties

PLA is often blended with polyesters like PBAT to improve the overall stiffness of the material, as PLA has a higher modulus compared to PBAT. Additionally, incorporating PLA can enhance the bio-based content and reduce the cost of fully biodegradable polymer blends, while maintaining compostability under industrial conditions. The Young's modulus, tensile strength at break, and elongation at break of the cast films were evaluated in both the machine direction (MD) and transverse direction (TD) with results are summarized in **Table 21**. Additionally, the mechanical properties are presented alongside their percent deviation relative to LDPE, serving as a reference material for comparison. Notably, several compositions exhibited significant enhancements in specific properties. For instance, Film 4 demonstrated over a 10-fold increase in MD Young's

modulus (1124%) compared to the reference, while Film 7 showed a over threefold increase in elongation at break (376%) in the MD. Additionally, PPeAT Films 4 and 7 showed a higher Young's modulus in MD compared to PBAT Films 3 and 6, respectively. In contrast, the same films exhibited a substantial reduction in elongation in TD. The substantial reduction is likely directly related to the very large increase in orientation, e.g. the number of chain entanglements in the TD direction yields a much less flexible material in that direction. These trends highlight the tunability of mechanical performance across different film compositions and processing conditions.

None of the other measurements with PPeAT, including blown film, showed this bad performance of PPeAT vs. PBAT. The only cause that we can use to explain these results is the PBAT is coupled with a diisocyanate. The diisocyanate is labile at elevated temperatures and high stress increases this ability to break, and such breaking would allow more relaxation by low molecular weight chains, which would be followed by reformation. Diisocyanate coupled samples would be expected to have lower orientations. Another possibility is a reaction between PBAT terminated with isocyanate and PLA, i.e. some linking between the two is occurring.

Table 21. Mechanical properties comparison of extruded films

Sample		Young's modulus		Yield Strength		Elongation at break	
		Result	Comparison	Result	Comparison	Result	Comparison
		MPa	%	MPa	%	%	%
LDPE	MD	112.9 ± 5.1	100%	13.3 ± 2.1	100%	252 ± 70.2	100%
	TD	118.4 ± 2.3	100%	10 ± 0.9	100%	370 ± 55.3	100%
1	MD	86.6 ± 2.4	77%	23.5 ± 2.9	177%	735.3 ± 63.6	292%
	TD	96 ± 6	81%	25.2 ± 2	252%	826.4 ± 52.8	223%
2	MD	694.8 ± 22.7	615%	25.7 ± 1	193%	319.9 ± 49.6	127%
	TD	312.2 ± 58.6	264%	13.8 ± 1	138%	43 ± 6.4	12%
3	MD	1147 ± 72.3	1016%	31.5 ± 5.4	237%	242.2 ± 99.4	96%
	TD	671.6 ± 62.3	567%	18.4 ± 1.5	184%	83.4 ± 16.2	23%
4	MD	1268.7 ± 133.8	1124%	24.5 ± 5.3	184%	176.4 ± 58.7	70%
	TD	908.6 ± 38.4	767%	18.8 ± 2.4	188%	19.8 ± 5.1	5%
5	MD	253 ± 18	224%	18.7 ± 1	141%	492.8 ± 34.5	196%
	TD	207.8 ± 19.7	176%	14.8 ± 1	148%	450.5 ± 44.6	122%
6	MD	150.9 ± 22.2	134%	21 ± 2.7	158%	541.3 ± 67.4	215%
	TD	134.6 ± 12.8	114%	18.9 ± 1.8	189%	562.7 ± 50.2	152%
7	MD	424 ± 21.9	376%	18.1 ± 0.7	136%	295.2 ± 31.3	117%
	TD	426.1 ± 86.3	360%	10 ± 0.9	100%	90 ± 28.1	24%

To confirm the poor performance of the PPeAT blends, Elmendorf tear and slow puncture for the cast films were measured and reported in **Table 22**. Elmendorf tear (ASTM D1922) quantifies propagated tear resistance after a notch is made in the sample while slow puncture (ASTM F1306) quantifies the force required for a 0.125-inch diameter probe to puncture a sample at low deformation rate. LDPE films were not tested since they do not have very good puncture or tear resistance. Cast films were all tested with the 1600g pendulum to provide a comparison. But data is not fully accurate below 160 grams when using the large pendulum, therefore films with lower tear were retested with the 200g pendulum. PPeAT cast films showed significantly lower tear resistance compared to the PBAT cast films. For the 45wt% PLA cast films, tear resistance in the TD was higher than MD whereas the opposite trend was observed in the films with 10 wt% PLA. Low tear

resistance indicates a brittle behavior, these results are consistent with the results obtained from the tensile tests. In puncture resistance tests, a lower peak force indicates that the film is more susceptible to puncture and likely exhibits brittle behavior. Additionally, low displacement at break suggests limited ductility, as the material fails quickly with minimal deformation. PPeAT cast films exhibited higher peak force and displacement compared to the commercial PBAT/PLA cast films, but lower values than those observed in the component-blended PBAT/PLA films.

Table 22. Slow Puncture and Elmendorf Tear test results of extruded films.

Sample		Pendulum Mass		Slow Rate Puncture	
		1600 g	200 g	Force	Displacement
		gf	gf	N	in
1	MD	910.1 ± 85.1	-	40.25 ± 12.09	2.54 ± 0.84
	TD	931.7 ± 45.3	-		
2	MD	103.0 ± 3.1	78.4 ± 8.4	11.21 ± 1.60	0.36 ± 0.01
	TD	808.5 ± 32	-		
3	MD	130.9 ± 10.2	113.8 ± 17.0	25.62 ± 3.27	0.41 ± 0.06
	TD	341.0 ± 48.2	-		
4	MD	54.7 ± 3.3	48.4 ± 2.8	20.49 ± 2.74	0.31 ± 0.08
	TD	77.8 ± 4.8	66.0 ± 4.4		
5	MD	1041.6 ± 30.5	-	7.69 ± 0.58	0.43 ± 0.02
	TD	858.6 ± 21.8	-		
6	MD	1074.3 ± 74.3	-	22.85 ± 1.84	1.14 ± 0.03
	TD	444.8 ± 19.0	-		
7	MD	51.4 ± 1.9	32.8± 5.2	16.85 ± 6.09	0.48 ± 0.11
	TD	90.1 ± 9.7	108.8 ± 19.6		

Barrier Properties

Barrier properties of the extruded cast films were measured and reported in **Table 23** alongside their percent deviation relative to LDPE, serving as a reference material for comparison. Polyesters tend to have a lower P_{O_2} than polyolefins due to the presence of carbonyl and ester bonds, which led to a more hydrophilic structure and thus a lower P_{O_2}. As expected, PPeAT cast films and PBAT cast films had a lower $\mathrm{P}_{O_2}$and P_{CO_2}than LDPE.

P_{O_2} of PPeAT films 4 and 7 was measured to be 24% and 30%, respectively, relative to that of LDPE. PPeAT Films 4 and 7 showed a lower P_{O_2} and P_{CO_2} compared to PBAT Films 3 and 6, respectively. The addition of 45 wt% PLA slightly lowered P_{O_2} and P_{CO_2} , however the addition of 10 wt% PLA didn't affect the barrier properties. A similar trend was observed in the water vapor transmission rate (WVTR), except for the PBAT and PPeAT cast films, which showed higher WVTR values than LDPE. This deviation is attributed to the presence of hydrophilic polar functional groups—such as hydroxyl, ester, and carboxyl—that promote hydrogen bonding with water vapor molecules.

Table 23. Barrier properties comparison of extruded films

Sample	P_{O_2}		P_{CO_2}		WVTR	
	Result Barrer	**Comparison %**	**Result Barrer**	**Comparison %**	**Result g.mm/m².day**	**Comparison %**
LDPE	1.7 ± 0.11	100%	6.0 ± 0.1	100%	0.3 ± 0.1	100%
1	1.2 ± 0.1	72%	13.9 ± 1.2	231%	6.3 ± 0.4	2100%
2	0.6 ± 0.01	36%	5.3 ± 0.1	88%	4.4 ± 0.2	1467%
3	0.8 ± 0.02	48%	4.6 ± 0.1	76%	3.9 ± 0.6	1300%
4	0.4 ± 0.02	24%	2.1 ± 0.1	35%	2.6 ± 0.2	867%
5	0.7 ± 0.01	42%	7.4 ± 0.1	123%	4.4 ± 0.2	1467%
6	1.1 ± 0.04	66%	11.5 ± 0.4	191%	6 ± 0.3	2000%
7	0.5 ± 0.2	30%	2.8 ± 0.9	46%	1.9 ± 0.2	633%

Area 4 – Chemical Recycling of Polyesters

The chemical recyclability of bio-derived polyesters was investigated under Task 3.0 – *Design of catalytic processes to chemically recycle polyesters* and Task 5.0 – *Scaling up of polyester synthesis and application.*

Task 3.0: Design of catalytic processes to chemically recycle polyesters

In this task we designed catalytic processes to selectively depolymerize the polyesters back into their monomer components. These tests were first conducted in batch reactors with a variety of different catalysts.

M 3.1.1 - Experimental batch reactor studies with solvents and catalysts: Deconstruction reactions with two PDO-based polymers that were synthesized at the University of Oklahoma in Brian Grady's group were evaluated for optimum operating conditions in 10 mL sand bath reactors. Monomer products from each reaction were quantified to assess reaction effectiveness. Optimized reaction times and temperatures were tested. These optimized conditions were based on work developed in a different project in our group at NREL; this work is covered by a provisional patent application (U.S. provisional patent application 63/485,294).

3.1.2 - Recycling of up to 80% of 1,5-PDO polyesters back into monomer components: Chemical recycling pathways were evaluated for PPeAT and poly(pentylene sebacicate-co-terephthalate) (PPSeT or PPeC10T in other conventions) that would generate the highest possible monomer yields. Optimized reaction conditions of 170 °C, 2 hours, 8:1 w/w methanol:polymer, 5 wt% catalyst produced monomer yields of 92%.

The general reaction scheme for methanolysis of the PPAT and PPSeT polymers is shown below in **Figure 49**.

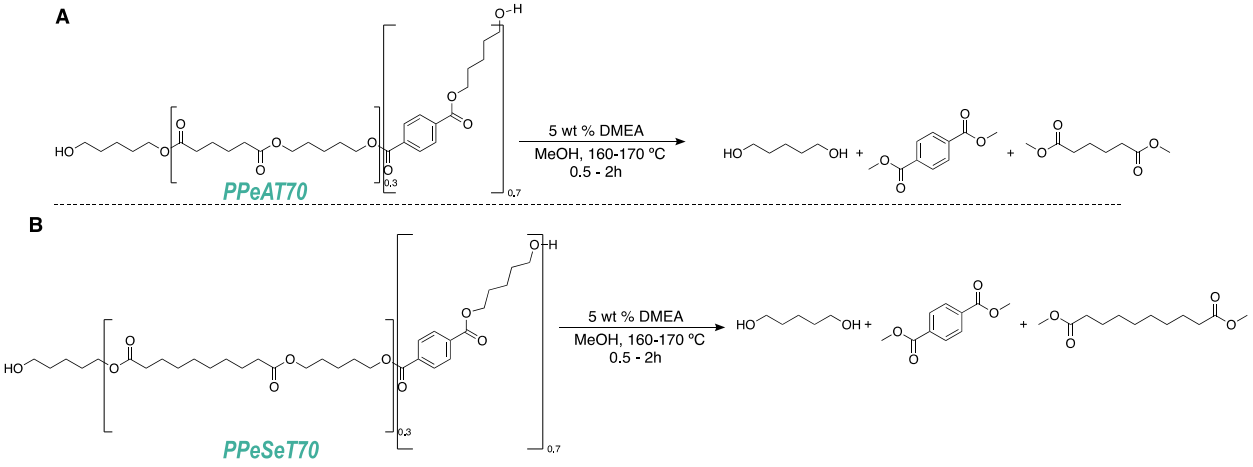

Figure 49. Representative depolymerization/methanolysis reactions with A) PPAT (PPeAT70) and B) PPeSeT70.

Methanolysis of the PPAT and PPSeT polymers indicates that 1,5-PDO and TPA can be recovered as methyl esters in >90% (molar) yield.

M 3.2.1 - Experimental batch reactor studies with solvents and catalysts: An amine catalyzed methanolysis system was developed to depolymerize each of the THFDM/FDM biodegradable polymers with >80% monomer yields. However, the optimization was not pursued because the collaborators at Oklahoma University found that polyesters derived from THFDM, HAH, and FDM did not have appropriate Tg and Tm to produce good films.

M 3.2.2 - Recycling of up to 80% of THFDM/FDM polyesters back into monomer components: The collaborators at Oklahoma University found that polyesters derived from THFDM, HAH, and FDM did not have appropriate Tg and Tm to produce good films. Therefore, these polyesters were not further synthesized or investigated, and focus would be on PPAT.

Task 5.0: Scaling up of Polyester Synthesis and Application Testing

M 5.10 – Optimization of Chemical recycling process at 100 mL scale: The chemical recycling of polyesters was performed in a Parker autoclave 300 mL stainless-steel mechanically stirred pressure reactor under 300 psi of nitrogen atmosphere. The polymer was loaded as 20 wt.% in methanol, 5 wt.% of DMEA (relative to polymer repeat unit). After loading the feed, the heating jacket was turned on, and reaction was run at 600 rpm, for 3 h at 190 °C. After reaction products were vacuum filtered. Analysis of solid fraction was performed via ^{1}H NMR using an internal standard. Liquid fraction was analyzed with both NMR and GC-MS. Chemical recycling was optimized for the PPAT formulation (PPeC6T60) chosen for scale-up to confirm that results obtained met required goals. Optimized conditions shown in **Figure 50**.

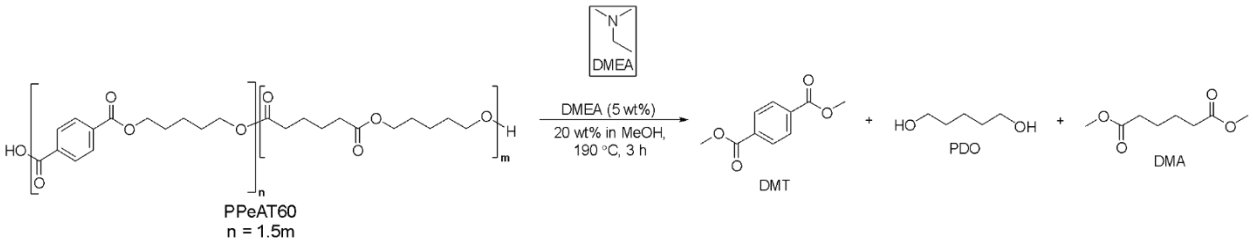

Figure 50. Representative depolymerization/methanolysis reactions with PPAT (PPeAT60)

Yields are shown in **Table 24**. The optimized scaled-up recycling process showed that yields of ≥ 80% were achieved.

Table 24. Summary of PPeAT60 Depolymerization Yields at 150mL Scale

Period	Polymer	Monomer	NMR yield (%)	GC yield (%)	Total yield (%)
12/8/23	PPeAT60	DMT	65	12	
		DMA	60	39	-
		PDO	-	85	85
1/25/24	PPeAT60	DMT	61	21	82
		DMA	72	63	-
		PDO	-	98	98
6/10/24	PPeAT60	DMT	44	19	63
		DMA	81	56	-
		PDO	-	99	99
6/17/24	PPeAT60	DMT	65	21	86
		DMA	60	67	-
		PDO	-	105	105
8/14/24 (Batch 1)	PPeAT60*	DMT	59	13	72
		DMA	64	38	-
		PDO	-	61	61
8/22/24 (Batch 2)		DMT	45	17	62
		DMA	59	37	-
		PDO	-	56	56

*This PPeAT60 sample was closer to PPeAT75, so maximum yield could not be achieved at these operating conditions. The depolymerized sample sent back contained 78% T and 28% A by mole fraction.

Area 5 – Techno-economic analysis and Life cycle assessment

We have developed a comprehensive process modeling framework that supports both techno-economic analysis (TEA) and life cycle assessment (LCA) of the broad range of polyesters studied in this project. Detailed methodology and results are provided in *Wang BX et al. ACS Sustainable Chem. Eng. 2024, 12, 24, 9156-9167* and *Wang BX et al. ACS Sustainable Chem. Eng. 2024, 12, 46, 16914-16923*. Our framework integrated rigorous process simulation tools with data sourced from both the literature and our own experimental research. This framework provided the basis to compare the benefits and drawbacks of different polyesters, identify key factors driving economics and environmental issues, and confirm that the new developed bio-based polyesters meet the intended performance and sustainability targets. All the work presented in this area was conducted under Task 4.0 - Techno-economic analysis (TEA) and life cycle analysis (LCA) of polyester and polyester recycling in milestones 4.1, 4.2, 4.3 and 4.3 and in Task 5.0 - Scaling up of Polyester Synthesis and Application under milestone 5.11. All five milestones were successfully completed.

TEA was performed for both the synthesis and recycling of each polymer, using experimental data generated during this project. LCA was used to estimate the environmental impacts of the proposed technologies. Together, TEA and LCA were used to assess multiple technology pathways, identifying the most promising as well as not viable options, and pinpointing critical bottlenecks. These analyses also provided valuable guidance for experimental design; specifically, TEA and LCA identified key missing pieces of information (e.g., technology performance), which were subsequently addressed through targeted experiments.

Furthermore, we developed supply chain and technology pathways models to understand the potential of scaling up biomass-based polymer production technologies. The process models were refined in BP3 using data obtained in Task 5 from our experimental collaborators. Results from Milestone 5.11 indicate that excess diol was not required for polyester synthesis and provided additional insights into diol degradation and mechanical strength properties. These findings were incorporated into the models, strengthening the validity of our conclusions.

Main differences between results obtained and initial plans were the following. The recycling model was developed by NREL and is proprietary; as such, we used basic estimates from their model to compare TEA/LCA of synthesis and recycling. In addition, our original goal was to conduct LCA for polyesters as used in multi-layer plastic films developed by Amcor; it was decided that this was not necessary in order to conduct our comparisons and instead we focused on estimating LCA impacts of the synthesis of polyesters.

Significant Accomplishments and Conclusions

Area 1 – Monomers from Biomass: We have successfully synthesized eight different biomass-derived monomers using chemical platforms such as furfural and 5-hydroxymethylfurfural (HMF). Selective production was achieved for key monomers including FDM, THFDM, HAH, PHAH, FHAH, and tetrol. From an industrial perspective, monomers such as 1,5-pentanediol and FDCA have been demonstrated at pilot scale by our industrial partners, Pyran and Stora Enso.

An important focus of this project was the transition from batch to continuous flow processes. Using FDM as a model monomer, we demonstrated how batch reactor systems can be translated into continuous flow setups, enabling scalable production while preserving product selectivity. Through kinetic studies, we optimized reaction conditions and gained a deeper understanding of reactor performance in both batch and continuous modes. Complete details about this study is to be presented in a future publication performed in the research group of Professor Huber and found in the products section of this report.

While this work has focused on monomers derived from furan-based biomass platforms, future exploration of alternative monomer classes, such as diacids and diols derived from fatty acids, may provide valuable new pathways for sustainable polymer production.

Area 2 – Polymer synthesis and characterization: In this project we have studied the production of aliphatic-terephthalate, aliphatic-furanoate and tetrahydrofuranoate polyesters. The main accomplishments demonstrated for this type of polyesters are:

- *Step-growth polymerization:* Almost 100 different polyesters, primarily based on pentanediol and FDCA, but also including terephthalic acid and THFDM, were synthesized to identify those that had the possibility of replacing LLDPE and LDPE based on Tg and Tm. Two were found, PPeAT and PDDF.

- *Cyclic Monomer Synthesis and Characterization:* We have developed efficient synthetic routes for cyclic aliphatic – furanoate and - tetrahydrofuranoate monomers, including PPeFL, DDFL, and THFDCA derivatives, *via* step-growth polycondensation (SGP) followed by catalyzed ring-closing depolymerization (RCDP). Monomer structures were confirmed by NMR and single-crystal X-ray diffraction (SCXRD), revealing stabilizing non-covalent interactions critical to solid-state packing.

- *High-Yield Monomer Recovery:* Substantial improvements in monomer recovery through RCDP have been achieved, with isolated yields of 35.6% for PPeFL and 71% for DDFL, enabling scalable production of high-purity cyclic monomers essential for ring-opening polymerization (ROP).

- *Controlled Ring-Opening Polymerization (ROP):* Ring-opening polymerization reactions employing Lanthanum- and Tin-based catalysts demonstrated the production of high molecular weight polyesters, including PPeF (M_n = 47.8 kDa, $Đ$ = 1.2) and PDDF (M_w = 1.08 MDa, $Đ$ = 1.41), demonstrating excellent control over polymerization and reproducibility.

- *Hydrogenated FDCA-Based Polymer Development:* Synthesized and characterized PDDTHF using colorless dmTHFDCA to address FDCA coloration issues, achieving targeted T_g and T_m values suitable for polyethylene replacement, with scalable hydrogenation protocol (99.9% yield, 99.0% purity).

- *Tailored Thermal and Mechanical Properties:* Polymers exhibited tunable thermal transitions and superior mechanical performance:
  - ✓ PPeAT: T_g = -15 °C, T_m = 95 °C, Young's modulus (E) = 150 MPa, stress at break (δ_b)= 25 MPa, elongation at break (ε_B)= 700 %,
  - ✓ PDDF: T_g = -10 °C, T_m = 95 °C, Young's modulus (E) = 225 MPa, δ_b= 25 MPa, ε_B= 250 %.

Two other polymers might be of interest. PPeF will not work for flexible film because of its high Tg, but might work as a barrier coating. PDDTHF has similar properties to PDDF but should have less color issues.

  - ✓ PPeF: T_g = 20°C, T_m = 70 °C, ε_B > 1000%,
  - ✓ PDDTHF: T_g = -20°C, T_m = 90 °C.

- *Barrier Performance:* PPeAT, PPeF and PDDF showed significantly reduced carbon dioxide and oxygen permeability compared to PBAT and LLDPE, and significantly reduced water vapor transmission rates compared to PBAT.

- *Biomass based content:* Assuming only pentanediol and FDCA are biobased, the biobased content of PPeAT and PDDF is 43 and 44% respectively, while PPeF is 100%. The addition of PLA, as is done commercially with PBAT, would increase biomass based content.

- *Biodegradability:* PPeAT is 60% biodegradable in 180 days by ASTMD6400 and is statistically identical to PBAT. PDDF does biodegrade but does not meet this standard.

- *Cost*: Because of their increased stiffness, the cost of PPeAT will be on the order of 50% less than PBAT on a use basis.

Area 3 – Polymer applications: We have demonstrated that biomass-derived polyesters PPeAT and PDDF have mechanical properties similar to those of LLDPE and better oxygen and carbon dioxide barrier properties which make these suitable for mono-layer films (M5.6) applications. Our deep characterization shows the technical feasibility of these two polyesters as sustainable alternatives to petroleum-based polymers for food

packaging. Regarding the polyesters studied for liquid packaging, blending PPeAT with PLA for extrusion coating applications (M5.8) resulted in materials with improved barrier properties compared to commercial PBAT and LDPE. This suggests that tailored biopolymer blends can outperform conventional materials in specific functional properties relevant to packaging. Despite the favorable mechanical and barrier properties identified in this research project, coloration of PPeAT and PDDF remains a concern for commercial food packaging applications due to consumer preferences for transparent of colorless films. Future directions for investigation of application of polyesters should focus on resolving the synthesis bottlenecks faced by the polymerization team, which hindered the investigation of our promising polyesters in multi-layer applications. In addition, further investigation is needed to address the removal of polyester's coloration through purification or formulation strategies.

Area 4 – Chemical Recycling of Polyesters: The project successfully demonstrated that bio-derived polyesters, particularly those based on 1,5-pentanediol such as PPeAT can be chemically recycled with high efficiency through catalytic methanolysis. Under optimized conditions, monomer recovery exceeded 90% yield, highlighting the viability of selective depolymerization as a circular strategy for polyester reuse. Importantly, the process was reproducible at an increased scale using a 300 mL pressure reactor, confirming that the optimized laboratory conditions could be translated into semi-pilot scale without loss in performance. The polyesters produced from this recycled monomer had properties equivalent to those from virgin monomers, except somewhere in the process a very small amount (<1% and possibly less than 0.1%) of an unidentified particulate contamination was present, which significantly reduced the elongation at break vs. the virgin material. In contrast, although similar recycling efficiencies were initially observed for polyesters derived from THFDM, HAH, and FDM, these materials were ultimately deemed unfit for application due to inadequate thermal properties, underscoring the importance of aligning recyclability with material functionality. Consequently, research and development efforts were concentrated on PPeAT formulations, which offered a favorable combination of mechanical properties and chemical recyclability, making them the most promising candidates for future application and scaling.

Area 5 – TEA and LCA: The main accomplishment of the process modeling team was demonstrating that the proposed bio-based polyesters can reduce carbon footprint by up to 50%, aligning with the original project targets. Reaching this conclusion required extensive process modeling and data collection. Notably, this reduction is enabled by the favorable mechanical strength properties of the bio-based polyesters, which allow for reduced resin usage while maintaining equivalent performance. Our analysis also revealed that feedstocks (diol and diacid) cost and environmental footprint account for 90% of polyester cost and emissions (i.e., the process for synthesis has limited impact

due to mild operating conditions). The cost and footprint of the diol is the dominant factor. In addition, diol degradation emerged as a key factor affecting overall process performance. We recommend that diol degradation should be carefully explored in future studies. From a scale-up perspective, we found that economies of scale are critical for achieving cost-competitive polyester production. Specifically, production scales of 20 kilotons per year or higher are favorable. Finally, we also found that the production costs and carbon footprints of recycling processes studied by NREL are comparable to those of virgin resin production

We found that bio-derived polyesters are cost competitive to fossil counterparts under certain market conditions (e.g., high oil prices) but there is a substantial amount of uncertainty in cost/footprint estimates due to uncertainty in bio-derived feedstocks (as such technologies are not commercial yet); as such, we recommend that more effort is spent in reducing such uncertainties by developing more detailed process models for monomer production and by conducting scale up studies of technologies. With additional data on the impact of diol/diacid ratio, an optimization framework can be developed to determine the optimal diol/diacid ratio (along with other design specifications throughout the process) to attain a minimum cost and carbon footprint in the production process.

Final Remarks Accomplishing Objectives of the Project

In the following lines we show again the initial objectives proposed for this project accompanied by a brief justification about how they were met as a metric to evaluate the success of the project.

- *50 to 70% lower energy input than conventional petroleum polymers*. Done with PPeAT and PDDF
- *Biomass based content from 50 to 100 wt.%:* Content was 44% for both PPeAT and PDDF. This small difference was judged to be acceptable.
- *Costs 30-50% lower than PBAT*: Done with PPeAT because of its higher stiffness. Approximate parity on per pound cost.
- *60% biodegradable in 180 days by ASTMD6400*: We have observed substantial degradation of biomass derived polyesters. As an illustration, for PDDF we observed that 60% of polyester biodegradation in soil occurs within 50 days.
- *Modulus at least 200 MPa and elongation at break at least 350% (similar to LDPE and linear-low density poly-ethylene (LLDPE)):* PDDF meets this without any additive, while PPeAT is ~150 MPa but does achieve this value in 90/10 PPeAT/PLA blend. This blend composition is very often used with PBAT.
- *Melting temperature 105-115 °C (similar to LDPE and LLDPE):* The glass transition temperature was achieved, but the melting temperature was 90-100°C for PPeAT and PDDF. This small difference was judged to be acceptable.

- *Haze index for a 25 µm film ~10 according to ASTM D1003 (similar to LDPE and LLDPE):* This objective was not achieved because of the dark color of the product. This dark color was attributed to the small batch synthesis used.
- O_2 transmission rate equal to or lower than ~8000 $cm^3/(m^2\ day)$ (LDPE and LLDPE): In this project we have demonstrated that PPeAT/PLAT blends might exceed substantially this objective.

3. Path Forward

Multiple research directions have been identified throughout this project that require continued development to advance and ultimately demonstrate the scalable production of biomass-derived polyesters. These key areas are outlined below:

1. **Scaling Up of Monomer Production**: Our research highlighted the need to refine crude 5-hydroxymethylfurfural (HMF) for the synthesis of key monomers, including FDM, THFDM, HAH, PHAH, FHAH, and 1,2,5,6-hexanetetrol. While a purification strategy was proposed to remove acidic and polymeric humin species, demonstration at larger scales is still required. Integration of this purification step into the overall process design, along with updated techno-economic (TEA) and life-cycle assessments (LCA), will be essential for evaluating its feasibility and sustainability.

2. **Overcoming Technical Barriers in Monomer Synthesis**: To achieve high conversion and yield in monomer production, most syntheses in this project were conducted in batch reactors. However, industrial-scale polyester production would greatly benefit from transitioning to continuous-flow monomer synthesis. While a comprehensive continuous-flow process was developed for FDM, other monomers were not synthesized in this manner. Nevertheless, the methodology and insights gained from FDM can be effectively translated to the synthesis of other monomers, especially those produced over heterogeneous catalysts.

3. **Development of Bio-Based Diols for Advanced Polyesters**: Toward the end of the project, PDDF (poly(dodecamethylene 2,5-furanoate)) was identified as a promising furan-based polyester with properties comparable to polyethylene. A key challenge now lies in identifying a sustainable source of dodecanediol. At UW–Madison, collaboration with Professor Brian Pfleger, an expert in microbial biosynthesis of hydroxy acids from sugars, offers a promising route. His work on 12-hydroxy dodecanoic acid could potentially be extended to produce 1,12-dodecanediol, establishing a biorenewable source of this diol for polyester synthesis.

4. **Pilot-Scale Demonstration of PPeAT Production:** Future research transfer efforts include ongoing collaboration with the Korean Research Institute of Chemical Technology (KRICT) to scale up production of PPeAT (poly(pentamethylene adipate-co-terephthalate)). A significant limitation during the project was the reliance on glass reactors, which restricted synthesis volumes. KRICT has a dedicated pilot plant to address these scale-up challenges. The facility will support the production of PPeAT using 1,5-pentanediol (1,5-PDO), produced at scale by Pyran, in combination with adipic acid and terephthalic acid. Demonstrating pilot-scale production is a critical milestone for validating PPeAT's commercial viability and industrial feasibility for

applications such as biodegradable mulch films and flexible packaging. Moreover, this effort represents a valuable opportunity for Pyran's 1,5-PDO to establish a new application niche, highlighting its role as a foundational building block for next-generation sustainable polyesters.

5. **Focus on Color:** The haze specification was not meant because of color concerns. For PPeAT, we believe those concerns were a result of our laboratory-scale synthesis procedure and KRICT results suggest that this diagnosis is correct. Fundamentally, we see no reason why PPeAT should be yellow while PBAT is not, assuming the pentanediol is not colored (which it is not). Our pilot-scale demonstration should solve this problem, but if not, this issue will be of concern.

6. **Monomer Ratio Control**: Preliminary analysis suggests that the effective TPA:AA mole ratio in the polymer post-polycondensation may have shifted to 70:30, deviating from the intended 60:40 feed ratio due to volatilization of AA. This discrepancy must be fully understood and managed under commercial synthesis conditions.

7. **PLA Compounding Considerations**: Although not discussed in detail here, blending with PLA has been shown to eliminate the need for additional nucleating agents. However, given that PPeAT exhibits approximately twice the stiffness of PBAT, the necessity of PLA compounding for mechanical enhancement may be moot. Further evaluation is needed to assess the trade-offs in performance and cost.

8. **Application Testing in Packaging:** Unfortunately, due to time constraints, we were unable to evaluate our polyesters in end-use applications such as mono- and multi-layer film formation for food packaging and extrusion coating for liquid packaging. However, the produced films demonstrate excellent mechanical and barrier performance compared to conventional LLDPE and PBAT. These application areas represent a critical next step in assessing the real-world viability of the materials developed. To date, we have identified two promising polyesters, PPeAT and PDDF, that exhibit biodegradability in both water and soil, partial bio-based content, and acceptable thermal and mechanical properties. Future research should prioritize application testing of these materials in packaging formats, which would offer a compelling opportunity to demonstrate their practical utility and potential for commercial adoption in sustainable packaging solutions.

4. Products

The following academic products were generated during this project.

Journal Publications Generated in this Project.

1. Kim, M. S.; Chang, H.; Zheng, L.; Yan, Q.; Pfleger, B. F.; Klier, J.; Nelson, K.; Majumder, E. L.-W.; Huber, G. W. A Review of Biodegradable Plastics: Chemistry, Applications, Properties, and Future Research Needs. Chem. Rev. 2023, 123, 9915-9939. DOI.
2. Zheng, L.; Kim, M. S.; Xu, S.; Urgun-Demirtas, M.; Huber, G. W.; Klier, J. Biodegradable High-Molecular-Weight Poly(pentylene adipate-co-terephthalate): Synthesis, Thermo-Mechanical Properties, Microstructures, and Biodegradation, ACS Sustainable Chem. Eng., 2023, 11, 13885-13895. DOI.
3. Wang, B-X.; Cortes-Peña, Y.; Grady, B. P.; Huber, G. W.; Zavala, V. M.; Techno-Economic Analysis and Life Cycle Assessment of the Production of Biodegradable Polyaliphatic–Polyaromatic Polyesters, ACS Sustainable Chem. Eng. 2024, 12, 24, 9156–9167. DOI.
4. Dastidar, R. G.; Chavarrio, J. E.; Jiang, Z.; McClelland, D. J.; Mavrikakis, M.; Huber, G. W.; Catalytic production of δ-valerolactone (DVL) from biobased 2-hydroxytetrahydropyran (HTHP) – Combined experimental and modeling study. Applied Catalysis B: Environment and Energy, 2025, 360, 124519. DOI.
5. Singh, O.; Aboukeila, H.; Klier, J.; Huber, G. W.; Grady, B. P.; Synthesis and characterization of biobased copolyesters based on pentanediol: (1) Poly(pentylene dodecanoate-co-furandicarboxylate). Polym Eng Sci., 2024, 1-12. DOI.
6. Aboukeila, H.; Singh, O.; Klier, J.; Huber, G. W.; Grady, B. P. Synthesis and characterization of biobased copolyesters based on pentanediol: (2) Poly(pentylene adipate-co-terephthalate). Polym Eng Sci. 2024. DOI.
7. Wang, B-X.; Zhuang, J.; Zavala, V. M. A Pathway Analysis Framework for Evaluating the Economic and Environmental Viability of Biomass-Based Plastic Production. ACS Sustainable Chem. Eng. 2024, 12, 46, 16914–16923. DOI.

Manuscripts under Preparation/Review

8. Wang, B.-X.; Zavala, V. M. A Fairness-Guided Supply Chain Framework for Polyester Production from Biomass. Computers & Chemical Engineering, (Under Review)
9. Chavarrio, J.E.; Votava, E.; Mavrikakis, M.; Huber, G.W. Catalytic Hydrogenation of HMF to BHMF over Copper Catalysts: Overcoming Challenges in the Production Process, (In Preparation)
10. Aboukeila, H.; Singh, O.; Mazaheri, M.; Edwards, E.; Rhue, M. A.; Klier, J.; Huber, G. W.; Grady, B. P. Film blowing of biobased biodegradable poly (pentylene adipate-co-terephthalate) and poly (dodecamethylene furandicarboxylate). ACS Appl. Polym. Mater. 2025 (Submitted)
11. Aboukeila, H.; Edwards, E.; Singh, O.; Klier, J.; Huber, G. W.; Grady, B. P. Synthesis and characterization of biobased copolyesters based on pentanediol: (3) Nucleation of poly(pentylene adipate-co-terephthalate) crystals. 2025 (In Preparation)

12. Chokkapu, E. R.; Aboukeila, H.; Tu, H.; Singh, O.; Klier, J.; Diment, W. T.; Huber, G. W.; Chen, E. Y.; Grady, B. P. Poly(dodecane furanoate) (PDDF): Synthesis, Characterization, and Polyethylene-Like Properties with Closed-Loop Circularity. Adv. Mater. 2025. (In Preparation)
13. Aboukeila, H.; Singh, O.; Mazaheri, M.; Cater, H.; Curley, J.; Klier, J.; Huber, G. W.; Grady, B. P. Closing the Loop: A Structure-Property Comparison of Virgin and Repolymerized Poly(pentylene adipate-co-terephthalate). Nat. Commun. 2025. (In Preparation)

Patents

14. Aboukeila, H.; Grady, B. P.; Klier, J. 1,5-Pentanediol-Based Polyester Compositions With Enhanced Crystallization Rates And Methods Of Manufacture; U.S. Provisional Patent Ser. No. 63/554,363, 2024.

Conferences where Results of the Project were Presented

15. Wang, B.-X.; Zavala, V. M. Evaluating Impacts of Carbon Taxes on the Economic Viability and Carbon Footprint of Plastic Production Pathways, AIChE, November 2022, Phoenix, Arizona. Link.
16. Singh, O.; Aboukeila, H.; Klier, J.; Grady, B. Biobased copolyesters poly(pentylene dodecanoate-co-furandicarboxylate): Synthesis, characterization, and thermo-mechanical properties, American Chemical Society Fall meeting, August 2023, San Francisco, California. Link.
17. Aboukeila, H., Singh, O.; Klier, J.; Grady, B. Characterization of high molecular weight Poly(pentylene adipate-co-terephthalate), American Chemical Society Fall meeting, August 2023, San Francisco, California. Link.
18. Aboukeila, H., Singh, O.; Klier, J.; Huber, G. W.; Grady, B. Synthesis and characterization of high molecular weight branched poly (pentylene adipate-co-terephthalate), American Chemical Society Southwest Regional meeting, November 2023, Oklahoma City, Oklahoma. Link.
19. Wang, B.-X.; Grady, B.; Huber, G. W.; Zavala, V. M. Techno-Economic Analysis and Life Cycle Assessment for Production of Biodegradable Polyesters, AIChE, November 2023, Orlando, Florida. Link.
20. Aboukeila, H., Singh, O.; Klier, J.; Huber, G. W.; Grady, B. Synthesis and Characterization of Biobased Copolyesters Based on Furandicarboxylic Acid. Poly(dodecamethylene furandicarboxylate), American Institute of Chemical Engineering – AIChE, October 2024, San Diego, California. Link.
21. Curley, J.; Liang, Y. ; DesVeaux, J.; Choi, H.; Uekert, T.; Clarke, R.; Michener, W.; Wu, Y.; Stanley, L.; Maurya, A. K.; Tassone, C.; Jacobsen, A., Mante, O.; Beckham, G.; Knauer, K. Closed-loop recycling of mixed polyesters via catalytic methanolysis and monomer reclamation. American Chemical Society National Meeting, March 2024, New Orleans, LA, Link.

5. Project Team and Roles

The project involves three main groups:

DOE personnel: The Department of Energy (DOE) personnel were responsible for overseeing the project's progress, evaluating milestone completion, and providing guidance on project objectives, including recommendations for renegotiation when necessary. Their roles ensured the alignment of project deliverables with DOE's standards and contractual obligations.

- **Jessica Phillips** – Technical Project Monitor
  Ensured the accuracy and completeness of documentation submitted as project deliverables and provided technical oversight throughout the project's duration.
- **Gayle Bentley** – Technical Project Officer
  Served as the primary interface between the DOE Office of Energy Efficiency and Renewable Energy (EERE) and the University of Wisconsin-Madison. She was responsible for the initiation and formal closeout of the award.
- **Alexandra Salvia** – Technical Closeout Coordinator
  Supported EERE programs by tracking the status of project deliverables and guiding them through the formal approval process required for closeout.
- **Ryan McCleary** – Grand and Contracting Officer
  Reviewed and approved project documentation to authorize and formalize the project closeout
- **Nathanael Heinz** - Grants Management Specialist
  Verified that all closeout deliverables conformed to the terms and conditions specified in the award agreement.

Academic partners: The academic collaborators were responsible for the technical development of the project, focusing on the synthesis of bio-derived polyesters and their chemical precursors. Their work was divided by the following institutions.

- **University of Wisconsin - Madison**
  Monomer synthesis – **Huber Research Group**: The Huber group led the synthesis of biomass-derived monomers using 5-hydroxymethylfurfural (HMF) as the starting platform. The team successfully developed and demonstrated the synthesis of several monomers, including tetrahydrofurandimethanol (THFDM), furandimethanol (FDM), 1,2,5,6-hexanetetrol (tetrol), hydroxyalkylated HMF (HAH), partially hydrogenated HAH (PHAH), and fully hydrogenated HAH (FHAH). These monomers were supplied to Professor Bryan Grady at the University of Oklahoma for subsequent polyester synthesis. The group was led by Professor George Huber, who also served as the project's principal investigator (PI). Graduate students Hoya Ihara, Javier Chavarrio, and Min Soo Kim were responsible for executing the monomer synthesis and

purification protocols to generate the quantities required for downstream polymerization.

Process evaluation – **Zavala Research Group**: The Zavala group conducted the techno-economic analysis (TEA) and life cycle assessment (LCA) of the polyester production process. Their work encompassed the evaluation of monomer synthesis pathways, esterification reactions, purification steps, and potential integration of chemical recycling strategies. These assessments aimed to determine the economic viability and environmental impact of the complete polyester value chain. The team was led by Professor Victor Zavala, with Bo-Xun Wang, a graduate student, contributing to the development and implementation of the modeling and analysis frameworks.

- **The University of Oklahoma** team, led by Professor Bryan Grady, focused on the production and scale-up of PPeAT (poly(pentamethylene adipate-co-terephthalate)) films as a potential replacement for PBAT in mulching applications. The team investigated processing conditions and film performance to meet agricultural application standards. Researchers Onkar Singh and Hesham Aboukeila contributed to polymer synthesis, film fabrication, and characterization studies.

- The **Colorado State University team**, led by Professor Eugene Chen, with John Klier, Eswar Chokkapu, and Hangfei Tu, focused on the synthesis and mechanical evaluation of novel polyesters. Their work emphasized the use of 2,5-furandicarboxylic acid (FDCA) as the diacid component, exploring multiple diols to produce a diverse set of furan-based polyesters including: PPeF (poly(pentamethylene 2,5-furanoate)), PDDF (poly(dodecane 2,5-furanoate)), PTDF (poly(tetradodecane 2,5-furanoate)), Emerging candidates such as P(GA-co-VL) (poly(glycolide-co-valerolactone)) and PDDTHF (poly(dodecane tetrahydrofuran)). Their goal in the project was to identify alternatives that could mimic or exceed the performance of conventional polyethylene films in packaging applications.

- **National Renewable Energy Laboratory (NREL)** focused on evaluating the chemical recyclability of the synthesized polyesters and predicting polymer properties using the PolyML machine learning tool. This work supported long-term circularity goals by identifying polymers with favorable degradation and recycling pathways. The NREL team was led by Dr. Gregg Beckham (PI), with key contributions from Brandon Knott, Henry Carter, Jeffrey Law, Julia Curley, and Laura Hollingsworth.

Industrial collaborators: The industrial partners played a critical role in scaling up the synthesis of monomers and demonstrating the applicability of the developed materials in packaging applications. Their specific contributions are detailed below.

- **Amcor** was responsible for evaluating the performance of our biomass-derived polyesters in the production of mono- and multi-layer films for food packaging. The Amcor team included Kevin Nelson and Steven Grey, who conducted material testing and provided feedback on film quality and process compatibility.
- **Pyran** led the demonstration of the scale-up production of 1,5-pentanediol (1,5-PDO) to quantities exceeding 1 kg. The effort was led by Dr. Kevin Barnett and Dr. Daniel McClelland, who showcased Pyran's proprietary process for converting furfural into 1,5-PDO. This pathway represents a renewable route to a key polyester monomer.
- **Stora Enso** contributed to the project by producing and supplying 2,5-furandicarboxilic acid (FDCA), a critical monomer for polyester synthesis. Additionally, they evaluated the use of synthesized PPeAT in extrusion coating applications for liquid packaging and compared the results to PBAT and PP control materials. The Stora Enso collaboration team included Gary Diamon, dirk Den Ouden, Laleh Maleki, Lars Kruger, and Staffan Torssell.

6. References

1. R. Geyer, J. R. Jambeck and K. L. Law, *Science Advances*, **3**, e1700782.
2. K. L. Sánchez-Rivera, A. d. C. Munguía-López, P. Zhou, V. S. Cecon, J. Yu, K. Nelson, D. Miller, S. Grey, Z. Xu, E. Bar-Ziv, K. L. Vorst, G. W. Curtzwiler, R. C. Van Lehn, V. M. Zavala and G. W. Huber, *Resources, Conservation and Recycling*, 2023, **197**, 107086.
3. L. Donkor, G. Kontoh, A. Yaya, J. K. Bediako and V. Apalangya, *Applied Food Research*, 2023, **3**, 100356.
4. S. Ronca, in *Brydson's Plastics Materials (Eighth Edition)*, ed. M. Gilbert, Butterworth-Heinemann, 2017, pp. 247-278.
5. X. Yang, S. Kang, S. L. Hsu, H. D. Stidham, P. B. Smith and A. Leugers, *Macromolecules*, 2001, **34**, 5037-5041.
6. S. Inkinen, M. Hakkarainen, A.-C. Albertsson and A. Södergård, *Biomacromolecules*, 2011, **12**, 523-532.
7. F. Carrasco, P. Pagès, J. Gámez-Pérez, O. O. Santana and M. L. Maspoch, *Polymer Degradation and Stability*, 2010, **95**, 116-125.
8. S. Y. Choi, I. J. Cho, Y. Lee, Y.-J. Kim, K.-J. Kim and S. Y. Lee, *Advanced Materials*, 2020, **32**, 1907138.
9. Y.-Y. Zhang, L. Yang, R. Xie, G.-W. Yang and G.-P. Wu, *Macromolecules*, 2021, **54**, 9427-9436.
10. T. F. Nelson, R. Baumgartner, M. Jaggi, S. M. Bernasconi, G. Battagliarin, C. Sinkel, A. Künkel, H.-P. E. Kohler, K. McNeill and M. Sander, *Nature Communications*, 2022, **13**, 5691.
11. L. Aliotta, M. Seggiani, A. Lazzeri, V. Gigante and P. Cinelli, *Journal*, 2022, **14**.
12. M. Adnan, A. J. Siddiqui, S. A. Ashraf, M. Snoussi, R. Badraoui, M. Alreshidi, A. M. Elasbali, W. A. Al-Soud, S. H. Alharethi, M. Sachidanandan and M. Patel, *Journal*, 2022, **14**.
13. A. Z. Naser, I. Deiab and B. M. Darras, *RSC Advances*, 2021, **11**, 17151-17196.
14. M. Denial, S. Karthikeyan, R. Godse and V. K. Gupta, *Polymer Science, Series C*, 2021, **63**, 102-111.
15. Z. Gan, K. Kuwabara, M. Yamamoto, H. Abe and Y. Doi, *Polymer Degradation and Stability*, 2004, **83**, 289-300.
16. Y. Ding, D. Huang, T. Ai, C. Zhang, Y. Chen, C. Luo, Y. Zhou, B. Yao, L. Dong, X. Du and J. Ji, *ACS Sustainable Chemistry & Engineering*, 2021, **9**, 1254-1263.
17. L. Wu, R. Mincheva, Y. Xu, J.-M. Raquez and P. Dubois, *Biomacromolecules*, 2012, **13**, 2973-2981.
18. Z. Terzopoulou, V. Tsanaktsis, D. N. Bikiaris, S. Exarhopoulos, D. G. Papageorgiou and G. Z. Papageorgiou, *RSC Advances*, 2016, **6**, 84003-84015.
19. G. Wang, M. Jiang, Q. Zhang, R. Wang and G. Zhou, *RSC Advances*, 2017, **7**, 13798-13807.
20. A. Künkel, J. Becker, L. Börger, J. Hamprecht, S. Koltzenburg, R. Loos, M. B. Schick, K. Schlegel, C. Sinkel, G. Skupin and M. Yamamoto, in *Ullmann's Encyclopedia of Industrial Chemistry*, 2016, pp. 1-29.
21. *United States Pat.,* US20170197930A1, 2017.
22. E. B. Gilcher, H. Chang, G. W. Huber and J. A. Dumesic, *Green Chemistry*, 2022, **24**, 2146-2159.

23. S. H. Krishna, M. De bruyn, Z. R. Schmidt, B. M. Weckhuysen, J. A. Dumesic and G. W. Huber, *Green Chemistry*, 2018, **20**, 4557-4565.
24. M. Balkenhohl, H. Jangra, I. S. Makarov, S. M. Yang, H. Zipse and P. Knochel, *Angew Chem Int Ed Engl*, 2020, **59**, 14992-14999.
25. V. Tsanaktsis, G. Z. Papageorgiou and D. N. Bikiaris, *Journal of Polymer Science Part A: Polymer Chemistry*, 2015, **53**, 2617-2632.
26. U. Fehrenbacher, O. Grosshardt, K. Kowollik, B. Tübke, N. Dingenouts and M. Wilhelm, *Chemie Ingenieur Technik*, 2009, **81**, 1829-1835.
27. P. Zemenová, R. Král, M. Rodová, K. Nitsch and M. Nikl, *Journal of Thermal Analysis and Calorimetry*, 2019, **141**, 1091-1099.
28. F. M. Sousa, F. B. Cavalcanti, V. A. D. Marinho, D. D. S. Morais, T. G. Almeida and L. H. Carvalho, *Polymer Bulletin*, 2021, **79**, 5327-5338.
29. R. K. Krishnaswamy and M. J. Lamborn, *Polymer Engineering & Science*, 2000, **40**, 2385-2396.
30. M. Härth and A. Dörnhöfer, *Polymers*, 2020, **12**, 1605.
31. V. Tsanaktsis, E. Vouvoudi, G. Z. Papageorgiou, D. G. Papageorgiou, K. Chrissafis and D. N. Bikiaris, *Journal of Analytical and Applied Pyrolysis*, 2015, **112**, 369-378.
32. Z. Terzopoulou, V. Tsanaktsis, M. Nerantzaki, D. S. Achilias, T. Vaimakis, G. Z. Papageorgiou and D. N. Bikiaris, *Journal of Analytical and Applied Pyrolysis*, 2016, **117**, 162-175.
33. V. Bourg, R. Valette, N. Le Moigne, P. Ienny, V. Guillard and A. Bergeret, *Polymers*, 2021, **13**, 652.
34. H. Münstedt, S. Kurzbeck and J. Stange, *Polymer Engineering & Science*, 2006, **46**, 1190-1195.
35. P. Micic, S. N. Bhattacharya and G. Field, *Polymer Engineering & Science*, 1998, **38**, 1685-1693.
36. L. Zheng, M. S. Kim, S. Xu, M. Urgun-Demirtas, G. W. Huber and J. Klier, *ACS Sustainable Chemistry & Engineering*, 2023, **11**, 13885-13895.
37. Y. Tokiwa and B. P. Calabia, *Appl Microbiol Biotechnol*, 2006, **72**, 244-251.
38. N. Lucas, C. Bienaime, C. Belloy, M. Queneudec, F. Silvestre and J. E. Nava-Saucedo, *Chemosphere*, 2008, **73**, 429-442.